VILNIUS GEDIMINAS TECHNICAL UNIVERSITY

Donatas GURAUSKIS

INVESTIGATION OF THE MEASUREMENT ERRORS FORMATION IN OPTICAL LINEAR ENCODERS

DOCTORAL DISSERTATION

TECHNOLOGICAL SCIENCES,
MECHANICAL ENGINEERING (T 009)

Vilnius, 2022

Doctoral dissertation was prepared at Vilnius Gediminas Technical University in 2017–2022.

Scientific Supervisor

Assoc. Prof. Dr Artūras KILIKEVIČIUS (Vilnius Gediminas Technical University, Mechanical Engineering – T 009).

The Dissertation Defense Council of Scientific Field of Mechanical Engineering of Vilnius Gediminas Technical University:

Chairman

Prof. Dr Habil. Rimantas BELEVIČIUS (Vilnius Gediminas Technical University, Mechanical Engineering – T 009).

Members:

Assoc. Prof. Dr Regimantas BAREIKIS (Vilnius Gediminas Technical University, Mechanical Engineering – T 009),
Dr Habil. Algimantas BUBULIS (Kaunas University of Technology, Mechanical Engineering – T 009),
Prof. Dr Arnas KAČENIAUSKAS (Vilnius Gediminas Technical University, Mechanical Engineering – T 009),
Dr Olga ORYNYCZ (Bialystok University of Technology, Poland, Mechanical Engineering – T 009).

The dissertation will be defended at the public meeting of the Dissertation Defense Council of Mechanical Engineering in the Senate Hall of Vilnius Gediminas Technical University at **9 a. m. on 16 June 2022.**

Address: Saulėtekio al. 11, LT-10223 Vilnius, Lithuania.
Tel.: +370 5 274 4956; fax +370 5 270 0112; e-mail: doktor@vilniustech.lt

A notification on the intended defending of the dissertation was sent on 13 May 2022. A copy of the doctoral dissertation is available for review at Vilnius Gediminas Technical University repository http://dspace.vgtu.lt and at the Library of Vilnius Gediminas Technical University (Saulėtekio al. 14, LT-10223 Vilnius, Lithuania).

Vilnius Gediminas Technical University book No 2022-024-M

doi:10.20334/2022-024-M

donatas.gurauskis@vilniustech.lt

VILNIAUS GEDIMINO TECHNIKOS UNIVERSITETAS

Donatas GURAUSKIS

MATAVIMO PAKLAIDŲ FORMAVIMOSI OPTINIUOSE LINIJINIUOSE KEITIKLIUOSE TYRIMAS

DAKTARO DISERTACIJA

TECHNOLOGIJOS MOKSLAI,
MECHANIKOS INZINERIJA (T 009)

Vilnius, 2022

Disertacija rengta 2017–2022 metais Vilniaus Gedimino technikos universitete.

Mokslinis vadovas

doc. dr. Artūras KILIKEVIČIUS (Vilniaus Gedimino technikos universitetas, mechanikos inžinerija – T 009).

Vilniaus Gedimino technikos universiteto Mechanikos inžinerijos mokslo krypties disertacijos gynimo taryba:

Pirmininkas

prof. habil. dr. Rimantas BELEVIČIUS (Vilniaus Gedimino technikos universitetas, mechanikos inžinerija – T 009).

Nariai:

doc. dr. Regimantas BAREIKIS (Vilniaus Gedimino technikos universitetas, mechanikos inžinerija – T 009),
habil. dr. Algimantas BUBULIS (Kauno technologijos universitetas, mechanikos inžinerija – T 009),
prof. dr. Arnas KAČENIAUSKAS (Vilniaus Gedimino technikos universitetas, mechanikos inžinerija – T 009),
dr. Olga ORYNYCZ (Balstogės technologijos universitetas, Lenkija, mechanikos inžinerija – T 009).

Disertacija bus ginama viešame Mechanikos inžinerijos mokslo krypties disertacijos gynimo tarybos posėdyje **2022 m. birželio 16 d. 9 val**. Vilniaus Gedimino technikos universiteto senato posėdžių salėje.

Adresas: Saulėtekio al. 11, LT-10223 Vilnius, Lietuva.
Tel.: (8 5) 274 4956; faksas (8 5) 270 0112; el. paštas doktor@vilniustech.lt

Pranešimai apie numatomą ginti disertaciją išsiųsti 2022 m. gegužės 13 d.

Disertaciją galima peržiūrėti Vilniaus Gedimino Technikos Universiteto talpykloje http://dspace.vgtu.lt ir Vilniaus Gedimino technikos universiteto bibliotekoje (Saulėtekio al. 14, LT-10223 Vilnius, Lietuva).

Abstract

The thesis investigates the displacement measurement errors of the linear encoder and the causing factors. To achieve the thesis objectives, the theoretical and experimental research of the linear encoder behavior was performed under different operating conditions, including thermal effects, mechanical vibration, and different scanning speeds. Analyzed and systematized results were used to develop methods for error compensation and offer possible technical solutions to improve the performance of linear encoders.

The dissertation consists of an introduction, analytical literature review, discussion of the research methodology, investigation results and conclusions, and four appended scientific articles.

The literature review systemized information about the optical linear encoders and their performance. The section on research methodology presents theoretical and experimental methods used to study the impact of different environmental effects on the measurement error formation in linear encoders. The third chapter briefly discusses the results obtained in each of the appended articles with the intention of relating them to the overall objectives and general conclusions of the thesis.

Based on analytical calculations, digital finite element analysis, and experimental research, Article 1 determines the mathematical models of thermal errors that are used for real-time compensation.

Article 2 presents an experimental realization of the real-time thermal and geometric error compensation approach for an optical encoder achieved by using a field-programmable gate array (FPGA) computing platform.

Article 3 presents the developed methodology for the estimation of linear encoder sub-divisional errors and the results of the experimental investigation based on the harmonic analysis of estimated errors.

Article 4 reveals the linear encoder behavior under mechanical vibration, determining the most dangerous resonant frequencies and performing the modal analysis by using the finite element method.

The appended scientific articles were published in four peer-reviewed scientific journals listed in the Clarivate Analytics Web of Science database with an impact factor. The other four related articles are printed in scientific journals listed in the Clarivate Analytics Web of Science database without the impact factor and other international databases. The results of the research were presented at three international conferences.

Reziumė

Šiame darbe tiriamos linijinių keitiklių poslinkių matavimo paklaidos ir jas sukeliantys veiksniai. Siekiant išspręsti darbe keliamus uždavinius, atliekami teoriniai ir eksperimentiniai linijinio keitiklio elgsenos, bei matavimo paklaidų susidarymo tyrimai vyraujant skirtingoms aplinkos sąlygoms, įskaitant temperatūros poveikį, mechanines vibracijas ir skirtingą poslinkio matavimo greitį. Išanalizuoti ir susisteminti rezultatai panaudoti sudarant matematinius matavimo paklaidų kompensavimo modelius..

Disertaciją sudaro įvadas, literatūros apžvalga, tyrimo metodikos aptarimas, rezultatai ir išvados, bei keturi pridedami moksliniai straipsniai.

Literatūros apžvalgoje susisteminta informacija apie optinius linijinius keitiklius ir jų veikimą. Tyrimo metodologijos skyriuje pristatomi teoriniai ir eksperimentiniai metodai, naudojami tiriant skirtingų aplinkos poveikių įtaką matavimo paklaidų susidarymui. Trečiame skyriuje trumpai aptariami kiekviename pridedamame straipsnyje gauti rezultatai, siekiant juos susieti su bendrais darbo tikslais ir bendromis disertacijos išvadomis.

Straipsnyje 1, remiantis analitiniais skaičiavimais, skaitmenine baigtinių elementų analize ir eksperimentiniais tyrimais sudaromas matematinis, tiriamojo keitiklio, termoelastinių paklaidų modelis, kuris gali būti pritaikytas realaus laiko temperatūrinių bei geometrinių paklaidų kompensavimui.

Straipsnyje 2 pristatomas praktinis realaus laiko temperatūrinių ir geometrinių paklaidų kompensavimo realizavimas panaudojant standartines technologines skaičiavimo priemones. Atlikti eksperimentiniai sukomplektuotos sistemos tyrimai.

Straipsnyje 3 pristatoma sukurta linijinio keitiklio metrologinių (interpoliacijos) paklaidų nustatymo ir analizės metodika, bei pateikiami eksperimentinių tyrimų, paremtų harmonine nustatytų periodinių paklaidų analize, rezultatai. Gauti rezultatai leidžia įvertinti linijinio poslinkio matavimo greičio įtaką paklaidų susidarymui, bei nusakyti fizikinę paklaidų prigimtį.

Straipsnyje 4 atskleidžiama tiriamojo linijinio keitiklio elgsena veikiant išorinėms mechaninėms vibracijoms. Eksperimentiškai nustatyti patys pavojingiausi rezonansiniai keitiklio dažniai, atlikta kompiuterinė modalinė analizė bei nustatyta rezonansinių dažnių įtaka matavimo paklaidos susidarymui.

Disertacijoje pristatomi straipsniai yra publikuoti keturiuose recenzuojamuose moksliniuose žurnaluose įtrauktuose į Clarivate Analytics Web of Science duomenų bazę, su cituojamumo rodikliu (angl. Impact Factor). Kiti keturi moksliniai straipsniai susiję su disertacijos tema atspausdinti kituose moksliniuose žurnaluose. Atliktų tyrimų rezultatai pristatyti trejose tarptautinėse konferencijose.

Notations

Abbreviations

CTE – coefficient of thermal expansion;
FEM – finite element method;
FFT – fast Fourier transformation;
FPGA – field-programmable gate array;
SDE – sub-divisional (interpolation) error.

Contents

Author's contribution to the publications

Publication[1]	Formal contribution[2]	Conceptualization	Data curation	Formal analysis	Investigation	Methodology	Software	Validation	Visualization	Writing – original draft	Writing – review & editing
Gurauskis, D. et al., 2019	0.250	joint	main	main	joint	joint		joint	sole	joint	main
Gurauskis, D. et al., 2021	0.333	main	main	main	joint	joint	joint	joint	sole	sole	sole
Gurauskis, D. et al., 2020	0.333	main	main	sole	main	main	sole	joint	sole	sole	sole
Gurauskis, D. and Kilikevičius, A., 2020	0.500	main	main	main	joint	main		joint	sole	sole	sole
Total or max[3]	1.417	main	main	sole	main	main	sole	joint	sole	sole	sole

[1] The published articles have been used here with the permission of the relevant publishers.

[2] The formal contribution is calculated as a fraction – $1/N_{\text{authors}}$.

[3] The total sum of the formal contribution values or the highest contribution achieved (in the increasing order: none, joint, main, or sole) in the specified 10 of 14 roles (according to the CRediT taxonomy, https://credit.niso.org/).

All the above-mentioned articles' co-authors have no motive to use this published data to prepare other dissertations.

All the authors of the above-mentioned articles have agreed on the author's contribution statement.

Introduction

Problem Formulation

Optical linear encoders are usually the most reliable devices for precise displacement measurement and motion control. Due to their high accuracy, resolution, repeatability, and low price, they are used in various applications. Some examples are manually controlled machine tools and computer numerical control (CNC) machines (Zhao *et al.,* 2018), automated production lines, medical or defense applications, monitoring, and fault diagnosis systems, tracking systems, and linear positioning stages (Lee *et al.,* 2011) and other precision positioning applications (Gao *et al.,* 2015). No wonder that with such diversity of applicability, encoders must work in a wide variety of operating conditions, which inevitably more or less affect the performance of the measuring device. Moreover, the requirements for these technological machines and their measuring systems are constantly increasing.

The accuracy and feasibility of the technological process performed by the machine depend on the reliability of the used measuring system. The superior performance of the linear encoder is critical. Unfortunately, rather often, the occurring dimensional errors of the technological process are attributed to direct strain, mechanical vibration, or thermal effects in the machine structure, assuming that the encoder has a small contribution to the total error (Alejandre and Artes, 2004).

Different kinds of measuring errors caused by mechanical strain or displacement, inaccurate production, thermoelastic deformation induced by thermal effects or shock, and vibration generated by an external mechanical excitation could corrupt the declared accuracy and repeatability of the linear encoder. The size of the dominant high-frequency sub-divisional error might even limit the highest resolution that could be reached. In applications where differential incremental signals of the encoder are used for motion control with direct-drive systems, the nonlinear interpolation error can result in loud noise, speed ripple, or additional heat generation (Ye *et al.,* 2019).

The minimization of measuring system errors and increasing high-quality requirements could only be met by developing new systems that respond to modern scientific and technical achievements, as well as improving existing measuring devices in accordance with the fundamental principles of precision engineering. Optical encoders and their working principles or manufacturing aspects are constantly analyzed by scientists in many parts of the world. The significant contribution to the design of linear encoders, the manufacturing process of glass and stainless-steel measuring scales, and the development of encoder calibration systems is made by Lithuanian universities and scientists.

This thesis focused on the theoretical and experimental investigation of the linear optical encoder displacement measurement error and the causing factors. The consistent research of the encoder behavior under different operating conditions, including ambient thermal effects, mechanical vibration, and different scanning speeds, is necessary to understand the nature of the measuring error. Analyzed and systematized results are used to develop methods for error compensation and offer possible technical solutions to improve the performance of linear encoders.

Relevance of the Thesis

In optical linear encoders, the displacement measurement errors may disturb the position estimation or the motion of the machine's moving unit. It leads to an impropriated technological process and sometimes could even damage the operating equipment. To avoid these consequences, close attention must be paid to the behavior of such measuring systems under various operating conditions.

The advanced photolithography manufacturing, system assembly, and calibration processes of the optical encoders are performed according to strict standards and requirements by using specialized clean and thermostable facilities and precisely calibrated equipment. The parameters, such as the accuracy of the device calibrated under such ideal conditions, are publicly declared. However, the impact

of thermoelastic deformation or mechanical vibration arising in a particular application on accuracy often remains the subject of debate. Any attempt to improve the performance of the linear encoder requires a deep understanding of its design and behavior. In practice, it is a challenging task because of the lack of knowledge, which is usually the "know-how" of the manufacturer. Therefore, universal measuring error estimation and analysis methodologies are needed.

On the other hand, the enhancement of accuracy at the expense of their production precision is not always possible and, moreover, technically and economically effective. The development of the encoder that is minimally sensitive to environmental conditions requires the most advanced scientific and technical achievements in optics, electronics, precise mechanics, materials science, and other fields. In this case, the measuring error minimization method as the real-time compensation opens wide possibilities when measuring errors are calibrated, memorized, and subtracted in the technological process.

The most optimal solution for these problems is only possible by performing complex research on the measuring system. The identified systematic behavior of the error could be attempted to eliminate by using compensation techniques, and the random error component could be reduced by the proposed technical solutions.

The Object of the Research

The research object is the optical linear encoder and its measurement error formation under the operating conditions. The main aspects of the research object investigated in the thesis are:

- analysis of the formation of thermoelastic deformations under different thermal conditions and its impact on measurement accuracy;
- analysis of the sub-divisional encoder error relation with different position scanning velocities;
- analysis of the external mechanical vibration impact on the measurement error formation and research of its minimization solutions.

The Aim of the Thesis

The thesis aimed to theoretically and experimentally investigate the measurement error of an optical linear encoder under real operating conditions in pursuance to develop methods and offer technical assumptions to improve the quality and performance of linear displacement measurement systems.

The Objectives of the Thesis

The following objectives were formulated to solve the stated problem and reach the aim of the thesis:

1. Summarize the knowledge of optical linear encoders based on the scientific and technical literature: analyze the main working principles and different designs of the encoder; comprehend the main aspects that disturb the measuring process; compose the measuring error budget and distinguish the main sources of error; analyze the methods used for a theoretical encoder error calculation and an experimental measurement error estimation; investigate the measurement error minimization techniques and possible technical solutions.

2. Use analytical and numerical methods for the theoretical investigation of linear encoder behavior under different operating conditions: thermal, displacement measurement, velocity, and vibration.

2.1. Create the numerical computer model to investigate the thermal error of the selected linear encoder caused by the thermoelastic deformations when the device under the test is affected by external heat sources and changing ambient temperature and develop the mathematical compensation model of the systematic error component.

2.2. Develop the methodology for the sub-divisional encoder error estimation and analysis under different displacement measurement velocities.

2.3. Develop the numerical computer model of the selected linear encoder to analyze its resonant frequencies (eigenfrequencies) and corresponding deformation shapes (eigenmodes).

3. Perform the experimental investigations:

3.1. Realize the practical approach for real-time geometric and thermal error compensation and evaluate its suitability and reliability.

3.2. Practically apply the developed methodology and experimentally investigate the periodic high-frequency error (sub-divisional) relationship with different scanning velocities.

3.3. Perform an experimental dynamic behavior analysis of the tested optical linear encoder under external mechanical vibrations. Link the measured oscillations of the encoder elements with the results of the performed computer modal analysis and determine which modes (encoder deformations) cause the maximum response amplitude. Evaluate the effect of external mechanical vibration on the formation of measurement error and offer technical solutions to improve the mechanical design of the encoder.

Research Methodology

The research methodology applied in this thesis is based on the relevant fields of science and was assessed using the analytical review of the scientific and technical literature.

The theoretical research performed in this thesis is based on the principles of material science and continuum solid mechanics, including the topics of thermomechanics and vibration of solids. The thermal behavior of the tested linear encoder was analyzed according to the laws of thermodynamics. The conservation of energy allowed to solve the heat transfer problem and evaluate the predominant temperature gradient. The calculation of introduced thermal stresses and thermal expansion helped to identify the thermoelastic deformation, which is related to the investigative measurement error. The dynamic behavior of the linear encoder was determined by the analysis of its eigenfrequencies and eigenmodes. The finite element method (FEM) was used as the most suitable numerical method for solving these partial differential equations in three space variables. The *"COMSOL"* Multiphysics simulation software was used for computer modeling.

The empirical data were collected during the experimental research. The tests were performed at the Institute of Mechanical Science (VGTU) and the laboratory facilities of JSC *"Precizika Metrology."* The *"Keysight 5530"* laser calibration system configured for linear measurement was used as the reference device for the linear encoder error estimation. Measuring instruments from the companies *"Brüel & Kjær"* and *"Hottiger"* were used to measure the vibration parameters. The experimental setup composed of the motorized direct-drive linear translation stage and the servo motion controller from the JSC *"STANDA"* was used for the investigation of the linear encoder's sub-divisional errors under different scanning speeds. The differential output signals of the encoder were recorded using data acquisition and processing equipment based on the digital oscilloscope *"PicoScope 3000"*. All experiments were performed based on the measurement theory to ensure the quality of measurements and minimize their uncertainty.

The reliability of the results was verified by mathematical statistics methods. A more detailed investigation of the obtained results was made based on fast Fourier transformation (FFT). The analysis of the collected data and the graphical representation of the results were performed by using numerical computing and advanced analytics software packages: *"MATLAB"*; *"Statistica"*; *"Origin"*; *"Microsoft Excel."*

Scientific Novelty of the Thesis

During the preparation of the thesis, the following novel results for engineering science were obtained:

1. The systematic regularities were revealed for position measurement errors of the closed type optical linear encoders under the impact of external environmental influences that can be subject to calculated error compensation.
2. The mathematical model of the thermal and geometric error compensation for an optical linear encoder was developed, investigated, and applied using technological calculation equipment.
3. The measuring technique of the sub-divisional encoder error was proposed, and the advanced error analyzation method based on harmonic analysis was presented.
4. The dynamic behavior of the linear encoder was determined under external mechanical excitation, and its impact on the displacement measurement process was estimated.

Practical Value of the Research Findings

The thesis solved a complex task, which included the necessary theoretical and experimental research in determining, analyzing, and understanding the ongoing processes in a linear displacement measurement system functioning under different working conditions. Such a task involves developing methodological and practical implementation techniques that enable solving analytical, empirical, and numerical assignments. The obtained results are used to evaluate the systematic behavior of the measurement error and develop the real-time compensation approach. The proposed method is convenient and easily realized using simple technological calculation equipment, which could be integrated into the application or the encoder itself.

The research methods and technical solutions proposed in the thesis could be useful for engineers and scientists working on the precise measuring systems in their development and improvement.

The Defended Statements

1. Thermoelastic and dynamic processes of enclosed linear encoders and their regularities could be investigated and evaluated using a complex methodology.
2. The geometrical and temperature errors of the linear encoders are recorded and compensated in real-time using simplified parametric functions.

3. The proposed real-time compensation approach is suitable for the thermoelastic and geometric encoder error compensation, stating that the declared performance of the encoder remains under different ambient temperatures.

Approval of the Research Findings

The research results were published in eight scientific publications:

- four articles were printed in peer-reviewed scientific journals listed in the Clarivate Analytics Web of Science database with an impact factor;
- one article was printed in an international peer-reviewed scientific journal listed in the Clarivate Analytics Web of Science database without an impact factor;
- three articles were printed in other international databases without an impact factor.
- The main results of the thesis are presented at the following three scientific conferences:
- annual national conference "Science – Future of Lithuania;"
- 15th international workshop on "Piezoelectric Materials and Applications in Actuators (IWPMA)," 2018, Kobe, Japan;
- 16th international workshop on "Piezoelectric Materials and Applications in Actuators (IWPMA)," 2019, Lyon, France.

Structure of the Dissertation

The dissertation contains an introduction, analytical literature review, discussion of research methodology, summarized investigation results and conclusions, references, four appended scientific articles, and a summary in Lithuanian.

The dissertation consists of 145 pages, 50 displayed equations, 28 figures, 2 tables, and 36 references cited in the thesis.

1

Review of Optical Linear Encoders, their Performance and Existing Measurement Errors

Chapter 1 provides a general review of the optical linear encoders and their performance and discusses the working principles and main areas of their application. The encoder performance is objectively described by its accuracy, repeatability, and resolution. The meaning of these parameters is described in terms of linear encoders. Also, the chapter discusses the physical nature of the measurement errors and their formation and presents the sub-divisional interpolation error within one signal period and its determination by using the Lissajous pattern.

1.1. Linear Encoders and Their Applications

A linear encoder is a device that transforms linear mechanical motion into electrical signals, which could contain information about the size of displacement, absolute position, and direction of the movement. After further signal processing by the numeric control device, this information could be used to determine the speed and to control moving units of various technological machines or other equipment.

There are various position measurement technologies based on different physical phenomena, such as magnetic, inductive, capacitive, eddy current, or optical.

Magnetic linear encoders usually use a self-adhesive magnetized or a passive variable reluctance scale. The information of the position could be sensed by using reading heads based on the Hall Effect, sense-coils, or magnetoresistance. This type of encoders is designed to perform in harsh environments, where high accuracy is not needed, e.g., packaging, woodworking, sawing, laser, or waterjet cutting, automation, and assembly systems (RLS, 2020). They are capable of operating at high speed with a typical resolution from several millimeters up to 1 μm.

Inductive technology-based linear encoders are robust and tolerant of dust, dirt, mechanical vibrations, shock, and mounting inaccuracies. The big air gaps up to 5 mm between the scale and the reading module could be introduced. The achievable resolution is up to 20 nm. The research presents fully integrated measuring systems with straightforward fabrication and ease of application, requiring no external light or magnetic field source (Podhraski *et al.,* 2016).

Capacitive encoders work by sensing the capacitance between a reading module and scale. Similarly, with inductive technology, this measurement method is usually used in measurement tools like digital calipers, etc. However, there are scientific articles presenting a capacitive type of linear encoder using electrostatic induction (Baniasadi and Modabberifar, 2016).

Optical linear encoders are the dominant type of sensors in the high-resolution market. They are insensitive to a magnetic field compared with magnetic encoders and have high accuracy, resolution, good repeatability, and low price. According to the mechanical construction, linear encoders may be enclosed or open (exposed).

Enclosed type linear encoders have an aluminum extrusion that encloses and protects the measuring scale and the reading head from dust, dirt, chips, or splashing coolant. Such configuration measuring systems, together with a digital readout, are used in various manually controlled machine tools (HEIDENHAIN, 2020), and more accurate versions are used in numerically controlled CNC machines (HEIDENHAIN, 2019). For typical manual control milling machines or lathes, the display steps of 10 μm or 5 μm and accuracy of ±10 μm per meter are sufficient. For more precise measurement and inspection tasks, grinding or jig boring machines, the display steps could reach 1 μm, and the accuracy of ±5 μm or ±3 μm is desirable. In modern CNC machines, those requirements could be even higher. Because of the sealed construction and self-guided scanning carriage along the measuring scale surface, the accuracy of such an encoder is limited by the friction and hysteresis effects.

Open type (exposed) linear encoders consist of a measuring scale attached straight onto the support of the application and a scanning head. The working

principle of such a configuration system is based on noncontact reflective scanning, which operates without any mechanical contact. They are used in machines that require very high accuracy, such as PCB assembly machines, high-accuracy machine tools, coordinate measuring machines (CMM) or other precise measuring devices, positioning stages, etc. [HEIDENHAIN Exposed 2020].

Despite the industrial applicability, more advanced and precise optical linear encoders are used in various scientific, medical, military, and surveillance or aerospace applications.

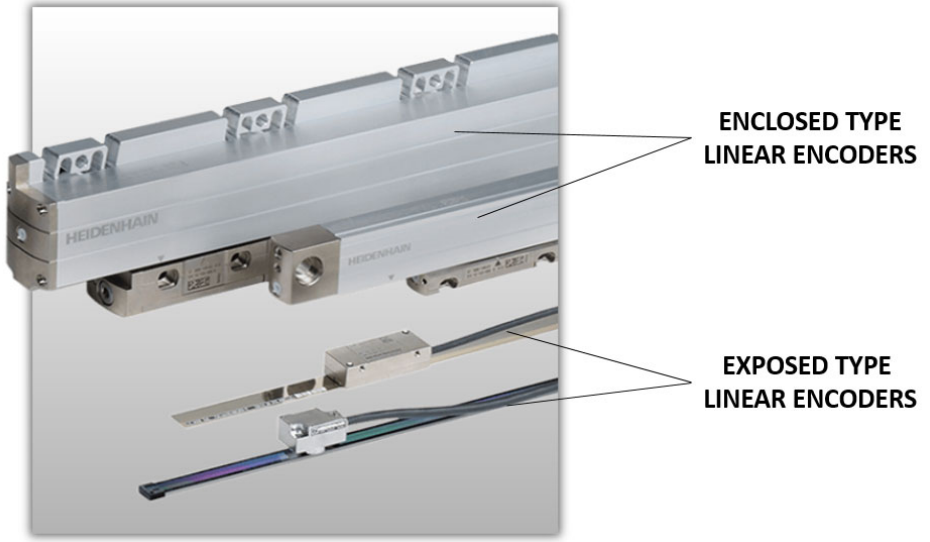

Fig. 1.1. Enclosed and exposed optical linear encoders of the company *"HEIDENHAIN"*

In this dissertation, the main attention is focused on the theoretical and experimental research of an enclosed type of optical linear encoders.

1.2. Working Principles of Optical Linear Encoders

In general, the working principle of an optical linear encoder is based on the light detection that propagates through the interaction of moving (scanning reticle/index grating) and stationary (measuring scale) gratings. A light source, scanning reticle, photodetectors, and all necessary electronics are integrated into the reading head of the encoder. In enclosed linear encoders, the reading head consists of two

parts: a housing and a scanning carriage (cursor). The housing of the reading head is usually attached to a moving unit, while the aluminum encoder's profile, with an integrated glass measuring scale, is usually fixed on the rigid support of the application. The cursor holds the scanning reticle and is preferably guided along the surface of the glass scale. As the housing or the reading head of the encoder are inaccurately mounted, or the motion is not perfectly straight, the flexible spring-based suspension between the housing and the scanning carriage is required. For a proper motion transmission to the cursor, these two parts must have a rigid contact point. Hardened or rigid stainless-steel parts like pins and grinded plates must stay connected while the measurement is processed in both directions. Those parts could be maintained together by using the force of extension springs, a magnetic field of a permanent magnet, etc. A typical structure of an enclosed optical linear encoder is shown in Fig. 1.2.

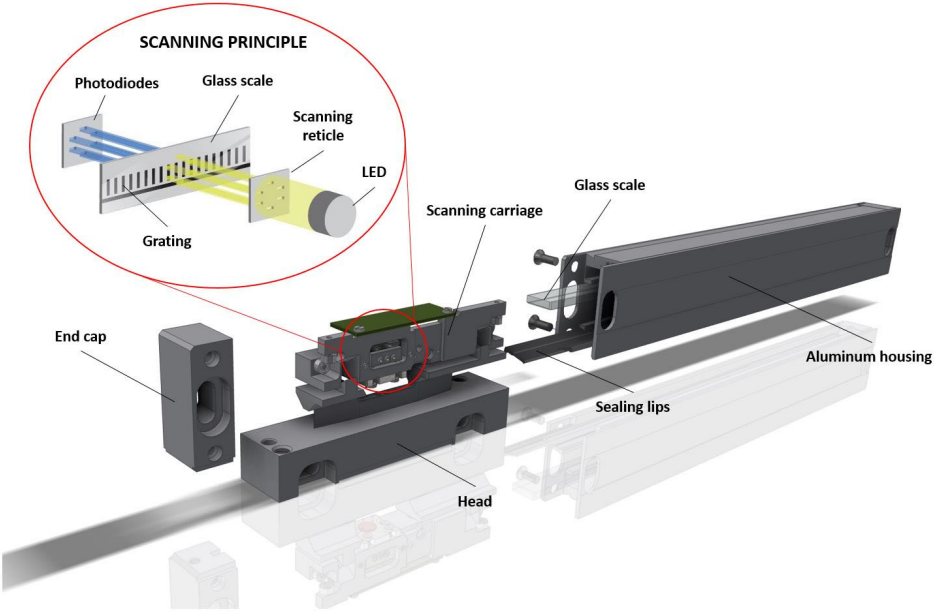

Fig. 1.2. Structure of an enclosed optical linear encoder

There are two most common methods to generate an electrical signal from the relative movement between a measuring scale grating and a reading head: imaging and interferential. Those methods and basic electric signal generation techniques are described in the following subsections.

1.2.1. Imaging Optical Encoder

The optical imaging technology-based encoders consist of an infrared light source with a collimating lens. The light beam propagates through an index grating that transmits 50 % of the light. The transmitted light could be imaged onto a measuring scale via shadow projection of the two mentioned gratings in near contact or by an optical imaging system. When the modulated light passes both gratings, its intensity *I* is sensed by the photodiode, which produces an electrical signal that is proportional to the light intensity. If both encoder gratings have a constant interval, the bar and space pattern (called Ronchi grating) are precisely aligned, and the index grating is sharply imagined on the measuring scale, the detected light intensity will vary triangularly with a reading head displacement, as shown in Fig. 1.3.

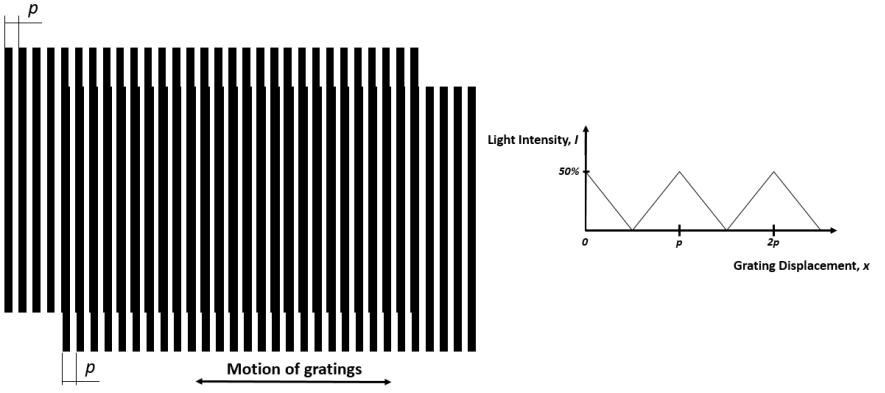

Fig. 1.3. Superposition of two precisely aligned identical Ronchi gratings

The transmitted light intensity is uniform over the grating area. Any displacement *x* between two gratings will generate an intensity signal that contains a fundamental spatial frequency of *1/p* plus successive harmonics of reduced amplitude (Luxmoore and Shepherd, 1983). Such a signal could be expressed as:

$$I_{(x)} = I_0 + I_1 cos\frac{2\pi}{p}(x - x^I) + I_2 cos\frac{4\pi}{p}(x - x^{II}) + I_3 cos\frac{6\pi}{p}(x - x^{III}) + \cdots, \tag{1.1}$$

where x^I, x^{II}, x^{III}, etc., indicate the position of the various maximum light intensities for each harmonic and are equal. Therefore, $(x - x^I)$ corresponds to the displacement between two gratings Δx.

If the superimposed identical grating patterns (with the same period p) are inclined by a small angle θ to one another, the angular fringes (Moiré interference patterns) are formed. The relative movement of one grating to another causes the fringes to move in a manner that magnifies the grating displacement. In this case, the small perpendicular motion of one grating along the other by one pitch (period p) will make the Moiré fringe move vertically by one fringe spacing T (Barakauskas *et al.,* 2017). The superposition of two slightly rotated gratings and the formation of the Moiré fringes are shown in Fig. 1.4.

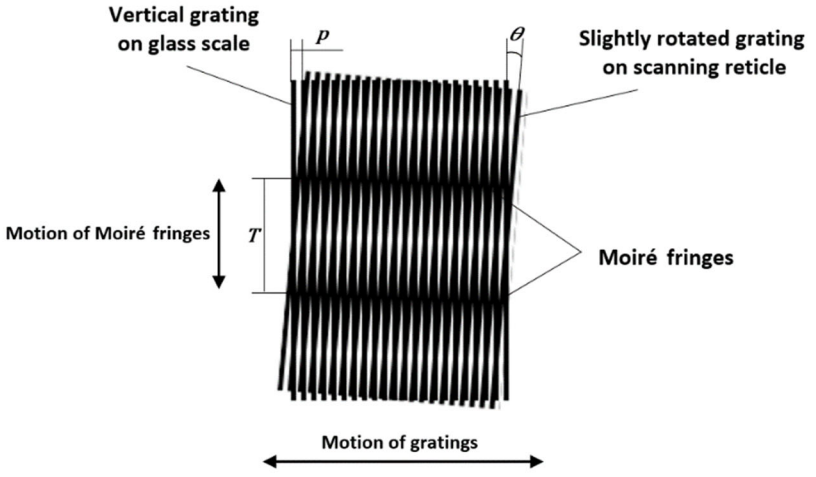

Fig. 1.4. Superposition of two slightly rotated gratings and the formation of the Moiré fringes

When one of the gratings has a slightly different period, Vernier fringes are seen in the superposition of the two gratings. The intensity variation of these fringes is given by:

$$I_{(x)} = I_0 + I_1 cos\frac{2\pi x}{p}\cdot\frac{\delta p}{p} + I_2 cos\frac{6\pi x}{9p}\cdot\frac{\delta p}{p} + I_3 cos\frac{10\pi x}{25p}\cdot\frac{\delta p}{p} + \cdots . \quad (1.2)$$

If the difference in period varies across the area of the grating, this variation can be presented as $\rho(x) = x\delta p/p$ (Luxmoore and Shepherd, 1983). In this case, the relative displacement between gratings perpendicular to the grating lines will generate the motion of Vernier fringes by one fringe spacing but in the same direction as the grating displacement. Such superimposition is shown in Fig. 1.5.

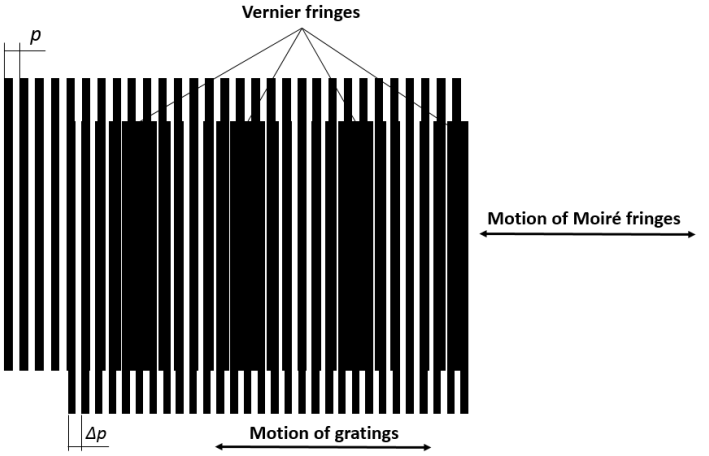

Fig. 1.5. Superposition of two gratings with slightly different periods and formation of the Vernier fringes

For accurate displacement detection by using phase quadrature interpolation and discerning the direction of the measurement, the optical system should be designed to generate two analog sinusoidal signals with a phase shift of 90 electrical degrees. The sharpness of the imaged grating is affected by the captured diffraction orders of the imaging system, the size and shape of the light source, and the distance between the gratings, optical noise fluctuations due to random changes in grating transmission or reflection over its length or by variations in light source intensity and sensitivity of the detectors. With a proper design of the encoder reading head, a sinusoidal modulation of the detector signal could be obtained (Cosijns and Jansen, 2018).

In practice, in optical linear encoders with the same period gratings, the scanning reticle (index grating) is designed with multiple grating areas that have predefined offsets to obtain various phase signals. The properly aligned separate photodetectors are generating sinusoidal electrical signals from four areas displaced by $n + ¼$ of the period. The schematic representation of the electrical signal formation is shown in Fig. 1.6. Nearly sinusoidal signals phase-shifted by 0, 90, 180, and 270 electrical degrees are generated.

$$I_0 = a + b\,cos\left(2\pi\frac{x}{p}\right);$$

$$I_{90} = a + b\,cos\left(2\pi\frac{x}{p} + \frac{\pi}{2}\right) = a - b\,sin\left(2\pi\frac{x}{p}\right);$$

$$I_{180} = a + b\,cos\left(2\pi\frac{x}{p} + \pi\right) = a - b\,cos\left(2\pi\frac{x}{p}\right); \qquad (1.3)$$

$$I_{270} = a + b\,cos\left(2\pi\frac{x}{p} + \frac{3\pi}{2}\right) = a + b\,sin\left(2\pi\frac{x}{p}\right),$$

where a — is the irradiance bias, b — is the modulation depth of the signal, and x indicates the position of the index grating (displacement inside one period). This signal generation method is known as 4-field scanning.

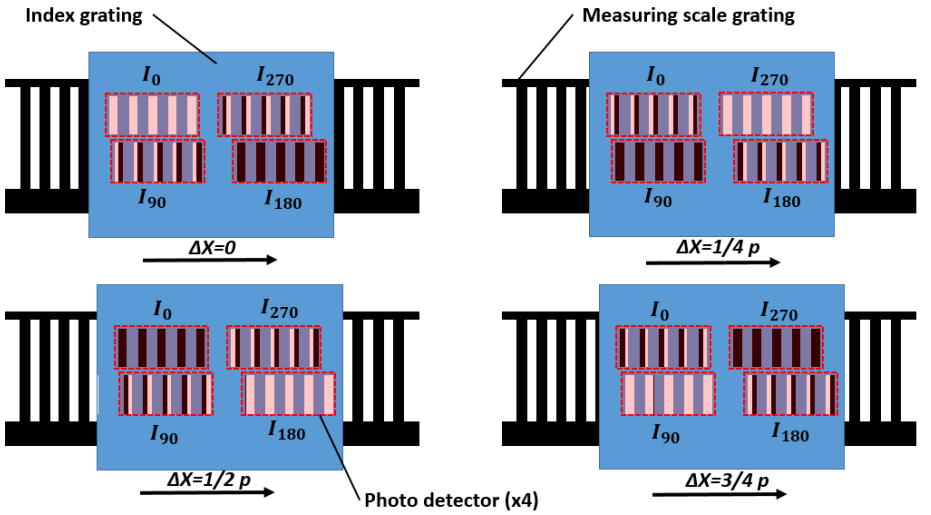

Fig. 1.6. Schematic representation of electrical signal formation in optical linear encoders with the 4-field scanning method

In optical linear encoders with Vernier fringes, the index grating is designed on a single wide-area with a slightly different pitch grating compared to the measuring scale. A segmented photodetector with specialized size pixels or a line camera is used to capture the formed fringes. This scanning method causes a type of optical filtering that allows the generation of homogeneous signals with a shape very close to a sine wave. Compared with the 4-field method, one large scanning area has indisputable benefits. Therefore, it is called a single-field scanning technique that is less sensitive to various contaminations. Better quality of generated electric signals leads to a small position error within one signal period (sub-divisional error), good control quality for direct drives, which means improved and finely tuned velocity control, and high repeatability. It allows for the management of high interpolation and achieves a resolution of 0.1 μm and finer. The signal

amplitudes are only slightly influenced by the scanning velocity, so the electrically permissible traversing speeds are high (HEIDENHAIN Single-field, 2006). The schematic representation of the signal formation from the Vernier fringes is shown in Fig. 1.7.

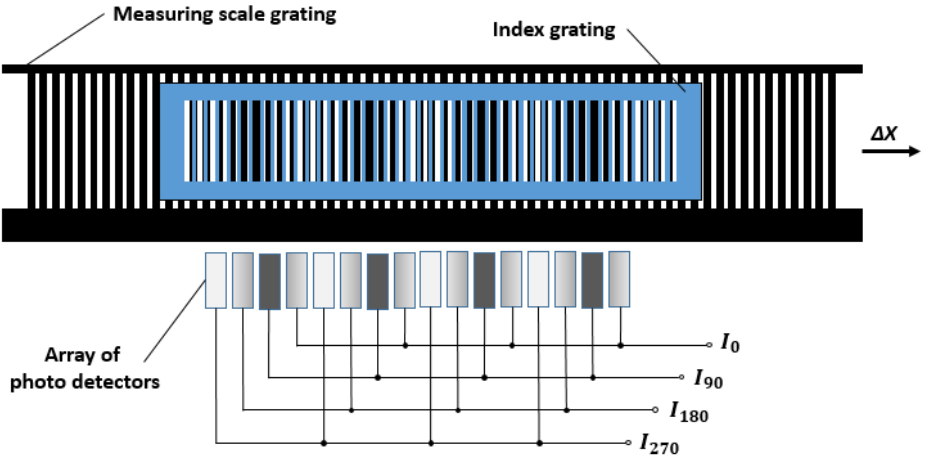

Fig. 1.7. Schematic representation of electrical signal formation in optical linear encoders with the single-field scanning method

Despite all its advantages, the single-field scanning method requires a special structured photosensor. The design and development of such a microtechnological device is a challenging and expensive task.

1.2.2. Interferential Optical Encoder

With a scale period p smaller than 10 μm, the diffraction effects become dominant. Interferential encoders typically function with grating periods of 8 μm, 4 μm, and finer. They use coherent light-emitting diodes or semiconductor lasers to generate a coherent and collimated beam of light. A step grating is used as the measuring scale. On a flat reflective surface, 0.2 μm height reflective lines are applied. The scanning reticle is designed as a transparent phase grating with the same period as the measuring scale. The reflected light beam is split into diffraction order m by the measuring scale. The +1 and -1 diffracted orders are combined to interfere at the photodetectors, where sinusoidal signals with a half period of the gratings are generated (Cosijns and Jansen, 2018).

$$\Delta\varphi(\Delta x) = \Delta\varphi_{m=+1} - \Delta\varphi_{m=-1} = 2\pi(+1)\frac{\Delta x}{p} - 2\pi(-1)\frac{\Delta x}{p} = 4\pi\frac{\Delta x}{p}. \qquad (1.4)$$

The generated signals are free of harmonics and could be highly interpolated by using proper electronics. Practically, the limitation of the interpolation is limited by the noise of the electrical signal. The linear encoders with interferential scanning are especially suited for high resolution and high accuracy applications. Fig. 1.8 schematically represents the working principle of the interferential linear encoder produced by the company "HEIDENHAIN."

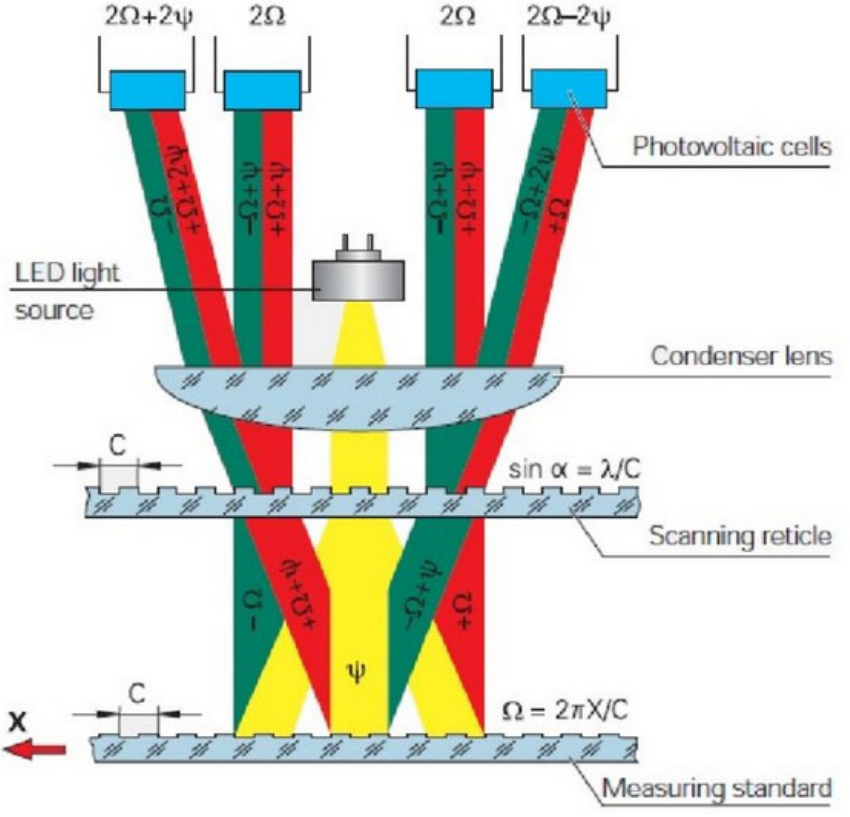

Fig. 1.8. Schematic representation of the interferential scanning principle of a "HEIDENHAIN" linear encoder

The notations in the Fig. 1.8 are: c — grating period, ψ — a phase shift of the light wave when passing through the scanning reticle, Ω — a phase shift of the light wave due to the motion X of the scale.

1.3. Performance of Optical Linear Encoders

An optical linear encoder by itself is only a converter of mechanical displacement into the corresponding electrical signals. For a proper interpretation of an exact position from the encoder reading, it must work together with a subsequent electronic unit. For manually controlled machines, it could be a digital readout (DRO) system, and for numerically controlled machine tools or other technological equipment, specialized controller units are used.

To ensure reliable communication between these devices, the output signal of the encoder reading is transmitted by various analog or digital interfaces (HEIDENHAIN Interfaces, 2019). However, the initial signal of the encoder-measured displacement from the incremental track is always analog. Usually, there are four nearly-sinusoidal signals phase shifted by 0, 90, 180, and 270 electrical degrees. An early industry standard was 11 μA peak-to-peak current signals. Nowadays, the most popular analog standard is 1 V peak-to-peak voltage signals. The biggest advantage of analog signals is their low bandwidth, which helps to minimize electromagnetic compatibility (EMC) emission. These signals are transmitted as differential signals to improve noise immunity. Later, these signals are driven through the differential amplifiers, and two quadrature sine and cosine signals are formed, as shown in Fig. 1.9.

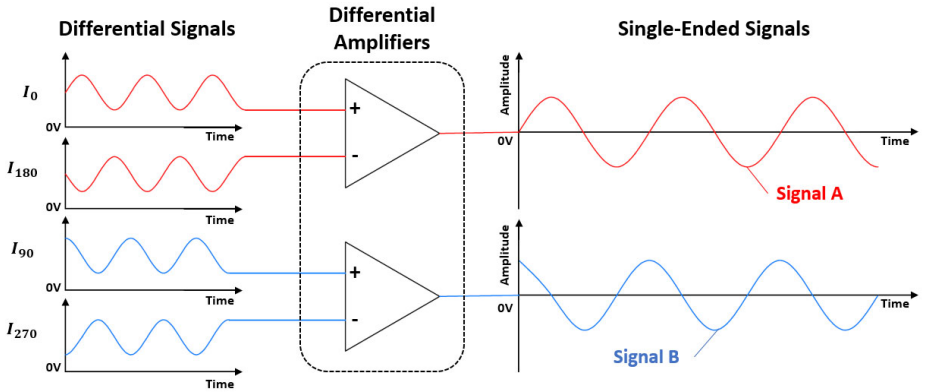

Fig. 1.9. Conversation of differential encoder output signals into single-ended quadrature sine and cosine signals

Later, both signals are interpolated and digitalized to achieve higher measurement resolution. The interpolation process is performed by a subsequent electronic, or it could be done inside the encoder. In this case, the output signals of the device are two digital A and B square-wave signals. The big advantages of the

incremental encoder signals are their high measurement accuracy, low signal latency, and improved noise immunity.

The absolute optical linear encoder, in combination with an incremental track, has another suitably encoded track. The absolute position could be traced by using Vernier, digital code, pseudo-random code, or multiple coded tracks. These encoders can determine an absolute position without movement or needing to find a reference position. The position reading is transmitted by using the serial communication protocol, such as SSI, BiSS, EnDat, DriveCliq, Panasonic, Yaskawa, Fanuc, and others. This type of encoder typically could reach high resolution and high accuracy because the position is determined and transmitted on demand rather than continuously. The performance and quality of absolute encoders mainly depend on the incremental track and initial analog signal formation, the same as in incremental encoders.

The performance of the optical linear encoder could be most appropriately described by its main parameters: resolution, accuracy, and repeatability. The meaning of these parameters in terms of linear encoders is described below.

1.3.1. Resolution

Resolution is the smallest positional increment that can be measured. In other words, it is the smallest distance the encoder can measure. The higher the resolution, the more precise positioning of the moving unit can be reached, and the more fluent motion can be generated by a closed-loop control system.

A resolution of an optical linear encoder is based on the measuring scale grating. The number of transparent and opaque lines defines the smallest measurable distance. The most frequently used grating pitch in Moiré effect-based encoders is 20 μm. Physically it is impossible to increase the resolution of already manufactured encoders, but there are other methods that allow doing that.

Most of the incremental linear encoders generate two quadrature output signals, A and B. Since these signals are phase-shifted by 90 degrees, it also allows sensing the direction of displacement. With such quadrature output, three types of decoding, X1, X2, and X4, could be used to increase resolution. The main idea of the decoding process is to count the different falling and rising edges of the output signals (Decoding Principles, 2015). All three possible types of decoding are shown in Fig. 1.10.

When a quadrature signal decoding X1 is used, the falling or rising edges of signal A are counted. The value of one count is equal to one full period of the measuring scale grating, and in the case of decoding X2, both the falling and rising edges of signal A are counted. The resolution is doubled up and reaches a half value of the measuring scale pitch. With X4 encoding, the rising and falling edges of both signals A and B are counted, and the resolution is increased by four times.

Thus, the optical linear encoder with a 20 μm grating pitch could reach the resolution of 5 μm after its electrical signals are decoded by an external microcontroller and integrated into the control unit of the machine tool or digital readout device.

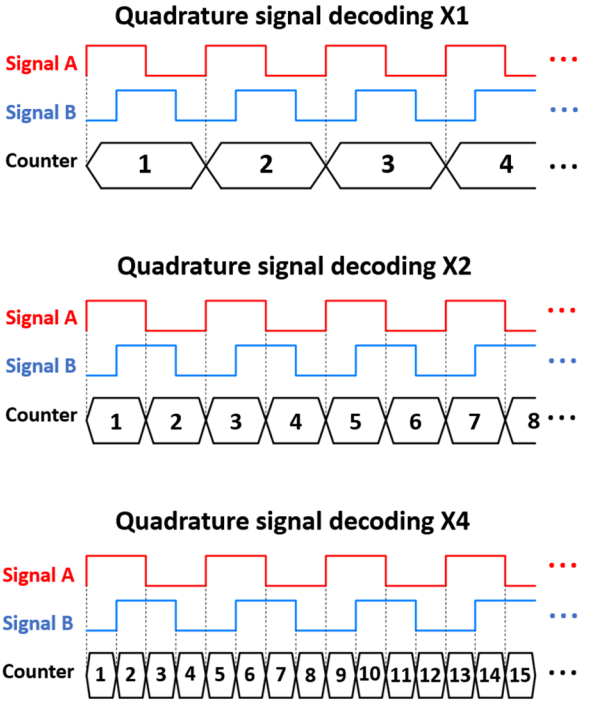

Fig. 1.10. Quadrature digital encoder output decoding X1, X2, and X4

To reach a higher resolution, the encoder's output signal processing called interpolation is used. However, the electrical signals from the encoder must have a sinusoidal shape. Each period of the sinusoidal signal could be represented in many finer possible positions. There are a lot of different methods for sinusoidal signal interpolation, like tracking loop, direct dual-sample-rate, direct high-sample-rate interpolators, etc. (Interpolators, 2018). Modern technologies allow sampling of sinusoidal signals at a higher than Nyquist rate with a great resolution even when the frequency of the encoder output signals is very high. Field-programmable arrays (FPGAs), together with analog electronics and noise filtering systems, are used for practical solutions (Jenkins and Hilkerk, 2008). The resolution of up to several nanometers is available. Interpolation electronics integration into the encoder becomes ordinary. It allows to minimize transmission path errors

and reject noise, which is the source of interpolation error in systems where the interpolation unit is external.

Aiming to reach the appropriate interpolation process, the quality of the encoder signals is essential. Sinusoidal signals gain versus speed, offset and phase errors between sin and cosine signals, and sampling errors are limiting factors of the accurate encoder data interpolation (Lepple, 2004). Therefore, the encoder's ability to generate good, undistorted signals is decisive in reaching a high resolution.

1.3.2. Accuracy

The accuracy of the encoder is the term that describes the difference between the target position (real position value) and the position determined by the encoder. According to ISO 5725-1 standard (accuracy of measurement methods and results), when the accuracy term is applied to sets of measurements of the same measurand, it involves a component of systematic error and a component of random error (ISO 5725-1 1994). In this case, the term "trueness" is used to describe the closeness of the mean of a set of measurement results to the real value, and the term "precision" is used to describe the closeness of agreement within a set of results. The graphical representation of the measurement accuracy is shown in Fig. 1.11.

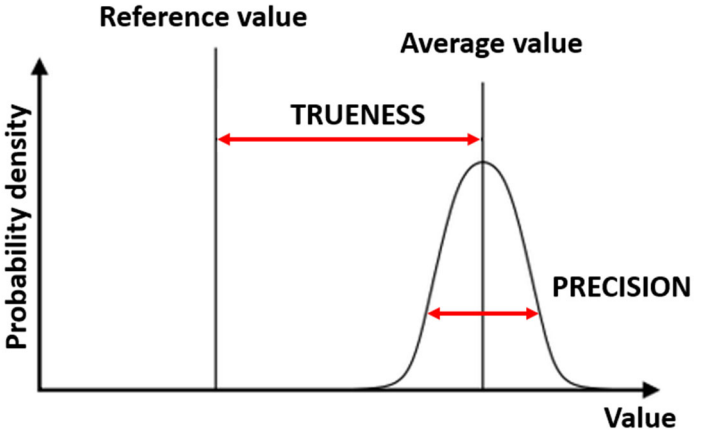

Fig. 1.11. Graphical representation of measurement accuracy according to the ISO 5725 standard

In the case of optical linear encoders, the trueness is accepted as the accuracy of the encoder, and the precision is used to describe the repeatability or reproducibility of the device. In practice, the encoder accuracy measurement is a specific procedure that requires well-calibrated equipment and a certain environmental condition. The calibrating encoder readings are compared with a reference device position indication, which is accepted as a real position value. Usually, a highly accurate encoder or a laser interferometer is used as a reference.

The calibration process is usually based on the international standard ISO 230-2. Several measurements (usually five) at relatively equally spaced positions are taken. Collected data are analyzed statistically, and the main parameters, like accuracy and repeatability, are estimated. The graphical representation of the unidirectional linear encoder measurement is presented in Fig. 1.12.

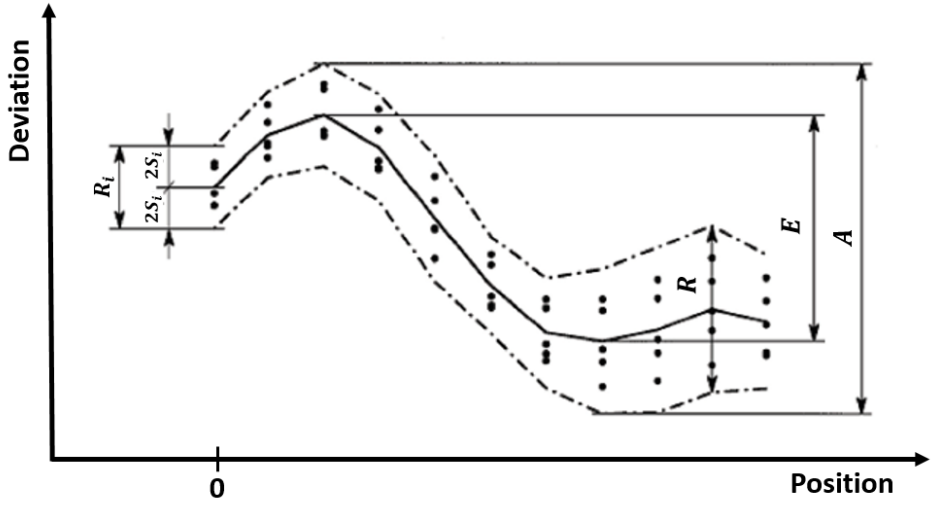

Fig. 1.12. Unidirectional accuracy and positioning repeatability according to ISO 230-2 international standard

The symbol *Si* denotes the estimator for the unidirectional axis positioning repeatability at a certain position. It is a standard uncertainty of the positioning deviations obtained by a series of *n* unidirectional approaches at a certain position:

$$S_i = \sqrt{\frac{1}{n-1}\sum_{j=1}^{n}\left(x_{ij} - \bar{x}_i\right)^2}, \tag{1.5}$$

where x_{ij} is the actual position reached by the functional point minus the target position and $\bar{x}_i$ — is the arithmetic mean of the positioning deviations obtained by a series of n unidirectional approaches to a certain position.

The unidirectional positioning repeatability at a certain position is noted as R_i and is calculated according to the following equation:

$$R_i = 4S_i. \tag{1.6}$$

The unidirectional positioning repeatability of a linear encoder is established as the maximum value of the positioning repeatability at any certain position along the encoder measuring scale:

$$R = max[R_i]. \tag{1.7}$$

The difference between the algebraic maximum and minimum of the mean unidirectional positioning deviations at any certain position along the encoder is accepted as the systematic positioning error:

$$E = max[\bar{x}_i] - min[\bar{x}_i]. \tag{1.8}$$

The range derived from the combination of the mean unidirectional systematic positioning errors and the estimator for the unidirectional positioning repeatability of a linear encoder using a coverage factor $k=2$ is accepted as the positioning error or accuracy:

$$A = max[\bar{x}_i + 2S_i] - min[\bar{x}_i - 2S_i]. \tag{1.9}$$

Such a calibration process is performed in a laboratory room with a stable nominal ambient temperature 20 ± 0.2 °C and minimized dynamic effects of the surroundings.

1.3.3. Repeatability

Encoder's ability to give the same value whenever a reading head reaches the same position is called repeatability. It is often referred to as precision. Usually, it is a small number specified as ± resolution and is several times better than the encoder's accuracy. In technological machines, like in pick-and-place applications, repeatability is even more important than accuracy.

However, such a parameter as repeatability must be summed up correctly and be considered regarding the equipment in which the linear encoder is installed. If the machine demonstrates high repeatability, the mismatch between the measured

value and the reference could be compensated, so the high repeatability of the encoder is required. On the other hand, the application with poor repeatability due to backlash in mechanical gears, friction effects, or hysteresis could not be upgraded even by the absolutely perfect repeatability encoder.

1.4. Nature of Measurement Errors

When speaking about the measurement error, the accuracy of the linear encoder is usually meant. This parameter is determined by (HEIDENHAIN, 2019):

- the quality of the measuring scale grating;
- the quality of the scanning process;
- the quality of the signal processing electronics;
- the error of the scanning unit guideway to the scale.

The biggest impact on the encoder's accuracy clearly has the quality of the measuring scale. The grating formed from transparent and opaque bars is usually produced by photolithography. For reflective type encoders, gratings are formed on a stainless-steel tape by using such technologies as electron beam writing (Kishimoto *et al.,* 1993; Yan *et al.,* 2004), nanoimprint lithography (Tang *et al.,* 2012), etc. The quality of the scale grating and various imperfections over its length are related to the optical noise fluctuations and electrical signal formation. The sensitivity of displacement measurement increases with the grating frequency. However, the fabrication of high-resolution gratings is a challenging task because of the technological process and material problems. Even a small deviation of the grating period affects the quality of the measurement.

The opening ratio and the form of the grating are also particularly important and have a strong effect on electrical signals. The intensity difference between the minimum and maximum values of the Moiré fringe pattern is the highest when the opening ratio of the measuring scale and the scanning reticle gratings are equal to 0.5.

The unwanted optical fluctuations could also be generated by the variation in light source intensity and sensitivity of the photodiodes. Non-perfectly collimated light also distorts the Moiré pattern and leads to poor contrast. The quality of the used components and precise alignment could help to avoid these harmful side effects.

The quality of the optical scanning process is essential to the formation of sinusoidal shape electrical signals. The presence of unwanted higher signal harmonics, immunity to a changing scanning speed, and various contaminants on the scale surface highly depend on the used optical scanning technique.

The scanning unit guideway along the measurement scale should ensure an appropriate position between the measuring scale and the scanning reticle. Any

relative motion like changing the distance between the gratings (air gap) or a tilt will lead to a formation of error.

One of the most important things is to ensure the high contrast of the Moiré fringes to get the high accuracy of the measurement. In the real mechanical construction of an encoder, the finite size gap between the gratings is introduced. Because of the nonperfect collimated light and diffraction effect, which becomes more significant in gratings with a period of 100–20 μm, the variation of the gap has a major influence on the fringe contrast (Sciammarella and Davis, 1968).

Kazuhiro Hane et al. (Hane *et al.,* 1985) suggested using an optical configuration in which the second grating is mounted with an adjusted tilt. A. Ieki *et al*. (Ieki *et al.,* 1999; Ieki *et al.,* 2000) introduced pitch-modulated phase grating. All these works are related to a reduction of the sensitivity to the air gap. Although sometimes, in real applications, it is hard to realize these improvements because they require more space and special technological solutions. Commonly, to not lose the contrast of the Moiré fringes and get good quality signals, the air gap between the glass scale and the scanning reticle should be around 50 μm (Ye *et al.,* 2015).

The formation and parameters of the Moiré fringes depend on the superposition of the two gratings. As it is shown in Fig. 1.4, the scanning reticle is slightly rotated to form a certain angle θ between the gratings. Spacing T of the formed fringes could be expressed as:

$$T = \frac{p}{2\,sin\left(\theta/_2\right)}. \tag{1.10}$$

Any changes in fringe spacing lead to an inappropriate formation of electrical signals because the photodetectors are aligned according to the location of the fringes. Even a small angle tilt between the gratings results in large displacement measurement errors of the encoder.

Ju-Ho Song et al. (Song *et al.,* 1999; Song *et al.,* 2000) represented the phase-shifted grating to reduce tilt errors. A scanning reticle with a specially formed grating could be used to compensate for the nonorthogonal error caused by the tilt of the index scale.

The measuring errors of the linear encoder are usually distinct in two main parts: the position errors over the entire measuring length and the sub-divisional (interpolation) errors within one signal period. The first type of error refers to the measuring scale, including the scanning unit, and is accepted as ± system accuracy. The measurement of this error is already described in Section 1.3.2., and the accuracy graph is shown in Fig. 1.12. The second type of error is described in the following section.

1.5. Sub-divisional Errors in Optical Encoders

Sub-Divisional Error (SDE) is a cyclic high-frequency error created by imperfections of the sine/cosine quadrature encoder output signals. This error appears in the interpolated counts and does not accumulate. Also, it can be referred to as an interpolation error. It is determined by the signal period of the encoder, the quality of the graduation, and the optical scanning. The size of SDE typically lies at ±2 % to ±0.5 % of the signal period (HEIDENHAIN, 2019). It is measured in the nm range, RMS. The graphical presentation of the interpolation error is shown in Fig. 1.13.

The mechanical inaccuracies and misalignment between the measuring scale and the scanning reticle are the main causes of SDE. Although, the harmonic disturbances can also cause distortions in the encoder signals. This type of error is especially important for the accuracy of positioning as well as for velocity control. The error leads to speed ripple, loud noise, and additional heat generation, particularly in direct drives. In applications such as machine tools, the SDE may result in the poor surface quality of the machined part (SDE, 2018).

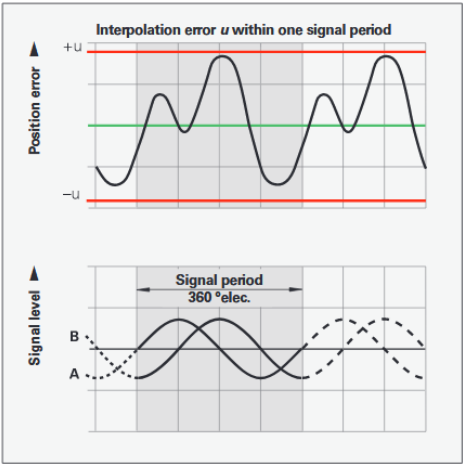

Fig. 1.13. Graphical representation of sub-divisional (interpolation) linear encoder error (HEIDENHAIN, 2019)

The quality of the analog sine/cosine signals of the encoder and SDE could be monitored by using an oscilloscope. Displayed signals in XY mode form a circular Lissajous figure. The high accuracy linear encoder with theoretically ideal signals will form a perfect circle. The formation of the Lissajous curve is shown in Fig. 1.14.

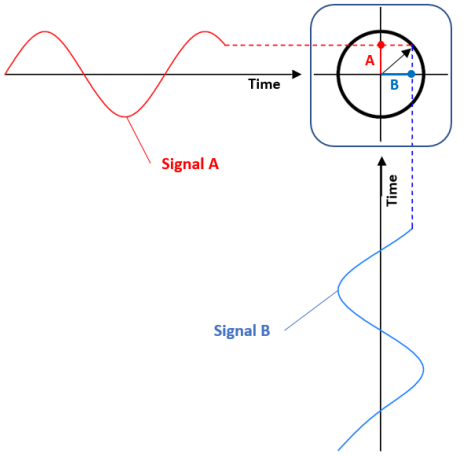

Fig. 1.14. Formation of the Lissajous figure from the linear encoder signals: Sine (Signal A) and Cosine (Signal B)

The signal inaccuracies will distort this figure and introduce the sub-divisional error. The offset of the signals from the mean 0 *V* level will offset the Lissajous curve from the center point (0, 0) coordinate. The difference between the amplitude values will produce the elliptical shape curve. If the signals are not phase-shifted by exactly 90 degrees, the Lissajous plot will be oval. Higher signal harmonics will shape the non-circular form curve. A more detailed explanation is provided in the introduction part of the appended Article 3.

1.6. Conclusions of Chapter 1

The general review of linear encoders and their performance showed that the optical encoders are the most widely used displacement measurement systems in precision applications, featuring high accuracy, good repeatability, and fine resolution. The optical imaging principle-based encoders are the most popular and cover most of the industrial and scientific applications. The mechanical design of the enclosed type of linear encoder allows it to work under harsher operating conditions compared to exposed encoders. For this reason, an enclosed type of optical linear encoder is chosen as the object of the complex investigation in this dissertation.

The distinguished important aspects of the research:

1. Optical imaging encoders could be realized by using different transmitted light imaging and electrical signal formation techniques. Each of these techniques

has its advantages and disadvantages. Encoders operating on the principle of the 4-field scanning were chosen for the research.

2. The formation of superior quality analog electrical signals is the most important process for an appropriate encoder performance. It is relevant to ensure the smooth running of this process during the operation of the encoder.

3. The quality of the sinusoidal shape quadrature signals is especially important for the interpolation process. Otherwise, the sub-divisional encoder error appears, and the fine resolution (high interpolation rate) of the device cannot be reached.

4. Calibration process of the linear encoder is performed under well-defined ambient conditions. Estimated accuracy, repeatability, and other parameters are accepted and declared. However, the meaning of these values may drastically vary when the encoder is operating under different conditions.

2

Assessing Methods of Measurement Errors Caused by Environmental Effects

Chapter 1 provided a general review of the scientific and technical literature about optical linear encoders. This chapter presents the theoretical and experimental research methodology used to investigate the impact of the specific external factors that cause measurement errors. In a real operating environment, linear encoders face a variety of effects that influence their performance. This thesis investigates thermal processes, different displacement scanning speeds, and mechanical vibrations and briefly discusses the procedures used for their studies in the following subsections.

2.1. Thermal Effects

When a linear encoder operates under the influence of internal and external heat sources, various thermal processes inevitably affect the measurement quality. The changing temperature has the greatest influence on the measuring scale. If the temperature increases, the parts of the encoder expand. The initial length of the scale becomes larger, as well as the period of the grating pattern. The moving

reading head counts less displacement. The difference between the real and measured lengths is positive. In the case when the temperature decreases, the measuring scale becomes shorter, and the moving reading head counts more displacement. The difference between real and measured lengths is negative (Alejandre and Artes, 2004). Theoretically, this expansion and contraction process occurs in the scale according to the coefficient of thermal expansion (CTE).

In practice, the thermal problem is somewhat complex. In enclosed optical linear encoders, the measuring scale is attached to an aluminum profile by a double-sided adhesive tape or by adhesive. The joint between these two encoder components must be flexible because of the different CTE values of the aluminum and the measuring scale material, which usually is glass or glass-ceramic. In differently designed linear encoders, long stainless-steel measuring scales are used to reach measuring lengths up to 30 meters or even longer. In such an assembly of the encoder, the actual CTE value acquires other meanings (Alejandre and Artes. Real CTE, 2004). The measuring scale expands more because, despite the initial CTE value, it is also stretched by an aluminum extrusion with a bigger thermal coefficient value. Meanwhile, the extrusion by itself expands less. Moreover, the nonlinear behavior of the CTE is noticed during the experimental research (Alejandre and Artes, 2006). To reach and maintain a wanted CTE value and a stable performance in a wide temperature range, the correct design of the encoder is essential.

Despite the thermal behavior of the encoder, the mounting type and thermal parameters of the machine support to which the encoder is attached have a great impact too. If the aluminum profile is tightly attached to the machine surface with a different CTE, the internal stress could be generated between the fixing bolts, as well as torsion, bending, unbalanced loads, etc. In practice, the linear encoder is usually fixed with only one permanent fixing point in the middle of the measuring length. In this case, the ends of the encoder could freely expand and contract independently to the mounting surface. Other fixing bolts are tightened through flexible parts.

2.1.1. Research Task of the Thermoelastic Deformation in a Linear Encoder

The selected optical linear encoder under investigation consists of:

- *Stainless-steel tape* with a laser engraved measuring scale on it;
- *Encoder housing.* An aluminum extrusion profile is used as a base for fastening the measuring scale and its tensioning mechanism. Such a housing protects the scale and the reading head from environmental pollution: dust, chips, an emulsion used in the operation of machine tools, etc.

- *Tensioning mechanism*. Used for proper stainless-steel tape pretension.
- *Reading head*. It carries all the optical and electronic components and ensures the operation of the encoder.

As the temperature of the steel tape changes, it lengthens or contracts. Such temperature deformations along the scale have a direct effect on the formation of measuring errors. The main object of the study is a simplified unit consisting of an aluminum housing and steel tape embedded in it, as shown in Fig.2.1.

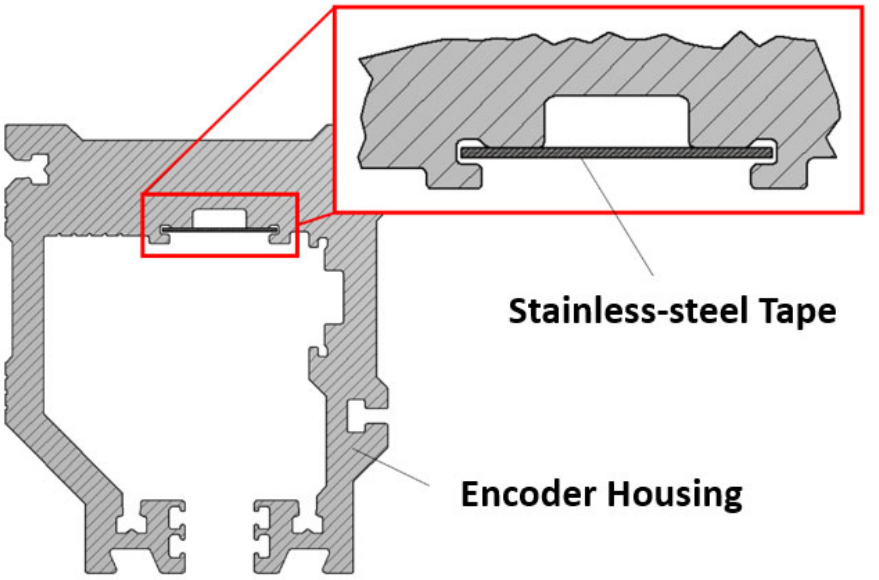

Fig. 2.1. Cross-section of the simplified encoder housing model under investigation

The steel measuring tape must be inserted into the cavity provided in the housing without restriction so that it is only held in its entire length and the surface with the raster track open and easily accessible to the scanning head. When the steel tape is inserted into the housing, one end is rigidly attached to the housing. For the measuring scale on it to function properly, the measuring tape must be tensioned with a certain force. This requires a special tensioning mechanism. It is based on a spring of appropriate stiffness, which causes tension. Such a mechanism must also prevent the tape from being overstretched. As the longitudinal dimensions of the tape change during this process, the scale formed by a laser during its manufacture has a smaller step. The measuring scale for one meter must be stretched by 10 μm. After a proper tensioning procedure, the stretched (elongated) tape is rigidly attached to the aluminum housing. Since the aluminum housing has

a higher coefficient of expansion (~ 23 μm/μmK) than the stainless-steel measuring tape (~ 10 μm/μmK), it is necessary to evaluate the temperature deformations of such an assembled unit and their influence on the measurement accuracy.

2.1.2. Calculation of the Tension Force on the Measuring scale

The one-meter-long tape is designed to be tensioned to 10 μm. To do this, the free end of the tape is pulled by a force F of a certain size.

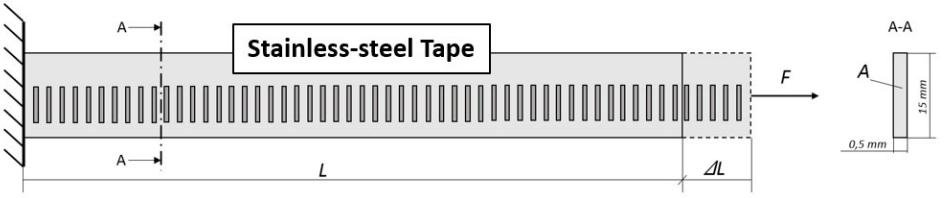

Fig. 2.2. Tensioning scheme of the stainless-steel measuring scale

Because the geometry of a steel tape is simple and its cross-sectional area does not change along the scale, the required tensile force can be determined using simple mechanical equations for the materials. The scale is made of steel AISI 420.

$$\Delta L = \frac{FL}{EA}. \tag{2.1}$$

Where: ΔL — absolute tape elongation (10 μm); E — Young's modulus (190 GPa); A — cross-sectional area of tape (7.5 mm2); L — initial tape length (1 m).

The required tensile force is given by the formula:

$$F = \frac{\Delta LEA}{L} = \frac{(1 \cdot 10^{-5}) \cdot (190 \cdot 10^{9}) \cdot (7.5 \cdot 10^{-6})}{1} = 14.25\ N. \tag{2.2}$$

The tension strength condition is described by:

$$\sigma = \frac{|F|}{A} \leq \sigma_{max}, \tag{2.3}$$

where: σ — stress in the cross-section of the tape; σ_{max} — normal allowable stress (1700–1900 MPa);

$$\sigma = \frac{|14{,}25\,|}{7{,}5 \cdot 10^{-6}} = 1.9\ MPa \leq \sigma_{max}. \tag{2.4}$$

The strength condition is met. The tensile force F determined in the following calculations can be used as a boundary condition for estimating stresses and temperature deformations.

2.1.3. Simplified Mathematical Model of Temperature Deformations

As the measurement accuracy of the linear encoder is mainly influenced by the temperature deformations in the longitudinal direction of the measuring scale, in the simplest case, the system of aluminum housing and steel tape can be considered as a system consisting of two beams.

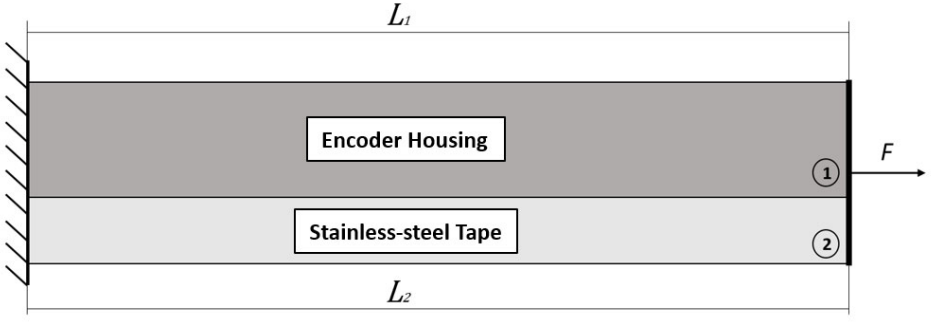

Fig. 2.3. Simplified representation of the aluminum housing and measuring scale as a system consisting of two beams

Since neither the cross-sectional area of the aluminum housing nor the cross-sectional area of the steel tape or the material properties (Young's modulus) changes along the system, the longitudinal deformations of these individual components at ambient temperature are calculated according to the following formulas:

Longitudinal deformations of the aluminum housing:

$$\Delta L_1 = \frac{\sigma_1 L_1}{E_1} + \alpha_1 L_1 \Delta T_1. \tag{2.5}$$

Longitudinal deformations of the stainless-steel tape:

$$\Delta L_2 = \frac{\sigma_2 L_2}{E_2} + \alpha_2 L_2 \Delta T_2. \tag{2.6}$$

Where: $\sigma 1$; $\sigma 2$ — stresses in the cross-sections of the aluminum housing and the stainless-steel tape; $\alpha 1$; $\alpha 2$ — coefficients of linear thermal expansion; ΔT1; ΔT2 — temperature difference.

The elongation/contraction of a common system is a combination of the thermal expansion of the individual comprising components. Considering the different cross-sectional areas, material properties (Young's modulus and coefficient of thermal expansion), acting temperatures and possible additional external forces, the elongation ΔL in the longitudinal direction of the total assembled stainless-steel measuring scale, and the aluminum housing assembly is defined as:

$$\Delta L = \frac{(A_1 E_1 \alpha_1 \Delta T_1 + A_2 E_2 \alpha_2 \Delta T_2) + F}{(A_1 E_1 / L_1) + (A_2 E_2 / L_2)}. \tag{2.7}$$

The force F in Equation (2.2) can be treated as a boundary condition if the assembled system is subjected to external forces. In the case of a linear displacement measuring system, this force can be understood as the temperature expansion of the object's surface on which the encoder is mounted. For example, a machine tool frame made of cast iron with a thermal coefficient of linear expansion of 10.4 μm/μmK will expand or contract less than the aluminum housing, which will cause additional external forces to affect the condition of the encoder itself.

In the elements of the general system, internal forces are created by the action of external forces. The measure of the intensity of such forces is stress. The stresses in the individual elements are defined by the following formulas:

Stress acting on the aluminum housing:

$$\sigma_1 = -E_1 \left[\frac{\alpha_1 \Delta T_1 - \alpha_2 \Delta T_2 \left(\frac{L_2}{L_1}\right) - (F L_2 / L_1 A_2 E_2)}{1 + (A_1 E_1 L_2 / A_2 E_2 L_1)} \right]. \tag{2.8}$$

Stress acting on the stainless-steel tape:

$$\sigma_2 = -E_2 \left[\frac{\alpha_2 \Delta T_2 - \alpha_1 \Delta T_1 \left(\frac{L_1}{L_2}\right) - (F L_1 / L_2 A_1 E_1)}{1 + (A_2 E_2 L_1 / A_1 E_1 L_2)} \right]. \quad (2.9)$$

Such a simplified mathematical model for the calculation of temperature deformations can estimate the total thermal elongation or contraction of a system at a constant temperature operating uniformly over the entire length of the system.

2.1.4. Influence of Measuring Scale Prestressing

The primary tensioning of the stainless-steel measuring scale F2 and the attachment of the pretensioned scale to the aluminum housing create a force F1 in the opposite direction, which compresses the aluminum housing. The force calculated by Equation (2.2) to tension a steel tape of one-meter length by the required 10 μm is equal to 14.25 N. A force of the same magnitude (only in the opposite direction) acts on the aluminum housing. Visually, this is illustrated in Figure 2.4.

$$|F_1| = |F_2|. \quad (2.10)$$

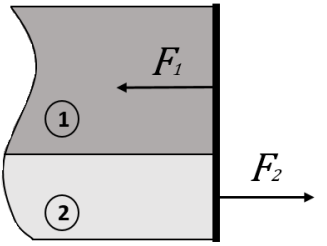

Fig. 2.4. Forces acting on the aluminum housing and the stainless-steel tape system result from the initial tension of the measuring scale

The shortening of the one-meter-long housing under the action of this force is calculated to evaluate such a force acting on the aluminum profile. Equation (2.1) is used. Housing is made of aluminum (Al Mg Si 0.5 (6060)):

$$\Delta L = \frac{FL}{EA} = \frac{-14{,}25 \cdot 1}{(70 \cdot 10^9)(0{,}113362)} = 1{,}796 \cdot 10^{-9}\, m = -0{,}0018\, \mu m. \quad (2.11)$$

Where: E — Young's modulus (70 GPa); A — cross-sectional area of tape (113362 mm^2); L — initial aluminum housing length (1 m).

The stress σ occurring in the cross-section of the aluminum housing under the action of the initial force F1 of the prestressed stainless-steel measuring tape:

$$\sigma = \frac{|F|}{A} = \frac{14{,}25}{0{,}113362} = 125{,}7\ Pa. \tag{2.12}$$

Since the shortening of the aluminum profile is an inadvertently small value (0.0018 μm) and the resulting stress is small in order and does not have a significant effect, the initial prestress of the stainless-steel tape effect on the aluminum profile can be eliminated by simplifying the calculations.

Temperatures below 20 ºC have a greater influence on the calculations. At these temperatures, and as the aluminum housing shortens, the steel measuring tape will not only shrink to its magnitude of linear thermal expansion but will also relax to its initial magnitude of 10 μm.

2.1.5. Spatial Thermoelastic Task

Because the thermal and elastic processes occurring in real conditions are complex, the simplified mathematical model discussed earlier is not accurate in precisely determining the behavior of the system. A spatial model of elasticity theory is used to obtain a higher precision answer. It requires a system of 15 equations to obtain the values needed to study the system.

Equilibrium equations (Navier's equations):

Stress is a measure of the intensity of the internal forces acting on the body. Differential equilibrium equations are found to describe their state, which is found using Newton's second law. To solve static problems, there are no material properties and displacements of the object under study in the equilibrium equations, except when extreme conditions (internal forces X, Y, Z) are included in the equations.

$$\frac{\partial \sigma_x}{\partial x} + \frac{\partial \tau_{xy}}{\partial y} + \frac{\partial \tau_{xz}}{\partial z} + X = \rho \frac{\partial^2 u}{\partial t^2}; \tag{2.13}$$

$$\frac{\partial \tau_{yx}}{\partial x} + \frac{\partial \sigma_y}{\partial y} + \frac{\partial \tau_{yz}}{\partial z} + Y = \rho \frac{\partial^2 v}{\partial t^2}; \tag{2.14}$$

$$\frac{\partial \tau_{zx}}{\partial x} + \frac{\partial \tau_{zy}}{\partial y} + \frac{\partial \sigma_z}{\partial z} + Z = \rho \frac{\partial^2 w}{\partial t^2}. \quad (2.15)$$

These differential equilibrium equations make it possible to determine with simple operations exactly which external surface forces *{p}* and external volumetric forces *{X, Y, Z}* cause a stress state characterized by stresses *{σ}*.

Geometrical equations (Cauchy`s equations):

The relationship between the displacements of a deformed test object and the resulting deformations depends on the geometry of the body and the chosen coordinate system. Force-causing deformations and material properties are not included in the geometric equations. Six equations for geometric deformation and displacement coherence:

Linear strain equations:

$$\varepsilon_x = \frac{\left(u + \frac{\partial u}{\partial x} dx\right) - u}{dx} = \frac{\partial u}{\partial x}; \quad (2.16)$$

$$\varepsilon_y = \frac{\left(v + \frac{\partial v}{\partial y} dy\right) - v}{dy} = \frac{\partial v}{\partial y}; \quad (2.17)$$

$$\varepsilon_z = \frac{\left(w + \frac{\partial w}{\partial z} dz\right) - w}{dz} = \frac{\partial w}{\partial z}. \quad (2.18)$$

Angular strain (shear) equations:

$$\gamma_{xy} = \frac{\left(u + \frac{\partial u}{\partial y} dy\right) - u}{dy} + \frac{\left(v + \frac{\partial v}{\partial x} dx\right) - v}{dx} = \frac{\partial u}{\partial y} + \frac{\partial v}{\partial x}; \quad (2.19)$$

$$\gamma_{xz} = \frac{\left(u + \frac{\partial u}{\partial z} dz\right) - u}{dz} + \frac{\left(w + \frac{\partial w}{\partial x} dx\right) - w}{dx} = \frac{\partial u}{\partial z} + \frac{\partial w}{\partial x}; \quad (2.20)$$

$$\gamma_{yz} = \frac{\left(v + \frac{\partial v}{\partial z} dz\right) - v}{dz} + \frac{\left(w + \frac{\partial w}{\partial y} dy\right) - w}{dy} = \frac{\partial v}{\partial z} + \frac{\partial w}{\partial y}; \quad (2.21)$$

$$\gamma_{xy} = \gamma_{yx}; \quad \gamma_{xz} = \gamma_{zx}; \quad \gamma_{yz} = \gamma_{zy} \tag{2.22}$$

Physical equations (Hooke`s equations):

Since the components of the system in question are homogeneous and isotropic, the relationships between stresses and strains can be expressed. The physical equations derived from Hooke's law express the dependence of stresses and strains on the properties of the material.

Linear strain equations:

$$\varepsilon_x = \frac{1}{E}\left[\sigma_x - \mu\left(\sigma_y + \sigma_z\right)\right] + \alpha\Delta T; \tag{2.23}$$

$$\varepsilon_y = \frac{1}{E}\left[\sigma_y - \mu(\sigma_x + \sigma_z)\right] + \alpha\Delta T; \tag{2.24}$$

$$\varepsilon_z = \frac{1}{E}\left[\sigma_z - \mu\left(\sigma_x + \sigma_y\right)\right] + \alpha\Delta T. \tag{2.25}$$

Angular strain (shear) equations:

$$\gamma_{xy} = \frac{\tau_{xy}}{G} = \frac{2(1+\mu)\tau_{xy}}{E}; \tag{2.26}$$

$$\gamma_{xz} = \frac{\tau_{xz}}{G} = \frac{2(1+\mu)\tau_{xz}}{E}; \tag{2.27}$$

$$\gamma_{yz} = \frac{\tau_{yz}}{G} = \frac{2(1+\mu)\tau_{yz}}{E}; \tag{2.28}$$

Temperature field equation:

To calculate the temperature stresses in the object under consideration, the distribution of temperature fields in the material must be determined first. In stationary systems, if the temperature and deformation do not change over time, the temperature distribution in an object can be determined independently of the deformation distribution in that object. In this way, the temperature distribution becomes a known quantity in solving the physical deformation equations.

Temperature transfer in solids is defined by the formula:

$$\rho C_p \frac{\partial T}{\partial t} - \nabla \cdot (k \nabla T) = Q. \tag{2.29}$$

Where: ρ — material density (kg/m^3); Cp — heat capacity (J/(kgK)); k — thermal conductivity (W/(mK)); Q — heat source (W/m3).

In stationary systems, the first term of the equation (2.29) is zero.

2.1.6. Modeling Temperature Fields and Deformations by using the Finite Element Method

The temperature field and error modeling is performed by using the finite element method (FEM) in the COMSOL Multiphysics software environment. A simplified 3D model of the aluminum profile and stainless-steel measuring tape of the encoder is developed. This model is then decomposed into finite tetrahedral elements. Such a fragmented linear encoder model is shown in Figure 2.5.

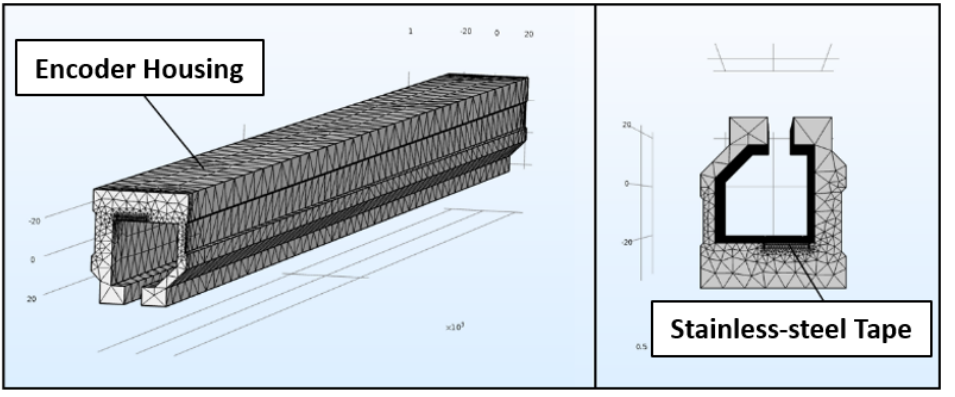

Fig. 2.5. Simplified 3D model of the linear encoder housing and the measuring tape divided into finite elements

The modeled thermo-mechanical task consists of the simulation of temperature fields and the modeling of mechanical deformations under the influence of the found temperature gradients. The first part of the problem is solved using the *Heat Transfer in Solids* mathematical package. Longitudinal deformations of the stainless-steel tape, which cause direct measurement errors in the encoder, are found by using the *Solid Mechanics* package. Combining these two tasks into a

common *Multiphysics* problem helps to find the right solution. With the help of computer modeling, the distribution of deformations (temperature expansion) along the stainless-steel measuring tape under different temperature gradients could be found.

Three-dimensional models of aluminum housing and a measuring scale include materials with specific mechanical (density, Young's modulus, Poisson's ratio) and temperature (thermal conductivity, heat capacity, expansion coefficient) parameters. The values of these parameters are given in Table 2.1.

Table 2.1. Mechanical and temperature parameters of materials used in computer modeling

Parameter	Encoder Parts	
	Housing	Measuring Scale
Material	Aluminum (Al 6060)	Stainless-steel (AISI 420)
Density, [kg/m^3]	2700	7700
Young's Modulus, [GPa]	70	190
Poisson's Ratio	0,33	0,28
Thermal Conductivity, [W/mK]	210	30
Heat Capacity, [J/kgK]	900	480
CTE, [1/K]	23	10

For visual data display, one end of the aluminum housing and the stainless-steel measuring tape assembly are rigidly fixed (*Fixed Constraint* function is used). Displacements in the direction transverse to the encoder are also limited. The *Roller* function used is placed on the mounting surface of the encoder housing. Such boundary conditions, which determine the mounting of the device under real conditions, are shown in Fig.2.6.

The *Prescribed Displacement* function is used to model the initial tension of the measuring tape, which is used to indicate the initial displacement of the tape end of the 10 μm. *Functions* are used to implement the distribution of the considered temperature fields. The desired distribution of temperature fields over the

entire length of the encoder is then described by using *Analytics* or *Interpolation* functions.

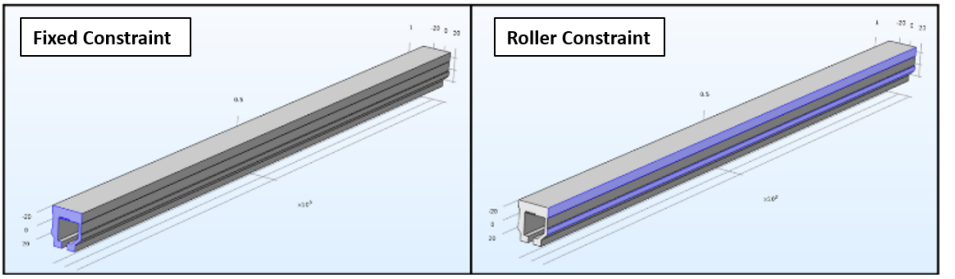

Fig. 2.6. Boundary conditions of the task: rigid fixation *Fixed Constraint* (left); surface limiting displacements across the aluminum housing *Roller Constraint* (right)

More detailed discussions about the thermal processes in measuring systems, thermal problem minimization methods, computer modeling based on FEM, and the benefits of computational error compensation techniques are presented in the appended scientific articles 1 and 2.

2.2. Effect of Different Scanning Speeds

The effect of different displacement scanning speeds appears to be the distortion of the analog converter output signals. This is due to the response of the used electrical components or the undesired relative motion between the optical components as the measuring scale and the scanning reticle. A distortion of the electrical signals, such as a reduced amplitude, offset from zero background, phase shift, or distorted shape, causes metrological (sub-divisional) errors in the encoder. These errors are periodic and occur in each period of the scanned measurement scale.

A convenient way to observe such errors is to analyze the Lissajous curve consisting of the two-analog encoder signals, A and B, phase-shifted by 90 electrical degrees.

2.2.1. Analysis of the Lissajous Curve by Using Arctangent Algorithm

The 2-argument arctangent function atan2(y, x) is defined as the angle in the Euclidean plane. It is given in radians, between the positive x-axis and the ray to the point $(x, y) \neq (0, 0)$. The function returns a single angle value Θ such that $-\pi < \Theta \leq \pi$.

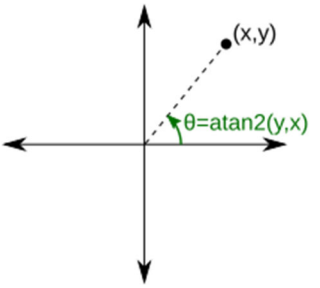

Fig. 2.7. Schematic atan2(y, x) function representation

If the $x > 0$, the given angle is:

$$\theta = atan2(y,x) = \arctan\left(\frac{y}{x}\right). \tag{2.30}$$

However, if $x < 0$, the given angle shows the direction opposite to the correct angle value. The value of $\pm\pi$ must be added to Θ:

$$atan2(y,x) = \begin{cases} arctan\left(\frac{y}{x}\right) & if\ x > 0, \\ arctan\left(\frac{y}{x}\right) + \pi & if\ x < 0\ and\ y \geq 0, \\ arctan\left(\frac{y}{x}\right) - \pi & if\ x < 0\ and\ y < 0, \\ +\frac{\pi}{2} & if\ x = 0\ and\ y > 0, \\ -\frac{\pi}{2} & if\ x = 0\ and\ y < 0, \\ undefined & if\ x = 0\ and\ y = 0. \end{cases} \tag{2.31}$$

Applying the arctangent algorithm to the analysis of the Lissajous curve, the values x and y correspond to the relative voltage values S_A and S_B of the electrical signals A and B of the linear encoder under study. One full revolution of the Lissajous curve (360 electrical degrees) corresponds to the period p of the measuring scale. Using the arctangent algorithm, it is easy to determine the relative position $X_{position}$ inside the period:

$$X_{position} = \frac{p}{2\pi}\arctan\left(\frac{S_A}{S_B}\right). \tag{2.32}$$

Such determination of the values of the internal period positions makes it possible to compare the magnitude of the displacement with the more accurate reference measure to determine the sub-divisional error of the encoder.

2.2.2. Constant Scanning Speed as a Reference for SDE Measurement

To evaluate the effect of different scanning speeds on the formation of the SDE error, the accuracy of the encoder must be measured at certain constant speeds by using a high-precision reference and all the necessary metrological equipment capable of performing calculations at high speed. It is somewhat difficult to realize this by practical means.

A different practical method for determining SDE errors at different position scanning speeds was realized during the experimental research of this work. This method is based on a constant-speed test and does not require a high precision reference. The reading head of the tested encoder was driven at different constant speeds, and the electrical output signals were recorded by using a digital oscilloscope. Because of the high sampling frequency, analog encoder signals were represented as a group of discrete points. The relative position values inside one grating period were calculated by applying the arctangent algorithm presented in the previous subsection by putting these discrete points of A and B signals into Equation (2.32).

Assuming that scanning speed is constant and knowing the used sampling rate that must be selected by considering the Nyquist–Shannon sampling theorem and the acceptable size of the sample, it is easy to compose the theoretically "true" position values at these points. For example, if the scanning speed is 100 mm/s, the grating period of the tested encoder is 20 μm, and the sampling frequency is 250 MHz, there are 50 000 sampling points per period. The first point corresponds to a zero-position value, and the last one (50 000) corresponds to 20 μm. All other points increase with a step of 0.0004 μm. Then, the calculated values according to the arctangent algorithm could be compared with theoretically determined "true" position values. The differences are accepted as metrological linear encoder errors inside one grating period. To obtain statistically reliable results, this procedure must be repeated for several periods or several separate measurements, and the average value must be used.

The accuracy of this methodology highly depends on the stability of the scanning speed and the precision of the used equipment. However, it is completely suitable to determine the magnitude level of the error and to notice its trend.

2.2.3. Harmonic Analysis of the SDE Curve

Because these errors are cyclic, their harmonic analysis could help to define what kind of signal imperfections cause them. Sub-divisional error curve representation as the superposition of basic waves (harmonics) can be helpful in analyzing and identifying the physical nature of the SDE. The first harmonic of the curve is a result of a non-zero background level of the A and B signals. The second harmonic could be caused by unequal amplitudes or a phase shift. Third and higher harmonics are the result of high-order distortions of the electric signals. Usually, they are caused by diffractive effects in optical light modulation processes.

Thus, an error decomposed into harmonics can be mathematically expressed:

$$\delta(x) = \sum_{i=1}^{n} \left(A_i cos\left(\frac{2\pi}{p} ix + \varphi_i\right)\right) + \varepsilon_n \ \ for\ 0 \le x \le p. \qquad (2.33)$$

Where $\delta(x)$ denotes the SDE inside one period of the encoder grating, A_i and φ_i indicate the amplitude and the phase of the harmonic, and x denotes the relative position inside a period p. The number of the harmonic is marked as n, and ε indicates the random error.

2.3. Mechanical Vibration Effect

External mechanical vibration is unavoidable in most applications. It is usually caused by an unbalanced motor, performed technological processes such as metal cutting or pick-and-place procedures, driving systems, etc. The elements of the linear encoder affected by these external excitations start to oscillate. The most dangerous motion is the lateral movement of the scanning carriage along the measuring scale. This type of motion will generate a continuously changing encoder reading around a particular position. In practice, the size of this oscillation is not big and is usually smaller than the period of the measuring scale. Nevertheless, this jumping of the position deteriorates the measurement repeatability and disturbs the interpolation process, because the analog signal of the encoder becomes more distorted.

The most dangerous scenario may happen if the frequency of these excitations matches with the natural frequencies of the encoder components. In this case, the amplitude of the vibration could significantly increase and damage the encoder or a whole application.

The dynamical behavior of the linear encoder depends on its stiffness and design. Scientific research shows that the scanning principle of the encoder may

increase its resistance to mechanical excitation (Lopez *et al.* 2012). Single-field type imaging optical encoders are less sensitive to oscillations compared to four-field electric output generation methods. Other research discusses the different mounting type influence on a measuring error formation (Lopez *et al.* 2011).

2.3.1. Finite Element Method for Mechanical Vibration Analysis

The finite element method is a numerical method for engineering design and analysis. It is a commonly used method for investigating the influence of mechanical vibrations, determining resonant frequencies, and performing modal analysis of the structure. The results of the application of the finite element method in modeling and analysis largely depend on the applied calculation and modeling procedures. Regardless of the scope of the method, digital modeling in use requires complete information about the space under consideration and its elements (geometry, elements, boundary conditions, loads, etc.).

2.3.2. Numerical Model of the Linear Encoder

The model under consideration depicts the elastic oscillations of the encoder's structural components. The dynamic equilibrium equation of one structural element is written in the form:

$$[M^e]\{\ddot{U}^e\} + [K^e]\{U^e\} = \{R^e\} + \{P^e\}. \tag{2.34}$$

Where: $[K^e] = \int_{V^e} \int [B]^T [D][B] dV$ — the stiffness matrix of the element; $[M^e] = \rho \int_{V^e} \int [N]^T [N] dV$ — the mass matrix of the element; $[B]$ — the matrix linking the displacements of the nodes with the deformations in the volume of the element. It is a function of the coordinates x, y, z and is obtained by differentiating the matrix of shape functions; $[N]$ — the matrix of shape functions of the element; $[D]$ — the stiffness constants of the material; $\{P^e\} = \int_{V^e} \int [N]^T \{b\} dV$ — the vector of node forces of the element due to the distributed volume forces; $\{b\} = \begin{Bmatrix} 0 \\ -\rho g \end{Bmatrix}$, ρ — material density; g — free-fall acceleration; $\{R^e\}$ — node force vector due to interelement interaction forces; V^e — the volume of the element.

When the element equations are assembled into a structural equation, their shape remains analogous to that of the element Equation (2.32). In solving the problem of elastic oscillations, the base of the encoder housing is considered fixed.

Eigenfrequency analysis:

Eigenfrequencies or natural frequencies are certain discrete frequencies at which a system is prone to vibrate. The non-damped natural oscillations of the encoder components are described by its dynamic equation with a zero right-hand vector:

$$[M]\{\ddot{U}\} + [K]\{U\} = 0. \tag{2.35}$$

Obviously, $\{U\} = 0$ is a solution to this equation that describes the state of the seriousness of an undeformed structure. However, this solution is not the only one. If there are other, non-zero, periodic solutions $\{U(t)\} = 0$, that satisfy this equation, they determine the natural oscillations of the structure (those that are possible without the action of external forces). These periodic solutions can be searched for in this form:

$$\{U\} = \{\widehat{U}\}\cos(\omega t). \tag{2.36}$$

Differentiating the expression Equation (2.34) twice and writing it to the starting Equation (2.33), we get the algebraic matrix equation:

$$([K] - \omega^2[M])\{\widehat{U}\} = \{0\}. \tag{2.37}$$

Non-zero solutions can be obtained only when the matrix of coefficients of Equation (2.35) is degenerate:

$$det([K] - \omega^2[M]) = 0. \tag{2.38}$$

The values need to be found for the angular frequencies ω of the oscillations to satisfy the algebraic Equation (2.36). This is a nonlinear equation of degree n, where n is the number of degrees of freedom of construction.

In the general case, the n-th degree algebraic Equation (2.36) has n roots ω_1, ω_2, …, ω_n, which are called the eigenvalues of Equation (2.35) or, in other words, the eigenfrequencies of the oscillations of the structure described by the Equation (2.33). If $[K]$ and $[M]$ were any, the eigenvalues ω_i, could be both real and complex. In reality, however, matrices of structures are always symmetric and positively defined, and as evidenced by matrix theory, their true meanings are always real and positive.

Writing any value of ω_i in Equation (2.35) and solving it results in a non-zero vector $\{\widehat{U}^{(i)}\}$, describing the amplitudes of the vibrations of the structure. Since at

value $\omega = \omega_i$ the matrix of system coefficients is degenerate, the value of the vector $\{\widehat{U}^{(i)}\}$ is not the only one. It is determined by the accuracy of a constant multiplier and determines the relative amplitudes of the nodes in the structure. Thus, by successively entering the real values ω_1, ω_2, ..., ω_n in Equation (2.35), we would obtain the corresponding vectors $\{\widehat{U}^{(1)}, \widehat{U}^{(2)}, \dots, \widehat{U}^{(i)}\}$, called eigenvectors.

The other more detailed aspects and the vibration-influenced error estimation methodology are presented in the appended article 4.

2.4. Conclusions of Chapter 2

The research methodology presented in this chapter includes theoretical and experimental research. The discussed methods are tailored to each of the three different studies of environmental effects: thermal, the effect of different scanning speeds, and mechanical vibrations.

1. The theoretical research performed in this work is based on the principles of material science and continuum solid mechanics, including the topics of thermo-mechanics and vibration of solids.
2. The finite element method is chosen to study the effects of temperature and mechanical vibrations. The modeling of introduced thermal stresses and thermal expansion helps to identify the thermoelastic deformation, which is related to the investigative measurement error. The dynamic behavior of the linear encoder is determined by the analysis of its eigenfrequencies and eigenmodes.
3. The experimental research consists of the composition of the required experimental setups and appropriate collection of data and its processing by mathematical-statistical methods.
4. Arctangent algorithm implementation in experimental research calculations helps to evaluate the sub-divisional error under different scanning speeds, while the Harmonic analysis and the fast Fourier transformation (FFT) enable a proper analysis and interpretation of these encoder errors.

3

Results and Conclusions of Theoretical and Experimental Research of the Measurement Errors Formation in Optical Linear Encoders

This part presents a summary of the findings of appended articles 1–4 in a common context. The intention is to relate the results of the papers to the overall thesis objectives. The research on each different environmental factor that determines the encoder's measurement error is presented in separate publications. A theoretical investigation of geometrical and thermal errors and the development of their compensation algorithm are presented in Article 1. The practical realization of the developed real-time compensation and performed experimental research are presented in Article 2. Article 3 presents an experimental study of the sub-divisional error at different displacement scanning speeds. The effect of mechanical vibrations on the measurement errors of the encoder is investigated and presented in Article 4. The general conclusions of the dissertation are also presented.

3.1. Investigation Results of Article 1

Article 1 presents the analysis of geometric and thermal errors of the linear encoder for real-time compensation. To get a better understanding of the prevailing problem, the thermal processes ongoing in measuring systems and the thermal error reduction methods are discussed. An enclosed type of optical linear encoder is used as the research object. The finite element method (FEM)-based computer modeling of emerging temperature fields and introduced thermal errors is performed. The obtained results reveal the systematic behavior of the thermal error while the encoder is working under constant thermal sources and changing ambient temperature. This allowed the development of a mathematical model for measuring error compensation. The proposed mathematical compensation model is based on the approximation of geometric and thermoelastic encoder errors by simple parametric functions and the calculation of the systematic linear errors according to ambient temperature variations. The two-dimensional function is the basis for the calculation of the compensation value Δ.

$$\Delta(q,T) = F_g(q) + F_{gr}(q) + F_a(\Delta T, q). \tag{3.1}$$

Its arguments are the displacement q and the temperature value T measured in one specially selected point of the encoder profile, which best describes the average temperature variation. $F_g(q)$ is the approximation function of the determined geometrical error; $F_{gr}(q)$ is the thermoelastic error approximation function when the thermal gradient along the linear encoder scale is steady, and ambient temperature is stable; $F_a(\Delta T, q)$ is the thermal error constituent that expresses a linear deformation of the measuring scale under the changing ambient temperature.

$$F_a(\Delta T, q) = \alpha_{corrected} \cdot \Delta T \cdot q. \tag{3.2}$$

Where: αcorrected is the corrected coefficient of linear thermal expansion of the measuring scale (determined by analyzing the interaction between the aluminum housing and the stainless-steel measuring scale); ΔT is the ambient temperature T difference from nominal T_n ($\Delta T = T_n - T$), and q is the measured displacement (linear position).

The visual representation of the total linear encoder error analyzed in Article 1 could be introduced as a 3D plot, as shown in Fig. 3.1.

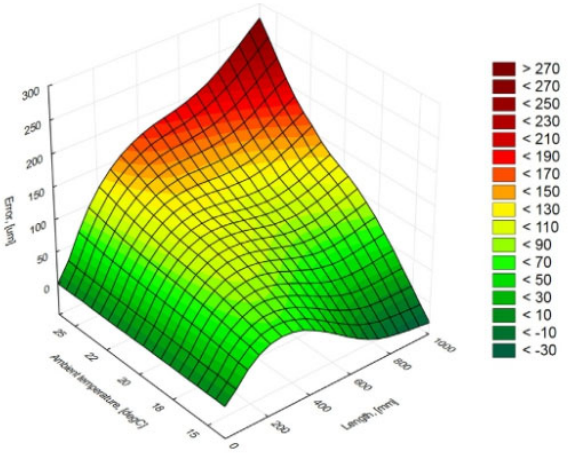

Fig. 3.1. Dependence of the compensated error on the measured displacement size and ambient temperature

Such a method could be realized by using simple standard calculation equipment that could be used as a subsequent electronics unit or be integrated into the encoder.

3.2. Investigation Results of Article 2

Article 2 presents the thermal and geometric error compensation approach for an optical linear encoder. In the previous article (Article 1), the developed mathematical model was realized by using a field-programmable gate array (FPGA) computing platform. The principal block diagram of the composed encoder position compensation setup is presented in Fig. 3.2.

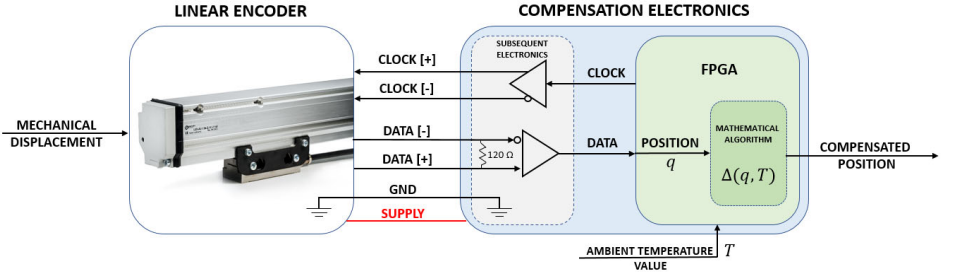

Fig. 3.2. Block diagram of the compensation setup with a field-programmable gate array

The calculation of a two-dimensional compensation function and the real-time correction of the linear encoder position readings are performed during the experimental research. The thermal behavior of the enclosed linear encoder is investigated under four different ambient temperatures. Determined encoder accuracy at 20 ± 0.2 °C temperature (measurement is performed in the thermostable laboratory room) is accepted as the non-compensated nominal accuracy of the encoder. The parametric function approximating this average position curve is derived and is used as the base for the further thermal and geometric error compensation value calculation. Comparative graphs of the non-compensated and compensated displacement position errors are given in Fig.3.3.

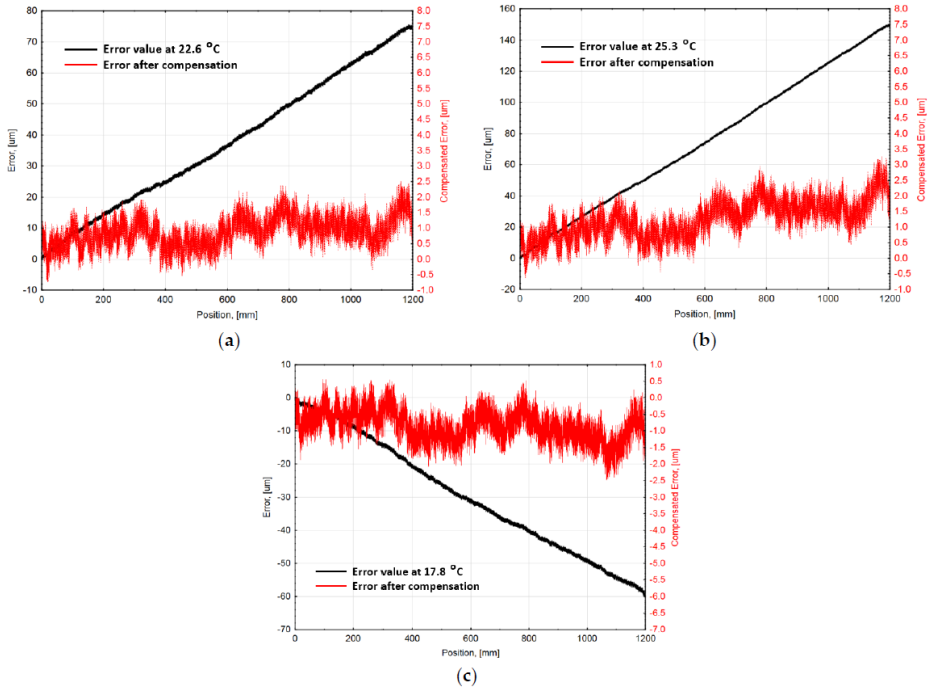

Fig. 3.3. Compensated linear encoder average accuracy graphs (red line/right Y-axis units) with corresponding uncompensated error values (black line/left Y-axis units), at different ambient temperatures: **(a)** at 22.6 °C; **(b)** at 25.3 °C; **(c)** at 17.8 °C

The results of the experiments show that the introduced thermal error could be significantly reduced up to 98 %. Moreover, the optimization method of the compensation algorithm is discussed. It is based on a calculation of the real coefficient of thermal expansion (CTE) value from the experimental data. A concise comparison of the results is given in Table 3.1.

Table 3.1. Investigation results of the experimental temperature error compensation

Parameter	Ambient Temperature			
	17.8 °C	20 °C	22.6 °C	25.3 °C
Average accuracy of non-compensated encoder [µm]	± 30.08	± 2.20	± 37.74	± 75.09
Average accuracy of compensated encoder [µm]	± 1.52	± 1.08	± 1.62	± 1.95
Theoretical encoder accuracy with experimentally estimated CTE value [µm]	± 1.42	-	± 1.46	± 1.48

The proposed selection of simply approximating functions and hardware ensure an appropriate calculation speed for a real-time application.

3.3. Investigation Results of Article 3

Article 3 presents the experimental investigation of linear encoder sub-divisional errors under different scanning speeds. In the beginning, the metrological process of optical encoders and the importance of the sub-divisional errors (SDE) are described. The methodology based on a constant-speed test is developed to investigate the influence of different scanning speeds on the SDE formation. During the performed tests, the reading head of the investigated linear encoder is driven at constant speeds from 100 mm/s to 1100 mm/s. The quadrature analog output signals of the encoder are recorded, and the approximate SDE values and the trend are estimated by adapting the arctangent algorithm (atan2). The statistical linear regression analysis shows the linear relationship between the magnitude of the SDE and the traversing velocity of the reading head (R-squared = 0.8581). Calculated total error values are plotted into one graph presented in Fig. 3.4.

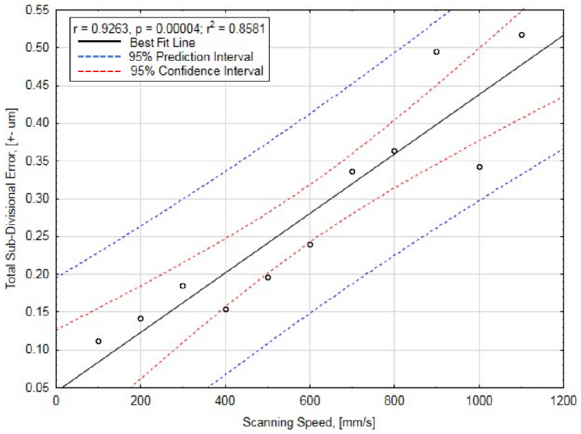

Fig. 3.4. Total SDE dependency on displacement scanning speed graph: data points and their statistical parameters

For a more detailed investigation, the harmonic analysis based on the fast Fourier transformation (FFT) is performed. The sub-divisional error determined at each constant speed is decomposed into separate harmonic components. The first three harmonics make up the bulk of the error and could define the nature of its formation. The biggest part of the SDE forms the second harmonic. It directly correlates to a scanning velocity and is caused by the occurring difference between the quadrature signal amplitudes or the increasing phase shift. The dependency graph of the three first harmonics and scanning speed is provided in Fig.3.5.

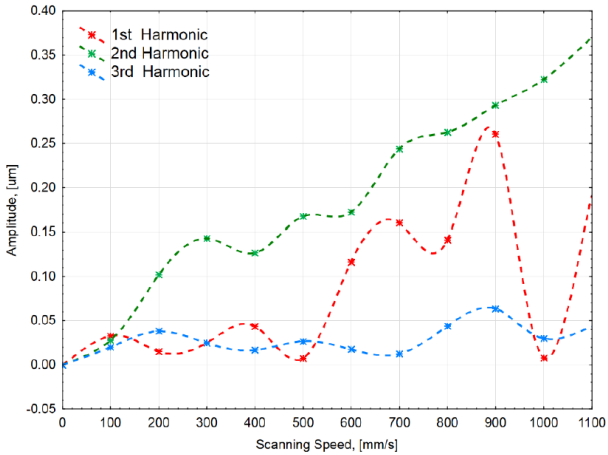

Fig. 3.5. Dependency of three first harmonics of determined SDE curves on different scanning speeds

The integration of less speed-sensitive single-field optical signal formation method or external signal monitoring and conditioning electronics are suggested as possible technical solutions to minimize this type of error. Another proposed method is computational compensation. The multivariable function could be derived after the extra processing of the experimental investigation data. The function could describe the approximated SDE value at a relative position inside the period of the measuring scale at any traversing velocity and could be used as a compensation value in real-time applications.

3.4. Investigation Results of Article 4

Article 4 presents the dynamic behavior analysis of the optical linear encoder under mechanical vibrations. The reading head and the aluminum profile of the enclosed type of linear encoder are mounted on the electrodynamic shaker in a fixed position during all experimental research. The additional unwanted motion of the scanning carriage along the measuring scale is the point of interest in this work. The shaker generates the known magnitude of the external mechanical excitation, while the piezoelectric accelerometers are used to estimate the dynamic response of the reading head and the aluminum extrusion. Recorded incremental analog encoder signals help to define the generated measuring error value by using the arctangent algorithm (atan2) and visually analyzing the corresponding arcs of the Lissajous curves. Firstly, the encoder's response to the sine sweep vibration test is received. The main resonant frequencies of the encoder are determined. Later, the shaker generates a discrete sine vibration of up to 2000 Hz with a step of 100 Hz, including the previously determined natural frequencies. This way, the dynamic response values (in the range up to 2000 Hz) of the reading head and the encoder extrusion become known. The finite element method (FEM)-based modal analysis of the digital 3D encoder model is performed. On that basis, the peak dynamic response values are related to the corresponding mode shapes of the encoder elements. Theoretically, the biggest error may appear due to a high amplitude motion of one of the encoder components: scanning carriage or measuring scale. Consequently, the differences in the determined response amplitude values are calculated and plotted in a graph (Fig.3.6).

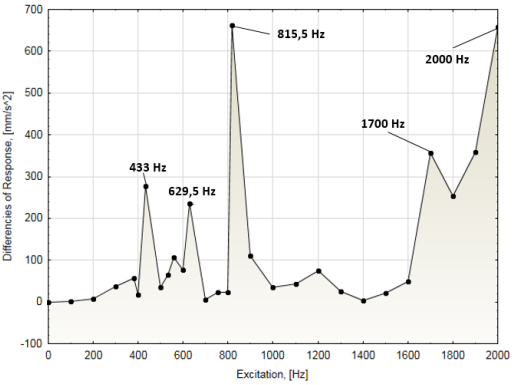

Fig. 3.6. Graph of differences between response amplitude values of the reading head and the aluminum extrusion

The results show potentially the most dangerous frequencies, which could generate displacement measurement errors. The determined measuring error values at these frequencies reach up to ~11 µm, which is a significant size compared to a measuring scale period of 40 µm. Electrical signals are recorded during the displacement measurement process to see how external mechanical excitation affects its performance. An example, the Lissajous curve of the working encoder under 815.5 Hz excitation is shown in Fig.3.7.

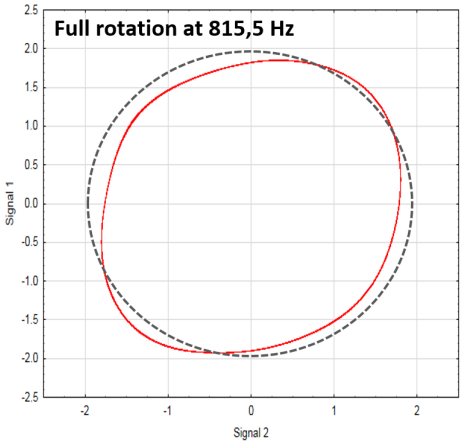

Fig. 3.7. Lissajous curve of a working encoder under 815.5 Hz external mechanical excitation: solid red line — Lissajous curve of the tested encoder; dashed black line — ideal circular curve

The nature of the determined error could be related to a specific modal swell type motion shape of the aluminum extrusion or the measuring scale, as well as various motions of the scanning head. Possible technical solutions are proposed for vibration error minimization, such as harder stretching of the stainless-steel measuring scale or the additional mechanical pin integration. The introduced analysis for dynamic linear encoder behavior could be widely applied to various engineering areas, including the design of precision applications or linear encoders.

3.5. General Conclusions

The problems of varied optical linear encoder behavior under real operating conditions were solved in terms of theoretical and experimental investigation. The following results were obtained:

1. The review of scientific and technical literature shows that the effect of real ambient conditions, such as thermal effects, mechanical vibration, various deformations, and displacements, has a significant impact on the formation of the measuring error. The revealed problem exposed the need for new reliable methods to deal with it. There is no comprehensive research on a linear encoder sub-divisional error formation under the dynamic effect of varying scanning speed.

2. The performed analytical and numerical research of linear encoder behavior under different operating conditions resulted in the following scientific conclusions:

2.1. The systematic regularities of the thermoelastic deformation were noticed, allowing to create preconditions to develop the introduced thermal error compensation model and realize it by simple technical means. The mathematical model adapted for real-time computational compensation was developed.

2.2. The methodology for the sub-divisional linear encoder error estimation at various scanning speeds was developed. The method allows to determine the prevailing trend of the interpolation error and analyze it with no need for a high-precision reference encoder or other metrological equipment.

2.3. Digital modal analysis of the linear encoder was performed. The resonant frequencies (eigenfrequencies) and modal shapes (eigenmodes) were determined to investigate the nature of the mechanical components' vibration.

3. The performed experimental research on the linear encoder allowed for these scientific conclusions:

3.1. The developed mathematical model is suitable for the geometric and thermoelastic error computational compensation for the enclosed type of linear encoders. The performed tests showed that the error could be minimized by 98 %. The realized compensation approach based on the field-programmable gate array

(FPGA) calculation platform demonstrated adequate computational speed performance and suitability for a real-time application.

3.2. The experimental investigation of the sub-divisional linear encoder error revealed the linear correlation between the SDE value and the scanning speed. As the traversing velocity of the encoder's reading head increased, the sub-divisional error magnitude increased. The second harmonic made up the bulk of the error value and could be interpreted as the phase shift or as an increasing difference between the amplitudes of the analog encoder signals.

3.3. The performed experimental research of the dynamic tested linear encoder behavior under the mechanical sinusoidal vibration (according to IEC/EN 60068-2 standard) showed the formation of the measuring error, which reached up to ~11 μm. The error formation was directly related to the swell type of motion of the stainless-steel measuring scale and aluminum profile, as well as to various motions of the scanning carriage.

The dissertation presented a complex methodology that can be applied to study the temperature and dynamic errors of enclosed linear encoders. The presented examples on the mathematical description of the identified errors and practical implementation of real-time error compensation can be integrated into the new generation of measurement systems or help to investigate and improve existing linear encoders.

In the future, the work presented in this thesis can be continued by applying specific technical solutions and performing experimental research, e.g.:

1. The mathematical model for the thermal error computational compensation could be improved by applying more advanced mathematical approximation methods. The dynamically changing impact of external heat sources and ambient temperature might be evaluated and added as a correcting value in the compensation algorithm.

2. During the performed experimental research (Article 3), mapped and approximated sub-divisional errors at different scanning speeds could be used as a multivariable function for positioning error compensation. It could be integrated into the advanced thermal error compensation algorithm to get a less sensitive linear encoder not only to thermal effects but also to a varying scanning speed.

3. A set of technical solutions could be added to the tested linear encoder to minimize the impact of mechanical vibration. Harder stretched stainless steel measuring tape or additional pins for measuring scale pressure in specific points could increase the stiffness and make the natural frequency of the encoder elements higher. The integration of single-field optical scanning methods could make the measuring system less sensitive to an external mechanical excitation as well as to changing traversing velocity.

Most of these improvements require changes in the mechanical design and technological manufacturing process of the linear encoder. Either way, more detailed theoretical and experimental investigation is needed.

References

Alejandre, L. and Artés M. 2004. Machine tool errors caused by optical linear encoders, *in Journal of Engineering Manufacture 218(1): 113-122.*
DOI: https://doi.org/10.1243/095440504772830255

Alejandre, I. and Artés, M. 2004. Real thermal coefficient in optical linear encoders, in *Experimental Techniques* 28(4), 18-22.
DOI: https://doi.org/10.1111/j.1747-1567.2004.tb00172.x

Alejandre, I. and Artés, M. 2006. Thermal non-linear behavior in optical linear encoders, in *International Journal of Machine Tools and Manufacture* 46(12-13), 1319-1325.
DOI: https://doi.org/10.1016/j.ijmachtools.2005.10.010

Baniasadi, H. and Modabberifar, M. 2016. Design, fabrication and development of a capacitive-type linear encoder using electrostatic induction, *in Modares Mechanical Engineering 16(3), 153-160.*

Barakauskas, A.; Barauskas, A.; Kasparaitis, A.; Kaušinis, S. and Jakštas, A. 2017. Error modelling of optical encoders based on Moiré effect, in *Journal of Vibroengineering* 19(1), 38-48.

DOI: https://doi.org/10.21595/jve.2016.17132

Cosijns, S.J.A.G. and Jansen, J. 2018. Advanced optical incremental sensors: encoders and interferometers, in *Smart Sensors and MEMs,* Book, Second Edition, 245-290.
DOI: https://doi.org/ 10.1533/9780857099297.1.230

Decoding principles 2015. *Decoding principles of quadrature encoder signals* [interactive] [20 February 2021]. Available online at: https://www.motioncontroltips.com/faq-what-do-x1-x2-and-x4-position-encoding-mean-for-incremental-encoders/

Gao, W.; Kim, S.W.; Bosse, H.; Haitjema, H.; Chen, Y.L.; Lu, X.D.; Knapp, W.; Weckenmann, A.; Estler, W.T. and Kunzmann, H. 2015. Measurement technologies for precision positioning, *in CRIP Annals, Measurement Tehcnologies for Precision Positioning 64(2), 773-796.*
DOI: https://doi.org/10.1016/j.cirp.2015.05.009

Hane, K.; Uchida, Y. and Hattori, S. 1985. Moire displacement measurement technique for a linear encoder, in *Optics and Laser Technology* 17(2), 89-95.

HEIDENHAIN 2019. *Linear encoders for numerically controlled machine tools* [interactive] [20 February 2021]. Available online at: https://www.heidenhain.com/fileadmin/pdb/media/img/571470-2C_Linear_Encoders_For_Numerically_Controlled_Machine_Tools.pdf

HEIDENHAIN 2020. *Linear encoders for manually operated machine tools* [interactive] [20 February 2021]. Available online at: https://www.heidenhain.com/fileadmin/pdb/media/img/208864-2G_Digital_Readouts_Linear_Encoders_For_Manually_Operated_Machine_Tools_en.pdf

HEIDENHAIN EXPOSED 2020. Exposed linear encoders [interactive] [20 February 2021]. *Available online at:* https://www.heidenhain.de/fileadmin/pdb/media/img/208960-2G_Exposed_Linear_Encoders_en.pdf

HEIDENHAIN Interfaces 2019. Interfaces of HEIDENHAIN Encoders [interactive] [20 February 2021]. Available online at: https://www.heidenhain.com/fileadmin/pdb/media/img/1078628-22_Interfaces_en.pdf

HEIDENHAIN Single-field 2006. *Technical Information. Linear Encoders with Single-Field Scanning* [interactive] [20 February 2021]. Available online at: https://www.heidenhain.us/wp-content/uploads/2-LinearEncodersSingleFieldScanning-1.pdf

Ieki, A.; Matsui, K.; Nashiki, M. and Hane. K. 1999. Compact optical encoder using modulated-pitch phase grating: suppression of harmonic noise and contrast change, in *Optical Engineering for Sensing and Nanotechnology* 3740.
DOI: 10.1117/12.347783

Ieki, A.; Matsui, K.; Nashiki, M. and Hane. K. 2000. Pitch-modulated phase grating and its application to displacement encoder, in *Journal of Modern Optics* 47(7), 1213-1225.
DOI: 10.1080/09500340008232168

Interpolators 2018. *Evolution of sinusoidal encoder interpolators* [interactive] [20 February 2021]. Available online at: http://www.deltataunews.com/pdfs/DeltaTau_WP_Auto-Correcting_Interpolator.pdf

ISO 5725-1 1994. *Accuracy (Trueness and Precision) of Measurement Methods and Results – Part 1: General Principles and Definitions* [interactive] [20 February 2021]. Available online at: https://www.iso.org/standard/11833.html

Jenkins, S.T. and Hilkerk, J.M. 2008. Sin/cosine encoder interpolation methods: Encoder to digital tracking converters for rate and position loop controllers, in *The International Society for Optical Engineering* 6971.
DOI: https://doi.org/10.1117/12.777741

Kishimoto, S.; Egashira, M. and Shinya, N. 1993. Microcreep deformation measurement by a Moire method using electron beam lithography and electron beam scanning, in *Optical Engineering* 32(3).

Lee, C.B.; Kim, G.H. and Lee, S.K. 2011. Design and construction of a single unit multi-function optical encoder for a six-degree-of-freedom motion error measurement in an ultraprecision linear stage, *in Measurement Science and Technology 22(10), 105901.*
DOI: https://doi.org/10.1088/0957-0233/22/10/105901

Lepple, C. 2004. Implementation of a high-speed sinusoidal encoder interpolation system, in *MSEE Thesis, Virginia Polytechnic Institute.*
URI: http://hdl.handle.net/10919/31139
DOI: https://doi.org/10.1117/12.61046

Lopez, J.; Artés, M. and Alejandre, I. 2011. Analysis of the optical linear encoder`s errors under vibration at different mounting conditions, *in Measurement 44(8), 1367-1380.*
DOI: https://doi.org/10.1016/j.measurement.2011.05.004

Lopez, J.; Artés, M. and Alejandre, I. 2012. Analysis under vibrations of optical linear encoders based on different scanning methods using an improved experimental approach, *in Experimental Techniques 36(6), 35-47.*
DOI: https://doi.org/10.1111/j.1747-1567.2011.00749.x

Luxmoore, A.R. and Shepherd, A.T. 1983. Applications of the Moiré *Effect,* in *Luxmoore A.R. (eds) Optical Transducers and Techniques in Engineering Measurement.* Springer, Dordrecht. 66-108.
DOI: https://doi.org/10.1007/978-94-009-6637-6_3

Podhraški, M.; and Trontelj, J. 2016. A differential monolithically integrated inductive linear displacement measurement microsystem, in *Sensors 16(3), 384.*
DOI: https//doi.org/10.3390/s16030384

RLS 2020. *HiLin High-accuracy Linear Magnetic Encoder System* [interactive] [20 February 2021]. Available online at: https://www.rls.si/eng/hilin.

Sciammarella, C.A. and Davis, D. 1968. Gap effect in Moire fringes observed with coherent monochromatic collimated light, in *Experimental Mechanics* 8, 459-466.

SDE 2018. *What is sub-divisional error (SDE) in linear encoders?* [Interactive] [20 February 2021]. Available online at: https://www.linearmotiontips.com/what-is-sub-divisional-error-sde-in-linear-encoders/

Song. J.H; Kim, K.C.; Kim, S.H. and Kwak, Y.K. 1999. A new error compensation method in linear encoders using phase shifted grating, in *Optical Engineering for Sensing and Nanotechnology* 3740.

Song. J.H; Kim, K.C. and Kim, S.H. 2000. Reducing tilt errors in Moire linear encoders using phase–modulated gratings, in *Review of Scientific Instrumentation* 71(6), 2296-2300.
DOI: https://doi.org/10.1063/1.1150445

Tang, M.; Xie, H.; Zhu, J.; Li, X. and Li, Y. 2012. Study of Moire grating fabrication on metal samples using nanoimprint lithography, in *Optics Express* 20(3), 2942-2955.
DOI: https://doi.org/10.1364/OE.20.002942

Yan, D.; Cheng, J. and Apsel, A. 2004. Fabrication of SOI-based nanogratings for Moire measurement using focused ion beam, in *Sensors and Actuators: A. Physical* 115(1), 60-66.
DOI: https://doi.org/10.1016/j.sna.2004.03.034

Ye, G.; Liu, H.; Fan, S.; Li, X.; Yu, H.; Lei, Y.; Shi, Y.; Yin, L. and Lu, B. 2015. A theoretical investigation of generalized grating imaging and its application to optical encoders, in *Optics Communications* 345, 21-27.
DOI: https://doi.org/10.1016/j.optcom.2015.05.023

Ye, G.; Xing, H.; Liu, H.; Li, Y.; Lei, B.; Niu, D.; Li, X.; Lu, B. and Lu, H. 2019. Total error compensation of non-ideal signal parameters for Moire encoders, in *Sensors and Actuators A: Physical* 298.

Zhao, L.; Cheng, K.; Chen, S.; Ding, H. and Zhao, L. 2018. An approach to investigate Moir*é* patterns of a reflective linear encoder with application to accuracy improvement of a machine tool, in *Proceedings of the Institution of Mechanical Engineers, Part B: Journal of Engineering Manufacture 233, 297-936.*
DOI: https://doi.org/10.1177/0954405417752506

Author‘s Publications Collection

Papers in the Reviewed Scientific Journals

[1]**Gurauskis, D.; Kilikevičius, A.; Borodinas, S. and Kasparaitis, A.** (2019). Analysis of geometric and thermal errors of linear encoder for real-time compensation, in *Sensors and Actuators A: Physical,* 296, pp. 145-154. [Article 1, see p.69]

[1]**Gurauskis, D.; Kilikevičius, A. and Kasparaitis, A.** (2021). Thermal and geometric error compensation approach for an optical linear encoder, in *Sensors,* 21 (2): 360 [Article 2, see p.79]

[1]**Gurauskis, D.; Kilikevičius, A. and Borodinas, S.** (2020). Experimental investigation of linear encoder`s subdivisional errors under different scanning speeds, in *Applied Sciences,* 10(5), pp. 1766. [Article 3, see p.95]

[1]**Gurauskis, D and Kilikevičius, A.** (2020). Dynamic behaviour analysis of optical linear encoder under mechanical vibrations, in *Mechanika,* 26 (1) pp. 35-41. [Article 4, see p.107]

[1] The dissertation is defended on the basis of these articles. Full-text articles are available at the end of the chapter “Author’s Publications Collection”. Articles published with the consent of the publisher /-s.

Papers in Other Editions

Fursenko, A.; Kilikevičius, A.; Kilikevičienė, K.; Borodinas, S.; Kasparaitis, A. and Gurauskis, D. 2018. Experimental investigation of friction transition on vibration of steel tapes, in *2ND International Conference On Chemistry, Chemical Process and Engineering*, 2029(1):020016. DOI:10.1063/1.5066478

Svilainis, P.; Kilikevičius, A.; Gurauskis, D.; Fursenko, A.; Matijošius, J.; Miknius, N.; Kobal, G. 2020. Precizinės ilgio matavimo sistemos dinaminių reiškinių tyrimai, in *Inžinerinės ir edukacinės technologijos = Engineering and educational technologies. Kaunas: Kauno technikos kolegija.* ISSN 2029-9303. 2020, Nr. 1, p. 77-84.

Fursenko, A.; Gurauskis, D.; Kilikevičienė, K.; Vainorius, D.; Kilikevičius, A.; Matijošius, J. and Čižiūnienė, K. 2017. Limbų plovimo įrenginio dinaminiai tyrimai, in *Inžinerinės ir edukacinės technologijos: mokslinių straipsnių žurnalas = Engineering and educational technologies: scientific journal. Kaunas: Kauno technikos kolegija.* ISSN 2029-9303. 2017, Nr. 1, p. 133-140.

Gurauskis, D.; Kilikevičius, A.; Fursenko, A. and Samy, M. 2017. Eksperimentiniai linijinio keitiklio sistemos tyrimai, in *Mokslas – Lietuvos ateitis = Science – future of Lithuania: Mechanika, medžiagų inžinerija, pramonės inžinerija ir vadyba = Mechanics, material science, industrial engineering and managemen.* Vilnius: Technika. ISSN 2029-2341. Vol. 9, no. 6 (2017), p. 593-596. DOI: https://doi.org/10.3846/mla.2017.1091

Article 1. Gurauskis et al. (2019). Analysis of Geometric and Thermal Errors of Linear Encoder for Real-time Compensation (https://doi.org/10.1016/j.sna.2019.06.055)

Sensors and Actuators A 296 (2019) 145–154

Contents lists available at ScienceDirect

Sensors and Actuators A: Physical

journal homepage: www.elsevier.com/locate/sna

Analysis of geometric and thermal errors of linear encoder for real-time compensation

Donatas Gurauskis [a], Arturas Kilikevičius [b], Sergejus Borodinas [b,*], Albinas Kasparaitis [b]

[a] Department of Mechanical Engineering, Vilniaus Gedimino Technical University, J. Basanavicius g. 28, Vilnius LT-03224, Lithuania
[b] Institute of Mechanical Science, Vilniaus Gedimino Technical University, J. Basanavicius g. 28, Vilnius LT-03224, Lithuania

ARTICLE INFO

Article history:
Received 31 December 2018
Received in revised form 25 June 2019
Accepted 30 June 2019
Available online 2 July 2019

Keywords:
Thermal error
Temperature sensor
Linear encoder
Thermo-plastic deformation

ABSTRACT

Thermal errors that cause temperature deformations is one of the main factors that influence the accuracy of precision machines. Displacement measuring systems are used in robotics, precision machine tools and other technological equipment, where exist abundant heat sources. The accuracy of linear encoder is affected by both: thermal sources and the changing external ambient temperature. Therefore, thermo-elastic deformations occurring due to the changes in the ambient temperature is an important factor that should be estimated in the process of machine operation. This article presents a study on the thermal errors of optical linear encoder. Compensation of thermal errors is considered a more convenient, effective and economical way in comparison to the ways of thermal error handling and reduction. On the basis of analytic calculations, digital FEM analysis and experimental research, the models of thermal errors that are used for the real-time compensation are determined. The methodology of thermal error compensation, which could be easily realized in a linear encoder itself is presented in the article.

1. Introduction

Requirements for technological machines and their measuring systems are constantly increasing. The enhancement of accuracy at the expense of their production precision is not always possible and, moreover, technically and economically effective. The calculated error compensation opens up wide possibilities, when errors are calibrated, memorised and subtracted in the technological process [1–5]. This is applied to particularly complicated technological machines that incorporate measurement systems [3,6].

The errors of precision measurement devices can be divided into several groups as follows [5,7]: geometric and kinematic errors; thermal errors; errors driven by force in the operation process and other errors that occur due to the mantling of measuring systems [8].

One of the main reasons of errors is the thermo-elastic deformation of the measuring system that appears due to thermal error, i.e. thermal processes and changes in temperature. In general, two types of heat sources exist in precision measurement systems: internal and external [9,10]. Internal heat sources [10–13] refer to the heat produced in the process of machine operation; heat resulting from the friction of turn points; and heat produced by motors. External heat sources include shifts in ambient temperature; solar and internal radiation.

Different methods are proposed to reduce thermal errors that can be grouped into three categories [14,15].

a) *Avoidance of thermal errors.* This strategy is based on the avoidance of possible thermal deformations by choosing an appropriate design and materials of construction elements that have the same or very close coefficients of heat expansion in frame details.

b) *Control of thermal phenomena.* Another way of reducing thermal errors is the control of heat transfer in precision measurement systems or avoidance of uneven temperature distribution.

c) *Compensation of thermal errors.* Compensation of thermal errors is a process when an error is corrected by introducing correction coefficients. Comparing to other two methods, compensation of thermal errors is a more convenient and economical way [5,11,15]. Besides, such model of compensation can be introduced at any stage of encoder design, exposition or mantling [16].

Real-time compensation of thermal errors has several main aspects: analysis, testing, modelling and realisation of compensation [5,9,11,14]. Analysis, testing and computer modelling is the basis and preparatory work for compensation. In a general case, the process of thermal error compensation [4,5,17,18] is to analyse and study the distribution of temperature and thermal errors in an

* Corresponding author.
E-mail addresses: donatas.gurauskis@vgtu.lt (D. Gurauskis), arturas.kilikevicius@vgtu.lt (A. Kilikevičius), sergejus.borodinas@vgtu.lt (S. Borodinas), albinas.kasparaitis@vgtu.lt (A. Kasparaitis).

https://doi.org/10.1016/j.sna.2019.06.055
0924-4247/

encoder in theoretical, digital and experimental ways; to create the models of thermal errors that most often describe the relationship between temperature and thermal errors on the basis of analysis or experimental results [19]; to predict thermal errors in accordance with the model, and on the basis of the predicted data, to correct the result of the encoder readings [6,9,18,20]. Hysteresis between temperature and thermal deformation can influence the accuracy of the model of thermal errors. A dynamic model and its evaluation [17,21,22] is used to reduce the influence of hysteresis. As far as linear encoders are concerned, it is possible to perform a simple correction when temperature is standard (20 °C) and the coefficient of the expansion of aluminum profile, as well as glass and steel measurement scales are known. Non-isothermal situations (when temperature increases or decreases with reference to standard temperature) demand a more complex processing of the data, when mutual effect of glass or steel and aluminum should be measured.

The present article analyses errors of the optical linear measuring system and their compensation in real-time exploitation conditions. The compensation of the so-called geometric errors is solved approximating their calibrating data by parametric functions [5,11,17,23]. Thermal processes, which occur in measuring systems being affected by thermal gradients of the environment and depending on time, thermal deformation and error, are analysed. An empirical method of geometric and thermal error compensation is proposed that is easy to realise.

2. Thermal processes in measuring systems

Even mechatronic equipment of especially high quality used in industry inevitably encounter with different factors that negatively affect the exploitation of the machine or its systems and condition different geometric and thermal errors. The latter are especially topical as machine elements being affected by temperature changes start to expand or shrink and can cause harmful deformations of the mechanism. Thermal errors in precision systems that influence the deformation of machine elements and other errors make approximately 40–70 % of the total of errors. This type errors are hardly predictable, since temperature fields are constantly changing depending on the regime of machine operation and environmental conditions.

Automated robotic systems, CNC machining centres, coordinate measuring machines, and similar mechanisms perform technological machining, transportation or measurement processes structurally are most often composed of three main parts [8,24]:

1 *The object.* In the technological process, an element or its template is processed, transported or measured.
2 *Machine construction.* The frame of the machine which supports the whole construction and combines individual parts of the system.
3 *Measuring systems.* An integrated measuring system creating a feedback, which helps to control actuators and perform precision movements.

Since optical linear encoders, as other measuring systems, are integrated in technological machines, the thermal sources and other harmful factors affecting them should be analysed by evaluating the whole mechatronic system.

The following internal and external sources of thermal errors are distinguished in such automated systems:

1 *Heat released during the machining process.* The heat generated during the cutting process by the numerical control centre or machining a part by the machine tool has a direct effect on the accuracy of the product as well as on the machine itself.
2 *Heat generated by the equipment (machine).* Relative movements between different elements of the machine cause heat release in the contact zones. Such heat sources can potentially include bearings; gears and hydraulic oil; various actuators and clutches; guides; pumps and motors. Heat can also be generated by electronic components or other external heat sources.
3 *Cooling-heating systems.* Some mechatronic devices have integrated cooling or heating systems that directly affect temperature phenomena (e.g. cooling emulsion during metal processing; electronic component fans, etc.).
4 *Influence of the working room.* The temperature of premises (room, workshop, thermo-stable laboratories, etc.) where technological machine is located.
5 *Operator's influence.* The heat is generated and transmitted by the operator during the contact with the device.
6 *Thermal influence of the previous environment.* A sudden change in the environment of the element, the machine, or its system is dominated by temperature gradients for some time until the settled temperature is reached.

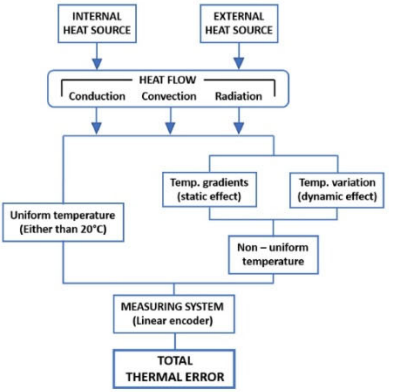

Fig. 1. Thermal effects of integrated measuring system.

According to the diagram of the thermal effects prevailing in machine tools developed by R. Ramesh et al. [8], a universal blocked scheme has been devised, which reveals the formation of thermal errors of integrated measuring systems in mechatronic devices. The scheme is presented in Fig. 1.

The heat flow generated by internal and external temperature sources is transmitted by thermal conductivity, convection and radiation techniques and forms appropriate temperature fields prevailing in the technological installation, including measuring systems. The resulting temperature fields can be homogeneous, i.e. have a constant temperature value. If such a settled temperature value differs from the standard 20 °C, all elements of the machine and measuring system will expand or shrink evenly, depending on their temperature expansion coefficients. Otherwise, temperature gradients start prevailing, which spread different temperatures unevenly. With variable temperature sources or cooling systems integrated in the mechanism, temperature gradients can change

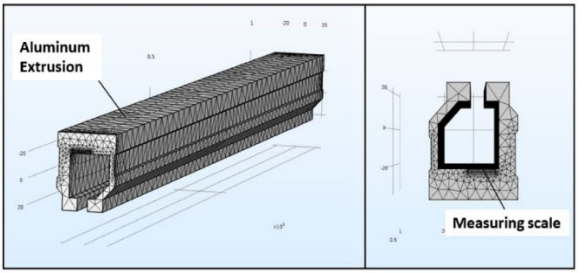

Fig. 2. The 3D model of linear encoder profile and measuring scale divided into finite elements.

dynamically over time. In this case, hysteresis effects have a significant impact.

Since photoelectric linear encoders are the most commonly used displacement measuring systems, understanding of the underlying thermal processes and analysing errors is particularly relevant.

Due to different thermal expansion coefficients and mounting methods, grating of the linear encoder and aluminum housing expands or contracts differently. These processes induce deformations that have direct influence on a displacement measuring accuracy. So thermal errors in linear encoders must be carefully considered.

In typical applications, the thermal behaviour of the linear encoder should match the one of the machine or measured objects. When temperature changes, it must expand or contract in a reproducible manner. On the other hand, in applications of nanotechnology, even a small change in the elements' geometry is crucial. In this case, one of the possible solutions to avoid the influence of temperature changes is to use special materials with minimal thermal expansion coefficients (a glass-ceramic with the expansion coefficient of $0 \pm 0{,}1 \cdot 10^{-6}$ K^{-1}). Another way to deal with thermal errors is compensation. The main idea of this method is to monitor the amount of inaccuracy and compensate it electronically.

Since thermal processes in applications as linear encoders are complicated because of constantly volatile thermal gradients and deviations of thermal coefficients of materials, errors of the measuring system are not repeatable or systematic. That is why it is hard to manage a proper compensation action. But in some cases, where thermal conditions do not change drastically, it would be very convenient to have a linear encoder which compensates its thermal errors in real-time.

3. Computer modelling of temperature fields and thermal errors in linear encoder

Temperature field and thermal error modelling is done by using the finite element method in the "COMSOL Multiphysics" environment. A simplified 3D model of linear encoder's aluminum extrusion together with stainless-steel measuring scale is created. Later, this model is divided into finite tetrahedron elements. This fragmented linear encoder model is shown in Fig. 2.

The modelled thermo-mechanical task consists of the simulation of temperature fields and modelling of mechanical deformations under the influence of found temperature gradients. The first part of the task is solved by using the mathematical package *"Heat transfer in solids"*. The longitudinal stainless-steel tape temperature deformations have a direct influence on encoder measurement accuracy. Such expansion or contraction of the measuring scale is the point of intertest in this work and are found by using the "*Solid Mechanics*" package. Combining these two tasks into a common "*Multiphysics*" task, the right solution is achieved.

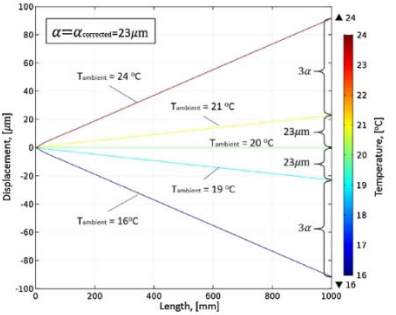

Fig. 3. Total displacement along aluminum extrusion at different uniform ambient temperatures.

3.1. Uniform ambient temperature effect. Determination of corrected coefficient of linear thermal expansion

Analysed optical linear encoder's fragment is composed of 1-meter long aluminum extrusion and a built-in stainless-steel tape with a measuring scale engraved by laser. The linear thermal expansion coefficient of aluminum profile is $\alpha = 23$ μm/m. Used stainless-steel tape has coefficient of $\alpha = 10.5$ μm/m. When measuring scale is mounted into extrusion, these coefficients start to differ due to different mass, geometric parameters and fixing type. Computer simulation, during which whole assembly expansion and contraction are determined at different uniform ambient temperatures, is done. The total displacement along the aluminum profile of linear encoder is plotted in Fig. 3.

As seen in the graph, there is no displacement at 20 °C. This ambient temperature is used as reference and all deformations are calculated according it. When temperature of an environment increases or decreases by one degree Celsius, 1-meter long profile relatively expands or contracts by 23 μm. Such value of the

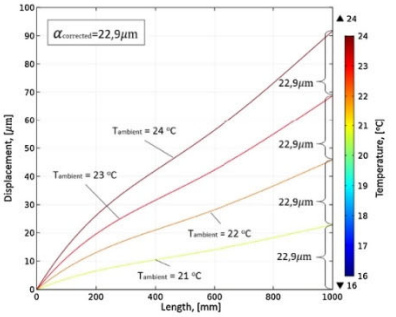

Fig. 4. Total displacement along measuring scale at different uniform ambient temperatures.

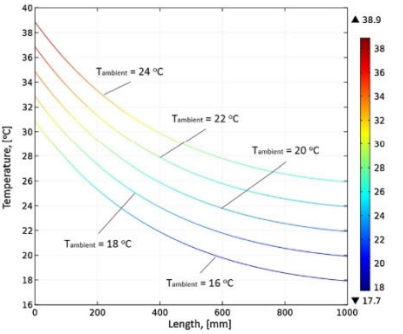

Fig. 5. Temperature distribution along aluminum extrusion at different uniform ambient temperatures, while one end of the encoder is affected by an external 35 °C heat source.

linear thermal expansion stays constant and could be accepted as corrected value: $\alpha = \alpha_{corrected} = 23\ \mu m/m$.

Similar graph is plotted for stainless-steel tape. It could be seen in Fig. 4.

Performed modelling shows, that 1-meter long measuring scale expands 22.9 μm per one degree of Celsius. The thermal expansion coefficient of stainless-steel tape is drastically changed, because the mass and geometric dimensions of the aluminum extrusion is much bigger, comparing with the measuring scale. It is also noticed, that the displacement profile of the measuring scale becomes less linear while ambient temperature increases. It will have impact to real-time compensation procedure, especially at temperatures which are much higher or smaller than 20 °C. However, in a small range of temperature ±5 degrees Celsius, such displacement distribution could be quite accurately approximated by a linear function. The corrected linear thermal expansion coefficient of a measuring scale could be accepted as: $\alpha_{corrected} = 22.9\ \mu m/m$.

3.2. Static thermal effects in linear encoder

When a measuring system is affected by a constant external heat source, a certain temperature gradient is established over time along the encoder's geometry. Such an uneven distribution of temperature fields also influences the occurrence of uneven temperature deformations. Below is an example, where one end of the optical linear encoder is affected by a 35 °C heat source. A steady temperature gradients and total displacements caused by a thermo-elastic deformation are simulated at several different ambient temperatures: 16 °C, 18 °C, 20 °C, 22 °C and 24 °C. Temperature distribution along the aluminum extrusion is plotted in Fig. 5.

Because aluminum is good heat conductor (thermal conductivity 210 W/(mK)), the heat generated by a source is conducted through all 1-meter long extrusion. The profile of temperature gradient maintains similar at each simulated uniform ambient temperature.

Temperature distribution along the measuring scale is plotted in Fig. 6.

Stainless-steel tape thermal conductivity is 30 W/(mK). It is seven times smaller comparing with an aluminum encoder's extrusion. The heat from a source distributes at the end, where it is generated. Temperatures, which are approximately equal to ambient, settle down after ~250 mm length of the measuring scale.

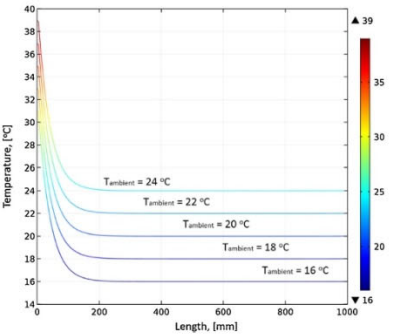

Fig. 6. Temperature distribution along measuring scale at different uniform ambient temperatures, while one end of the encoder is affected by an external 35 °C heat source.

According these simulated temperature gradients, the thermo-elastic deformations caused by them are modelled. Total displacements along aluminum extrusion and measuring scale are respectively plotted in Fig. 7 and Fig. 8.

Presented graphs show that displacements along the analysed encoder parts, caused by a thermo-elastic deformation, distribute differently. However, such distributions maintain approximately the same profile while the ambient temperature is changed, and only the slopes of the graphs vary. This variation is constant and could be linearly approximated by using corrected values of a linear thermal expansion coefficient. Therefore, if the heat generated by an external heat source stays constant, and only the ambient temperature is changing, the once determined displacements could be easily recalculated in real-time if the ambient temperature is known.

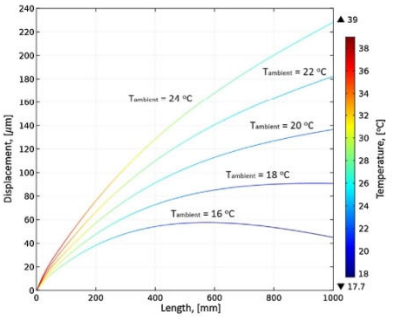

Fig. 7. Total displacement along aluminum extrusion at different uniform ambient temperatures, while one end of the encoder is affected by an external 35 °C heat source.

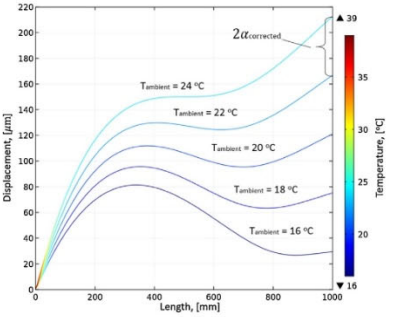

Fig. 8. Total displacement along measuring scale at different uniform ambient temperatures, while one end of the encoder is affected by an external 35 °C heat source.

3.3. Dynamic thermal processes in linear encoder

An experiment was carried out to determine the dynamics of the temperature processes occurring in the measurement system. The obtained data are used to correct the created computer model. During the experiment, with the help of a laboratory furnace, one end of the linear encoder was heated, and the temperature variation observed in real time at four points distanced from the heated end by 150 mm, 450 mm, 750 mm, and 1000 mm respectively.

The experimental scheme is shown in Fig. 9 (a). The equipment used during the tests is shown in Fig. 9 (b):

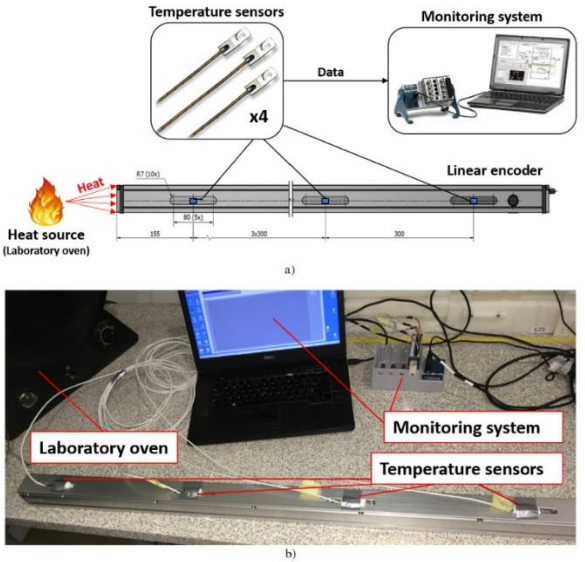

Fig. 9. The scheme of the experiment (a); the picture of the experimental equipment (b).

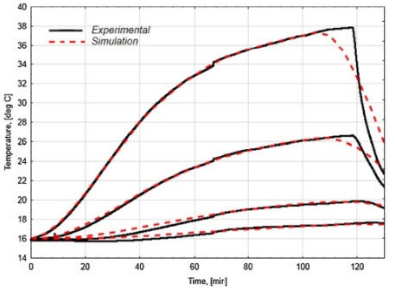

Fig. 10. Data of the experiment and computer simulation.

1 Laboratory furnace.
2 Temperature sensors of resistance type *Tj-PL1; Pt100*.
3 Controller *National Instruments cDAQ-9174*.
4 Input module for temperature sensor data *NI-9217*.
5 Portable computer DELL.

During the experiment, the ambient temperature was ~16 °C. The external heat source was turned on and the end of the encoder was slowly heated for about 120 min. The heating was then switched off and the encoder was left to cool at the ambient temperature. With such an experiment, the dynamics of thermal processes could be monitored when the heat flow spread along the measuring encoder. The cooling process was also monitored, and the effect of hysteresis was evaluated. Experimental and computer modelling data are presented in Fig. 10.

The obtained results demonstrate that the simulation model in the heating section quite accurately reflects the results of the experiment. The maximum error is 0.38 °C. However, there is a discrepancy observed during the cooling of the encoder. This is associated with the changing environmental conditions and coefficients important for modelling.

From the performed simulations, we can see that the modelling of the measuring system integrated in a real application requires a complex FEM model, which must evaluate many factors, such as geometrical form, dimensions and mass of a system, various material and environmental parameters, etc. Since linear displacement measuring systems can have a different design, various measurement lengths and different mounting methods, it is very difficult to evaluate and create a universal model that covers all variables. Complicated approximations and computations require a lot of resources, which makes it a difficult task to realise. The rapid calculation machines can significantly increase the price of a linear encoder, and the small size of the device complicates the integration process.

Therefore, several assumptions are made when evaluating the encoder model for a real-time compensation:

- Since the stainless-steel measuring tape is thin and fixed only at the ends, the contribution of the hysteresis effects therein to the accuracy of the measuring system is not high. They are, therefore, not considered during the compensation process.
- Dynamic thermal processes that occur due to different materials and geometry of the encoder require a sophisticated and highly accurate computer model and are, therefore, not evaluated. Only a well-established temperature gradient and its thermo-elastic deformations are studied.
- The effect of the ambient temperature on the system is assessed.

Below is a simplified error model of the analysed optical linear encoder, based on a static gradient variation analysis and minimisation of temperature and geometric errors.

4. The model of error compensation in measuring system

The essence of error compensation is the calculation of errors according to the changing values of arguments and their deduction from the results of displacement measurement in real-time. For this reason, the dependence of the displacement measurement errors on the displacement size and temperature is determined. These errors are approximated by parametric functions, which compute real-time error compensation values that are deducted from the indications of the displacement measuring system. The error compensation model encompasses thermal and geometric errors.

Linear encoder error δ is considered to be random and, in general, dependent on the measurement displacement q and temperature T. Then, the mathematical model of error is recorded as:

$$\Delta(q,T) = F(q,T) + \varepsilon \tag{1}$$

Where: $F(q, T)$ – parametric function approximating a systematic error component, ϵ – residual random error component.

The error compensation K is equated to the value of the approximating parametric function with the opposite sign of the systematic error component, i.e.

$$K = -F(q,T) \tag{2}$$

When the ambient temperature is constant and unequal to standard, i.e. T = const., $T \neq Tn = 20$ °C, geometric and temperature errors are approximated by parametric functions depending on the two-dimensional argument. Accepting the non-standard temperature constant in accordance with Taylor equation $\delta(q, T)$, the error is recorded by the formula:

$$\delta(q,T) \approx \delta(q,T_0) + \frac{\partial}{\partial T}\delta(q,T)\, I_{T=T_0} \cdot (T - T_0), \tag{3}$$

Where temperature T deviations from the recorded temperature T_0 are insignificant. The parametric function approximating the error analogous to Taylor's equation, is expressed as:

$$F(q,T) = G(q,\ T_0) + K(q,T_0) \cdot (T - T_0) \tag{4}$$

Where: $G(q, T_0)$ – approximation of measurement system errors at set, fixed temperatures (hereinafter geometric errors), when temperature $T = T_0$; $K(q, T)$ – thermal error compensation, when $T = T_0$; T_0 – fixed thermal value.

The equation for the thermal error compensation function $K(q, T_0)$ was obtained after a series of theoretical and experimental studies. From accumulated experience, the error compensation function is written by the equation:

$$K(q,T_0) = Co + C_1 q + C_2 q^2 \tag{5}$$

The thermal error can then be conveniently expressed by the following special function:

$$SF = \left(C_0 + C_1 q + C_2 q^2\right) \cdot (T - T_0),\ 0 \le q \le q_{max} \tag{6}$$

The first member of the equation C_0 represents the displacement of the entire measuring system due to the temperature deformations of the structures on which the measuring system is installed. The second member $C_1 q$ represents the thermal deformation of the measuring scale according to the law of thermal expansion of the metal. Member $C_2 q^2$ reflects more complex deformations of several connected bodies with different linear elongation coefficients.

Table 1
Parameters of thermo-elastic error approximation.

Parameters	Ambient temperature				
	16 °C	18 °C	20 °C	22 °C	24 °C
Standard deviation with respect to approximating function, S_{gr}	±6.14 μm	±2.13 μm	±0.06 μm	±1.52 μm	±2.93 μm
Maximal computer modelled thermo-elastic error	81.42 μm	95.72 μm	121.15 μm	167 μm	212.87 μm

A precision measuring machine approximating the calculation of function parameters must be designed on the basis of the results of the calibration of a measuring system.

$$\delta_j = \delta_{ij} = \delta\left(q_i, T_j\right),\ i = 1, 2, \ldots,\ m;\ j = 1, 2, \ldots,\ n \tag{7}$$

Where: q_i – value of the argument q (displacement), which help to estimate the error δ; T_j – temperature of j realisation.

The mean value is considered as the basic temperature:

$$T_0 = T = \frac{1}{N}\sum_{j=1}^{N} T_j \tag{8}$$

Such a choice of T_0 allows distinguishing the procedures of calculating the parameters of functions G and K. The parameters of functions G and K depend on T_0 value.

The standard deviation is accepted as a parameter for approximation accuracy evaluation.

$$S_p = \sqrt{\frac{1}{N}\sum_{j=1}^{N}\frac{1}{M}\sum_{i=1}^{M}\left[\delta_{ij} - F\left(q_i, T_j\right)\right]^2} \tag{9}$$

For the practical realisation, it is proposed to express the second member of the formula (4) by the sum of two functions. Thus a thermal error compensation is described by a function $F_{gr}(q)$ which depends on a constant heat source caused thermal gradient located in space (along the measuring scale) and $F_a(\Delta T)$ which indicates changes of this gradient slope in time, when ambient temperature varies.

Then, the mathematical model of the error compensation is expressed by the following formula:

$$\Delta(q, T) = F_g(q) + F_{gr}(q) + F_a(\Delta T, q) \tag{10}$$

Where: $F_g(q)$ – geometric error approximation; $F_{gr}(q)$ – thermo-elastic error approximation when thermal gradient is steady and ambient temperature is stable; $F_a(\Delta T, q)$ – thermal error constituent that expresses a linear deformation of the measuring scale under the changing ambient temperature.

$$F_a(\Delta T, q) = \alpha_{corrected} \cdot \Delta T \cdot q \tag{11}$$

Where: $\alpha_{corrected}$ – corrected coefficient of linear thermal expansion of the measuring scale, ΔT – ambient temperature difference from nominal ($\Delta T = T_n - T$), q – measured displacement.

4.1. Approximation of geometric errors

Errors attributable to geometric ones are related to inaccuracies and deformations in the production of measuring systems and also occur due to mounting process. In this case, the error compensation model assumes that the ambient temperature is constant and equal to standard, i.e. $T = Tn$. The error depends on one argument. Such an error is approximated by a single parametric function whose argument is the displacement q:

$$\Delta(q) = F_g(q) + \varepsilon_g \tag{12}$$

The optimal approximating function $F_g(q)$ is chosen depending on the nature of error change. When the error changes in a linear way or directly over the whole interval of displacement, the optimal approximating function is an algebraic polynomial (*API*).

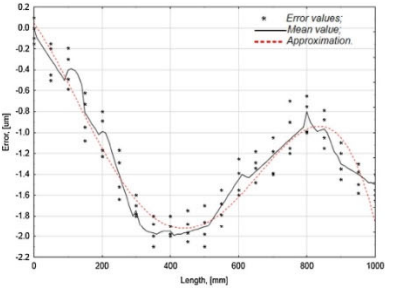

Fig. 11. Dependence of geometric linear encoder error and the approximation of its mean on displacement.

$$F_g(q) = a_0 + a_1 q + \ldots + a_m q^m, \tag{13}$$

The parameters of the approximating function – ($a_0, a_1 \ldots, a_m$).

When the variation of the error is within the range of displacement of different intensity, the optimal approximating function is the algebraic polynomial spline (*SPL1*).

$$F_g(q) = \sum_{i=0}^{m} a_i q^i + \sum_{j-1}^{\nu}\sum_{k=1}^{d} b_{jk}(q - u_j)^{m+1-k} \tag{14}$$

Where: m- spline element, $m = 1, 2\ldots$; γ - number of nodes, (u_1, $u_2 \ldots, u_\gamma$); d – spline defect, $d = 1, 2 \ldots m + 1$

If the error is periodic in the displacement range, the optimal approximating function is the trigonometric polynomial (*TP1*).

$$F_g(q) = \mu + \sum_{j=1}^{m} R_j \cos\left(\frac{2\pi}{T_j} q + \varphi_j\right) \tag{15}$$

The parameters of the approximating function ($\mu, R_1, T_1, \varphi_1 \ldots, R_m, T_m, \varphi_m$).

The geometric error of the measuring system is determined during a calibration process. Displacement measurement values of the tested device is compared with the values given by a laser interferometer or some kind of length etalon. Differences between these measures are considered as the error of the encoder. Usually such a comparation process is done in laboratories with well-defined thermal and dynamic conditions. Assuming that environment affect is minimal, the calculated errors are accepted as geometric.

Analysed linear encoder is tested in thermostable room, where temperature is 20 ± 0.2 °C. It's measures are compared with readings of the laser interferometer. Four realisation values, the mean value and their approximation with the fourth order polynomial are shown in Fig. 11.

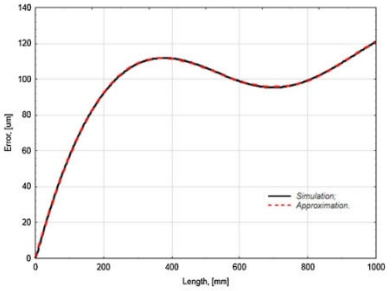

Fig. 12. Computer modelled thermo-elastic error at 20 °C ambient temperature approximated by the fourth order polynomial.

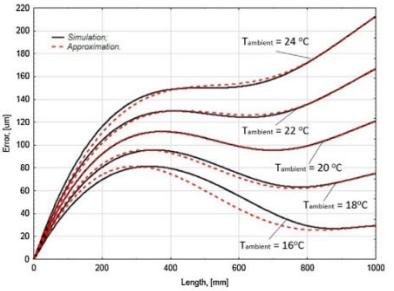

Fig. 13. Computer modelled thermo-elastic error at different ambient temperatures and their approximations by empirical functions.

Equation of the approximating polynomial:

$$F_g(q) = 0,048 - 0,0046q - 1,5734 \cdot 10^{-5} q^2 + 5,0732 \cdot 10^{-8} q^3 - 3,2276 \cdot 10^{-11} q^4 \quad (16)$$

The approximation accuracy could be evaluated by a standard deviation of mean values with respect to the approximating function:

$$S_g = \sqrt{\frac{\sum_{i=0}^{N} (\bar{x}_i - F_{geometic}(q_i))^2}{N}} = \pm 0.122\,\mu m \quad (17)$$

Where: $(\bar{x}_1, \bar{x}_2, \ldots, \bar{x}_N)$ – mean values of calibration process realizations. In order to evaluated ~96% of measurements, standard deviation value is multiplied by 2.1.

$$2.1 \cdot S_g = \pm 0.257\,\mu m \quad (18)$$

4.2. Estimation and approximation of the thermal error

Estimation of the thermal errors consists of temperature gradient measurement along the linear encoder and calculation of the thermo-elastic deformations of the measuring scale by the finite element method.

The thermal fields operating on a linear encoder in a real application are measured by means of temperature sensors. Experimentally measured multiple point temperature data are interpolated and a temperature gradient is obtained along the encoder profile. Later, such a gradient is introduced into a computer model of finite elements. The model evaluates the design of the encoder, the attachment type, etc. According to the measured temperature gradient, temperature deformations of the linear encoder are calculated along the measuring scale. After that, the simulated total displacement values are approximated with a parametric function, which is used to calculate the thermal error size in compensation process.

According to the data presented in Fig. 8, the plot of the thermo-elastic error at 20 °C ambient temperature is conveniently approximated by the fourth order polynomial. This is illustrated in Fig. 12.

The approximating function:

$$F_{gr}(q) = 0.002302 + 0.6764q - 0.001036q^2 - 5.32 \cdot 10^{-7} q^3 + 1.974 \cdot 10^{-9} q^4 - 9.616 \cdot 10^{-13} q^5 \quad (19)$$

The standard deviation that evaluates ~96% of data points is:

$$2.1 \cdot S_{gr} = \pm 0.129\,\mu m (20)$$

The maximum thermo-elastic error value of simulation at 20 °C ambient temperature is ~121 μm. So the meaning of standard deviation is only 0,1% of the maximum thermal error.

Linear encoder errors at other different ambient temperatures could be approximately evaluated by adding a linear deformation of the measuring scale (Eq. 11) to the founded approximating function (Eq. 19). Comparation of calculated functions at 16 °C, 18 °C, 20 °C, 22 °C and 24 °C ambient temperatures and computer modelled values are plotted in Fig. 13.

In this particular case, the accuracy of approximations could be evaluated by the following parameters listed in Table 1.

From the graph (Fig. 13) it is seen, that when the ambient temperature starts to vary from 20 °C the absolute value of the thermo-elastic error changes and the deviation of approximating functions increases. The biggest standard deviation value is ±6.14 μm, at ambient temperature of 16 °C. The biggest modelled error value at this temperature reaches 81.42 μm. The meaning of standard deviation is 7,5% of the maximum error value, which could be compensated by using this method. Evaluating 96% of data points (i.e. $2.1 \cdot S_{gr}$), the maximum deviation of presented thermal error approximation is up to 15% of the maximum compensated value at 16 °C.

In application, where the range of ambient temperatures are well known, the best fit approximating parametric function could be derived not only for a total displacement data at one chosen temperature, but also including multiple other data points of simulation at various ambient temperatures in that range. Or all simulated data could be approximated by a more complex multivariable function *f(q,T)*. This would help to reduce maximum deviation value.

4.3. Total error as real-time compensation size

The total error is found by Eq. (10), by summing the approximating geometric error function (Eq. 16) with the approximating function of the thermal error (Eq. 19) and adding a linear deformation of the measuring scale (Eq. 11). The visual representation of the total analysed linear encoder error is introduced as 3D plot and is shown in Fig. 14.

The illustration indicates the dependence of the amount of total error on the measured displacement and ambient temperature. In order to perform calculations according to this formula, we should have approximations of individual errors, know the value of the

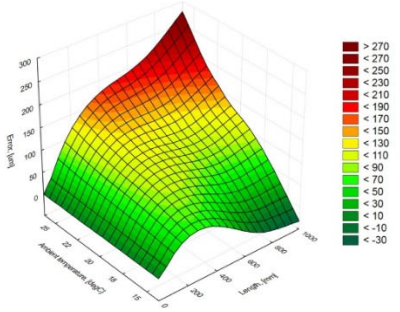

Fig. 14. Dependence of the compensated error on the measured displacement size and ambient temperature.

measured displacement q, which is indicated by the measuring system, and the value of the ambient temperature in one specially selected characteristic point of the encoder profile, which best describes the average temperature variation. This information could be obtained during the operation of the encoder in real-time.

The calculated total error could be considered as a compensation size and has to be respectively added or subtracted from the encoder readings. In cases, when temperatures are higher than nominal, the measuring scale expands, and the optical system of the encoder counts less raster elements of the measuring scale. So the total error values at higher temperatures than nominal should be subtracted from the device readings and added, when total error is calculated for lower temperatures.

The accuracy of the presented compensation model might be generally described as:

$$S_m = \sqrt{S_g{}^2 + S_{gr}{}^2 + S_a{}^2} \quad (21)$$

Where: S_a – standard deviation of a linear deformation of the measuring scale (S_a = 0.182). It depends on the accuracy of used temperature sensor and it's fixing point ability to describe an average temperature of an encoder.

Standard deviation of the compensation model, when the termo-elastic error is approximated with minimal deviation (i.e. at 20 °C, S_{gr} = 0.06 μm):

$$S_m = \pm 0.227\,\mu m \quad (22)$$

When the deviation of termo-elastic error approximation is maximal (i.e. at 16 °C, S_{gr} = 6.14 μm):

$$S_m = \pm 6.144\,\mu m \quad (23)$$

In practical applications, the compensation accuracy highly depends on existing external heat sources and their stability; determination of a settled down thermal gradient; the quality of FEM model and how accurate it represents real conditions; mathematical approximations of the simulated total displacement along the measuring scale; and accuracy of used temperature sensor.

5. Conclusions

The current article analyses the thermal processes occurring in the linear displacement measuring system and thermo-elastic deformations caused by them, when a linear encoder is influenced by heat sources and the changing temperature of the working environment. Having conducted the scholarly literature review, systematised the collected information, as well as having performed calculations and experimental research, the article provides a generalised method of the compensation of the thermal error of photo-electric linear encoder. On the basis of the performed study, the following conclusions are drawn:

1 Under real conditions of linear encoder exploitation, the component of the uncertainty of the displacement measurement is significant and has a big numerical value.
2 The method of finite elements is convenient for the identification of thermal deformations, yet such a computer model is rather complex and difficult to realise in the encoder for the recalculation of the thermo-elastic errors in real-time.
3 The proposed compensation model of the linear encoder displacement measuring errors is based on the approximation of geometric and thermal errors by simple parametric functions and calculations of linear errors according to ambient temperature variations. The compensation value is calculated on the basis of the two-dimensional function, whose arguments are displacement and thermal value calculated at one point of the encoder profile. Such a method is convenient and easily realised using simple technological calculation equipment, which could be integrated in the encoder itself.

References

[1] A. Jakstas, S. Kausinis, R. Barauskas, A. Kasparaitis, A. Barakauskas, Thermal error analysis in precision length measurements, Measurement 51 (May) (2014) 133–146.
[2] C. Jin, B. Wu, Y. Hu, P. Yi, Y. Cheng, Thermal characteristics of a CNC feed system under varying operating conditions, Precis. Eng. 42 (October) (2015) 151–164.
[3] H.-W. Lee, K.-Y. Huang, H.-T. Peng, C.-H. Liu, A real time error measuring device for meso-scale machine tools, Sens. Actuators A Phys. 244 (June) (2016) 213–222.
[4] Y. Li, J. Zhang, D. Su, C. Zhou, W. Zhao, Experiment-based thermal behavior research about the feed drive system with linear scale, Adv. Mech. Eng. 10 (11 (November)) (2018), p. 168781401881235.
[5] Y. Li, W. Zhao, S. Lan, J. Ni, W. Wu, B. Lu, A review on spindle thermal error compensation in machine tools, Int. J. Mach. Tools Manuf. 95 (August) (2015) 20–38.
[6] T. Fei, X. Xu, Z. Zhang, M. An, C. Zhang, Modeling and reduction of thermally induced non-reciprocal error in differential interference fiber optic gyroscope sensing coil, Optik 126 (July (13)) (2015) 1295–1299.
[7] C. Zhang, F. Gao, L. Yan, Thermal error characteristic analysis and modeling for machine tools due to time-varying environmental temperature, Precis. Eng. 47 (January) (2017) 231–238.
[8] R. Ramesh, M. Mannan, A. Poo, Error compensation in machine tools — a review, Int. J. Mach. Tools Manuf. 40 (July (9)) (2000) 1257–1284.
[9] Z. Ge, X. Ding, Design of thermal error control system for high-speed motorized spindle based on thermal contraction of CFRP, Int. J. Mach. Tools Manuf. 125 (February) (2018) 99–111.
[10] M. Liess, H. Karagözoglu, H. Ernst, Reducing thermal transient induced errors in thermopile sensors in ear thermometer applications, Sens. Actuators A Phys. 154 (August (1)) (2009) 1–6.
[11] T.N. Reddy, V. Shanmugaraj, V. Prakash, S.G. Krishna, S. Narendranath, P.V.S. Kumar, Real-time thermal error compensation module for intelligent ultra precision turning machine (iUPTM), Procedia Mater. Sci. 6 (2014) 1981–1988.
[12] T. Liu, et al., Analytical modeling for thermal errors of motorized spindle unit, Int. J. Mach. Tools Manuf. 112 (January) (2017) 53–70.
[13] X. Mao, K. Mao, F. Wang, B. Yan, S. Lei, A convective heat transfer coefficient algorithm for thermal analysis of machine tools considering a temperature change, Int. J. Adv. Manuf. Technol. 99 (November (5–8)) (2018) 1877–1889.
[14] H. Liu, E.M. Miao, X.Y. Wei, X.D. Zhuang, Robust modeling method for thermal error of CNC machine tools based on ridge regression algorithm, Int. J. Mach. Tools Manuf. 113 (February) (2017) 35–48.
[15] J. Wang, C. Zhu, M. Feng, W. Ren, Thermal error modeling and compensation of long-travel nanopositioning stage, Int. J. Adv. Manuf. Technol. 65 (March (1–4)) (2013) 443–450.
[16] Y. Zhao, D.L. Trumper, R.K. Heilmann, M.L. Schattenburg, Optimization and temperature mapping of an ultra-high thermal stability environmental enclosure, Precis. Eng. 34 (January (1)) (2010) 164–170.
[17] J. Wang, C. Zhu, M. Feng, W. Ren, Thermal error modeling and compensation of long-travel nanopositioning stage, Int. J. Adv. Manuf. Technol. 65 (March (1–4)) (2013) 443–450.

[18] I. Alejandre, M. Artes, Thermal non-linear behaviour in optical linear encoders, Int. J. Mach. Tools Manuf. 46 (October (12–13)) (2006) 1319–1325.
[19] Z.-D. Zhou, L. Gui, Y.-G. Tan, M.-Y. Liu, Y. Liu, R.-Y. Li, Actualities and development of heavy-duty CNC machine tool thermal error monitoring technology, Chinese J. Mech. Eng. 30 (September (5)) (2017) 1262–1281.
[20] Z.-S. Yan, W.-H. Lin, C.-H. Liu, Measurement of the thermal elongation of high speed spindles in real time using a cat's eye reflector based optical sensor, Sens. Actuators A Phys. 221 (January) (2015) 154–160.
[21] B. Tan, et al., A thermal error model for large machine tools that considers environmental thermal hysteresis effects, Int. J. Mach. Tools Manuf. 82–83 (July) (2014) 11–20.
[22] Y. Echerfaoui, A. El Ouafi, A. Chebak, Experimental investigation of dynamic errors in coordinate measuring machines for high speed measurement, Int. J. Precis. Eng. Manuf. 19 (August (8)) (2018) 1115–1124.
[23] T. Li, F. Li, Y. Jiang, H. Wang, Thermal error modeling and compensation of a heavy gantry-type machine tool and its verification in machining, Int. J. Adv. Manuf. Technol. 92 (October (9–12)) (2017) 3073–3092.
[24] J. Bryan, International status of thermal error research (1990), CIRP Ann. Manuf. Technol. 39 (2) (1990) 645–656.

Biographies

Donatas Gurauskis holds MSc in mechanical engineering. Doctoral dissertation topics related to research of precision measurement systems.

Artūras Kilikevičius received the PhD degrees in Technological Science from Vilnius Gediminas Technical University, Lithuania, in 2009. He is director of Institute of Mechanical Science (MMI) at Vilnius Gediminas Technical University, Faculty of Mechanics, and teaching professor. Research interests include Vibrations and Acoustics; biomechanics and dynamics of human musculo-skeletal system, Dynamic System Analysis; Control and Mechatronics; Signal Processing and Measurements; Applied Mechanics (theoretical, numerical, and experimental study of the response of solids and fluids to external forces); Measurement and dynamics of precise mechatronic systems.

Sergejus Borodinas received the PhD degree from Vilnius Pedagogical University in 1998. He is currently a senior researcher in Institute of Lithuanian University of Educational Sciences, assoc. prof. of Civil Engineering faculty in Vilnius Gediminas Technical University (VGTU) and Head of the Department of Applied Mechanics (VGTU). His research interests include driving and control of ultrasonic piezoelectric systems, mechatronic systems modelling and process simulation, microcontroller systems, piezomechatronic systems design and optimization.

Albinas Kasparaitis graduated Kaunas University of Technology (former KPI) in 1967 and obtained Degree of Engineer in Precision Machine Tools. He graduated with a candidate of Technical Science Degree (Ph.D.) from KTU in 1972 and later received the degree of Doctor of Habilitation from Moscow Machine-Instrument Institute (Moscow) in 1991. He currently works in company Precizika Metrology and is a Professor at Vilnius Gediminas Technical University. His main research interests include accuracy analysis and synthesis of precision mechatronic measurement systems, system design and development of measurement methodologies. He was actively involved in developing form measurement and precision displacement measurement systems, coordinate measurement machines and precision calibration units.

Article 2. Gurauskis et al. (2021). Thermal and Geometric Error Compensation Approach for an Optical Linear Encoder (https://doi.org/10.3390/s21020360)

sensors

MDPI

Article

Thermal and Geometric Error Compensation Approach for an Optical Linear Encoder

Donatas Gurauskis [1,*], Artūras Kilikevičius [2] and Albinas Kasparaitis [1]

[1] Department of Mechanical and Material Engineering, Vilnius Gediminas Technical University, J. Basanavičiaus g. 28, 03224 Vilnius, Lithuania; albinas.kasparaitis@vgtu.lt
[2] Institute of Mechanical Science, Vilnius Gediminas Technical University, J. Basanavičiaus g. 28, 03224 Vilnius, Lithuania; arturas.kilikevicius@vgtu.lt
* Correspondence: donatas.gurauskis@vgtu.lt

Abstract: Linear displacement measuring systems, like optical encoders, are widely used in various precise positioning applications to form a full closed-loop control system. Thus, the performance of the machine and the quality of its technological process are highly dependent on the accuracy of the linear encoder used. Thermoelastic deformation caused by a various thermal sources and the changing ambient temperature are important factors that introduce errors in an encoder reading. This work presents an experimental realization of the real-time geometric and thermal error compensation of the optical linear encoder. The implemented compensation model is based on the approximation of the tested encoder error by a simple parametric function and calculation of a linear nature error component according to an ambient temperature variation. The calculation of a two-dimensional compensation function and the real-time correction of the investigated linear encoder position readings are realized by using a field programmable gate array (FPGA) computing platform. The results of the performed experimental research verified that the final positioning error could be reduced up to 98%.

Keywords: measuring scale; thermoelastic deformation; coefficient of thermal expansion

Citation: Gurauskis, D.; Kilikevičius, A.; Kasparaitis, A. Thermal and Geometric Error Compensation Approach for an Optical Linear Encoder. *Sensors* **2021**, *21*, 360. https://doi.org/10.3390/s21020360

Received: 3 December 2020
Accepted: 5 January 2021
Published: 7 January 2021

1. Introduction

The vast majority of industrial and scientific applications use optical encoders for a position measurement and closed-loop position control, for example, machine tools [1–5], tracking systems [6–8], industrial robots [9–13], positioning stages [14–17], and so on. All these technological machines work under various environment conditions such as temperature, humidity, mechanical vibration, etc. In turn, these effects inevitably generate a corresponding error. According to Ramesh et al. [18,19], the thermal factors account for 40–70% of the total dimensional and shape errors in machine tools. Much scientific research has been performed to analyze, model, and compensate the influence of thermal positioning error in manually or computer-numerical-control (CNC) machines [20–28]. The majority of this research analyzes only the machine tool structure, considering that the used measurement system is not the source of the error by itself [29].

Working environment adversely affects the accuracy of the integrated encoder. Lopez et al. investigate optical encoder errors under vibration at different mounting conditions [30] and optical scanning principles [31]. They also present a methodology for a vibration error compensation [32]. Performance of the encoder could be improved by correcting its output signals in real-time. This could be done by using look-up tables, digital filtering, or other techniques [33–37]. These methods help to reduce a high frequency sub-divisional encoder error that repeats at each period of a scale grating. Temperature changes introduce strains that change the width of a grating period. Therefore, the thermal errors could not be compensated by using these techniques.

The thermal behavior of the encoder is also a very important factor. One way to deal with a changing temperature impact is by using low thermal coefficient (CTE) materials. Glass ceramics like ZERODUR (CTE = 0 ± 0.1 µm/m°C) or ROBAX (CTE = ~ 0 µm/m°C) are used for a measuring scale manufacturing. Another way is trying to match the thermal coefficients between used linear encoder, machine tool support, and a workpiece material. In this case, the change in a workpiece size has the same value as the expanded or contracted encoder, so the thermoelastic error is practically eliminated. A well-defined and reproducible thermal behavior of the encoder must be ensured. Unfortunately, it is quite challenging task to do. For example, an enclosed type linear encoder consists of an aluminum extrusion and a measuring scale, usually made from glass or stainless steel. The scale is attached to extrusion by adhesive or a double-sided adhesive tape. Such an assembly demonstrates a complex thermal behavior because of the combination of different CTE materials. Alejandre et al. [38] present the method to determine the real thermal coefficient of a linear encoder. In this research, they investigate an enclosed-type linear encoder and established that the real CTE is influenced by the bonding material between the aluminum extrusion and the glass scale. Moreover, during another study [39], a non-linear thermal behavior in optical linear encoders was noticed. This could be explained as a consequence of varying stresses transmitted from the extrusion to measuring scale.

The thermal error compensation could be an effective and economic method to improve optical encoder accuracy. This procedure is based on encoder error correction by introducing correction coefficients derived by using various mathematical ways and experimental research. Yu et al. [40] improve the rotary encoder accuracy by using Fourier expansion-polynomial fitting technique. In 2020, Jia et al. [41] proposed the compensation approach based on Fourier expansion-back propagation neural network technique optimized by a genetic algorithm. This group of scientists minimized rotary encoder error from 110.2 arc sec to 2.7 arc sec. Hu et al. [42] used the empirical mode decomposition and the linear least square fitting methods for a linear encoder error compensation at different temperatures. In general, there is not much information about the real thermal behavior of optical encoders and their accuracy under a real ambient condition. Even less information is published about a practical realization capability of the embedded error compensation solution.

In a previous work [43], the theoretical investigation of the linear encoder thermal behavior was done using the finite element method. The performed computer simulation analyzed the occurring thermal processes and introduced thermoelastic deformations, when a linear encoder is influenced by various heat sources and the changing temperature of the working environment. The results showed that the analyzed encoder demonstrated systematic behavior, which could be approximated by a simple parametric function. This could be used to compensate the final encoder position value, in order to improve its accuracy.

In this work, the real-time geometric and thermal error compensation approach is proposed. The article is based on theoretical and experimental research of the tested optical linear encoder and practical realization of the composed compensation algorithm. The presented method is optimized by experimentally estimating actual CTE of the linear encoder under test and could reduce the thermoelastic error to the accuracy range specified by the manufacturer. In Section 2, the error compensation background is discussed. Section 3 presents the setup used for the experimental investigation. Equipment used for the tested encoder accuracy measurement at different ambient temperatures and the composed subsequent electronics which realize the error compensation in real-time are specified. Obtained results and performed compensation algorithm optimization, based on a real CTE calculation, are described in Section 4. The discussion about the collected data and a short summary are written in Section 5. In Section 6, the main findings and conclusions are listed.

2. The Error Compensation Method for Linear Encoder

The accuracy of the encoder is one of the most significant parameters. This term describes the difference between the target position (real position value) and actual position—

the encoder position reading. Mathematically, the position reading of the encoder Q could be expressed as:

$$Q = Q_{real} + \delta, \quad (1)$$

where Q_{real}—is a real linear position value, δ—is an error component. Therefore, the accuracy of the encoder is directly related to the size of a measurement error and is sometimes called the position error. In practice, the encoder accuracy measurement is a specific procedure that requires a well-calibrated equipment and a certain environmental condition. The calibrating encoder readings are compared with a reference device position indication, which are accepted as a real position value Q_{real}. Usually, second, a highly accurate encoder or a laser interferometer is used as a reference.

According to ISO 5725-1, when the accuracy term is applied to sets of measurements of the same measurand, it involves a component of systematic error and a component of random error [44]. In this case, the term "trueness" is used to describe the closeness of the mean of a set of measurement results to the actual value and term "precision" is used to describe the closeness of agreement among a set of results. In practice, the trueness is accepted as the accuracy of the encoder and the precision is used to describe the repeatability or reproducibility of the device. In general, linear encoder error δ depends on the position q and the temperature T. Then, the mathematical model of the error is written as:

$$\Delta(q, T) = F(q, T) + \varepsilon, \quad (2)$$

where $\Delta F(q, T)$—parametric function approximating a systematic error component, ε is the residual random component. In optical linear encoders, glass or stainless steel scales with a precise grating patterns are used for a linear position measurement. The manufacturing inaccuracies, like a varying duty cycle of the grating; any kind of scale deformations during the encoder assembly or mounting procedure; and a thermal expansion or contraction of the encoder due to ambient temperature or other temperature sources cause the systematic error component that could be measured, approximated by a parametric function and compensated. The error compensation K is equated to the systematic error component approximating function value with an opposite sign, i.e.,

$$K = -F(q, T). \quad (3)$$

Other effects, like accidental mechanical vibrations or a shock, dust, metal chips or any other contaminants on the measuring scale surface, etc. represent the random error component and cannot be easily compensated.

Theoretically, the simplified mathematical error model for compensation could be expressed as:

$$\Delta(q, T) = F_g(q) + F_{gr}(q) + F_\alpha(\Delta T, q), \quad (4)$$

where the first member is $F_g(q)$—geometric error approximation function. The calibration process of the encoder is done at nominal temperature $T_n = 20\ ^\circ C$, in a special thermostable laboratory room, where ambient temperature varies only about $\pm 0.2\ ^\circ C$. Tested encoder error values are plotted in graph according to the linear position values. Such a plot is called an encoder accuracy graph and is added to each manufactured encoder as a document to ensure the accuracy of the calibrated device. In this case, the compensation model assumes, that the ambient temperature stays constant and is equal to a nominal $T = T_n$. The calibrated encoder error plot is approximated by a single parametric function whose argument is the position value q.

$$\Delta(q) = F_g(q) + \varepsilon_g, \quad (5)$$

The second member $F_{gr}(q)$—thermoelastic error approximation, when thermal gradient is steady and ambient temperature is stable. In real applications, there are various temperature sources around the measuring system. Those sources generate a relative temperature gradient along the encoder. That causes an unwanted deformation of the

measuring scale. Estimation of the approximating thermal error function consists of the temperature gradient measurement by means of temperature sensor values in multiple points along the encoder, and calculation of the thermoelastic deformation of the measuring scale by the finite element method. The simulated total displacement values of the scale are approximated by a single parametric function, which is later used to estimate the thermal gradient error size in compensation process.

The third member $F_a(\Delta T, q)$—thermal error component—expresses a linear deformation of the measuring scale due to changing ambient temperature.

$$F_a(\Delta T, q) = \alpha_{corrected} \cdot \Delta T \cdot q, \quad (6)$$

where $\alpha_{corrected}$—corrected coefficient of linear thermal expansion (CTE) of the measuring scale and ΔT—ambient temperature difference from the nominal temperature ($\Delta T = T_n - T$).

The total error value calculated according the Equation (4) could be considered as a size for the real-time compensation. The determined compensation value at specific position should be relatively added or subtracted from the encoder position readings, in order to get the compensated position value.

3. Experimental Setup

The prototype absolute linear optical encoder LK50 of the company JSC "Precizika Metrology" was chosen for the experimental research. It is a reflective type optical encoder with a measuring scale pattern engraved onto the stainless steel tape surface by a laser. The tape is fitted into the encoder's aluminum extrusion, stretched by using a special rigid spring based mechanism and tightened at both ends. Another stainless steel tape is used as a guideway for a precise positioning and motion of the scanning carriage. The cross-sectional view of the tested optical linear encoder is shown in Figure 1.

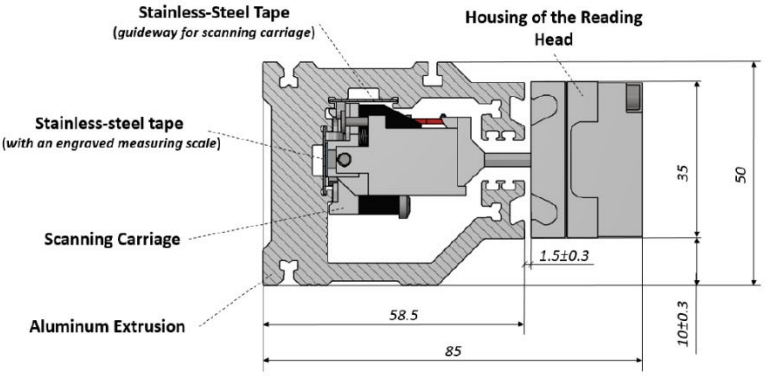

Figure 1. Cross-sectional view of the tested optical linear encoder LK50.

The main parameters of the tested encoder, such as dimensions, measuring length and so on, are specified in Table 1.

In order to investigate the thermal behavior of the encoder, all experiments were carried out in a laboratory room, where the stable ambient temperature could be maintained. The specially customized technological stand was used for encoder mounting and imitation

of an appropriate reading head motion along the measuring scale. The aluminum extrusion of the tested encoder was mounted onto the stainless steel support fixed on the granite base. The extrusion was attached with only one fixing screw in the middle of its length. In this way, the ends of the encoder could freely move during the thermal expansion and contraction. The reading head is attached to a moving carriage with an aerostatic bearing.

Table 1. Parameters of tested optical linear encoder.

Concept	Value	Units
Measuring length (ML)	1200	mm
Accuracy (to any meter within the ML)	±5	µm/m
Resolution	0.1	µm
Interface	BiSS-C	-
Aluminum extrusion	Dimensions: 50 × 58.5 × 1485	mm × mm × mm
	Thermal coefficient (CTE): 23×10^{-6}	m/(m °C)
Stainless steel tape	Dimensions: 12 × 0.5 × 1440	mm × mm × mm
	Thermal coefficient (CTE): 10.5×10^{-6}	m/(m °C)

During the tests, readings of the linear encoder were compared to a linear position indication of the laser calibration system "Keysight 5530". The interferometer assembly was placed at the end of the technological stand. The retroreflector assembly is located at the moving carriage. To avoid uncertainties and compensate laser measuring system errors due to changing temperature, the "E1736A USB Sensor Hub" and relatively mounted temperature sensors "E1737A" were used. The composed experimental setup is shown in Figure 2.

The content of the used experimental setup is listed in Table 2 according the position numbers marked in Figure 2.

Table 2. Content of the experimental setup.

Position	Object
1	Granite base
2	Stainless steel support (for encoder mounting)
3	Moving carriage (with aerostatic bearings)
4	Optical linear encoder (device under test)
5	Fixing screws (for encoder reading head)
6	Fixing screw (for encoder aluminum extrusion)
7	Subsequent electronics (for error compensation)
8	Ambient temperature sensor (E1738A)
9	Laser (5519A/B)
10	Interferometer assembly (linear interferometer, linear retroreflector, base, height adjuster, and post)
11	Retroreflector assembly (linear retroreflector, post and height adjuster, base)
12	Temperature sensors (E1737A)
13	USB sensor hub (E1736A)
14	USB axis module (E1735A)
15	PC (with an appropriate software)

Considering the linear position compensation implementation into a real application, the response of the encoder becomes an important factor. For incremental encoders, the response is limited to a specific input signal frequency. The latency depends on the analog amplifier bandwidth, interpolation process, and the resolution. In practical applications, the incremental interface encoder latency is usually ignored, given that the edges of digital output signals have the real-time nature [45]. Unfortunately, the thermal error compensation process realization in incremental encoder is a hard task, because the output signals did not contain any information about the absolute position. They indicate the size of the reading head linear displacement. The absolute linear encoders usually consist of low resolution absolute position track and high resolution incremental track. The combination

of the two tracks determines the absolute position value with a high resolution. These data are given on the demand of an application controller by a serial interface. The data transmission time depends on the bit length and overall speed.

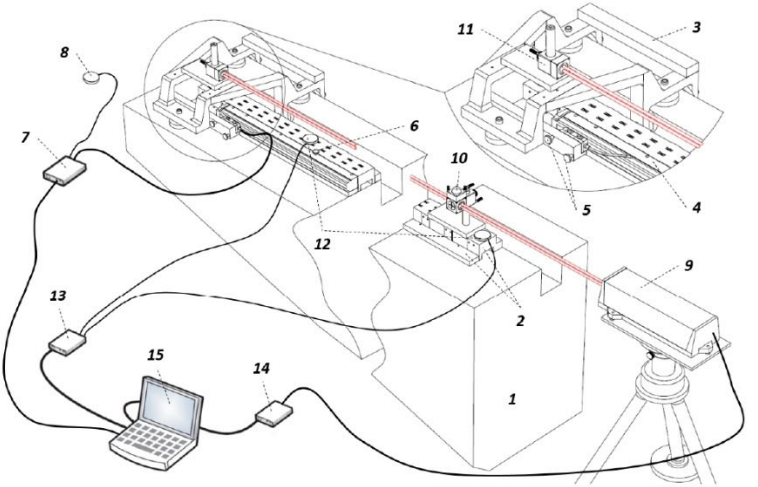

Figure 2. Experimental setup based on "Keysight 5530" system configured for a linear measurement.

The selected absolute optical linear encoder transmits its position by using a bidirectional synchronous serial interface BiSS. Usually it is used in industrial applications, where high transfer rates are required [46]. Depending on cable length, the encoder could handle clock frequencies up to 4 MHz and the calculation time is ≤ 5 µs. The maximum traversing speed is limited up to 2 m/s. The chosen resolution position is outputted with a 30-bit format. Taking into account the calculation time, the absolute position is transmitted upon ≤ 13 µs. Thermal and geometric encoder error compensation is realized by using the composed subsequent electronics. The programmable gate array (FPGA) platform "S7 Mini" with "Xilinx Spartan-7 7S25" is used as a master to request and get the linear encoder position readings, calculate the compensation value according to an integrated mathematical algorithm and external ambient temperature sensor data, and output the compensated position at the real-time. The vanishingly small calculation time of the FPGA could perform the compensation process almost instantly. If the compensation is processed by subsequent electronics, the FPGA has to receive, recognize, compensate, and generate the absolute position value. The whole process takes approximately double the time of the encoder transmission time. In this case, a compensated position is outputted ≤ 26 µs. If the proposed mathematical algorithm could be installed into the integrated FPGA or other controller, the calculation time might be drastically reduced.

The measuring length of the tested linear encoder is 1200 mm. The rectilinear velocity of the moving carriage is 0.2 m/s. To reduce the uncertainty and maintain the reproducibility of the successive measurements, the digital incremental encoder signals are also recorded. According the counted edges of these signals, the absolute position request is

sent to the encoder at every 1000 counts i.e., at each 0.1 mm. In such a way, there are 12,000 equally spaced measured positions along the linear encoder.

Additionally, the "Texas Instruments" THVD 1451 RS-485 transceivers are used to deal with differential encoder CLOCK and DATA signals. The simplified block diagram of the composed compensation electronics is shown in Figure 3.

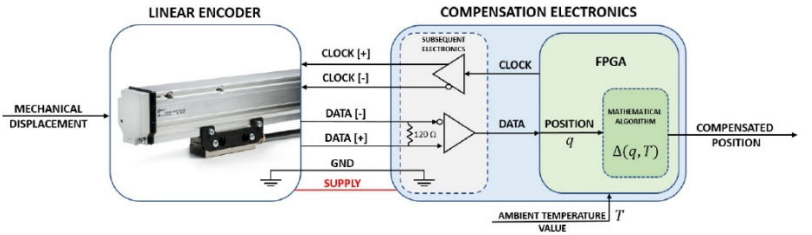

Figure 3. Block diagram of the compensation electronics with a field-programmable gate array (FPGA).

The encoder readings, compensated encoder position values, and respective indications of the laser interferometer measuring system are recorded simultaneously during all experiments. Collected data are processed by using a numerical computing software environment "MATLAB" for the estimation of approximating function, further data analyzation, and graphical representation.

4. Results

Firstly, the whole experimental setup was left in the laboratory room at fixed nominal ambient temperature $T_n = 20 \pm 0.2$ °C for 5 h to stabilize. During the tests, the ambient temperature was changed, so this stabilization process was repeated four times, at each settled temperature (i.e., 20 °C, 17.8 °C, 22.6 °C , and 25.3 °C). Because in the laboratory room there were a number of electronic components which generate approximately the same amount of heat all the time, it is stated that along the linear encoder existed a steady thermal gradient. Temperature differences in various part of the encoder induced thermoelastic deformations of the measuring scale. Encoder mounting could also be the source of the linear position measurement error, because of misalignment or deformations during fixation, lack of support stiffness, inaccurate guideway of the carriage, and so on. All these factors introduced the geometric error component. These conditions are relatively close to some of a real application, where such an encoder could be used.

Five separate unidirectional measurements are taken at each temperature. The average value of these five measurements is calculated. Based on standard ISO 230-2, the half peak-to-peak value of the resulting average position error curve is accepted as the unidirectional systematic positioning error of the encoder. The compensation and minimization of this systematic error is the main goal of this work.

The first five measurements at 20 °C ambient temperature were recorded. The error values at corresponding positions and the average meaning curve are presented in Figure 4. The unidirectional systematic positioning error of the encoder was ±2.2 µm. This value is accepted as the accuracy of non-compensated tested encoder.

The parametric function approximating the average position error curve could be accepted as the combination of the geometric $F_g(q)$ and the thermoelastic $F_{gr}(q)$ error components, i.e., the sum of the first two members of the Equation (4). The fitted approximating function is shown in Figure 5.

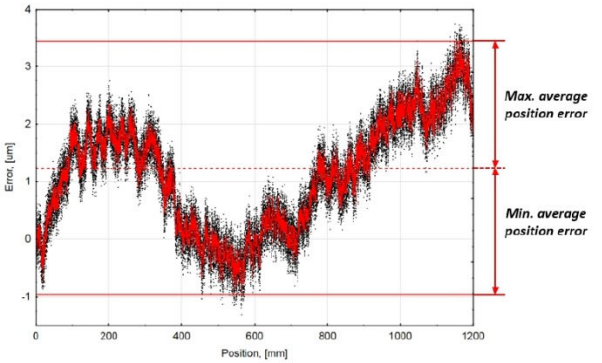

Figure 4. Accuracy graph at 20 °C ambient temperature. (Black dots—the measured error values at corresponding positions; Red curved line—the resulting average position error curve).

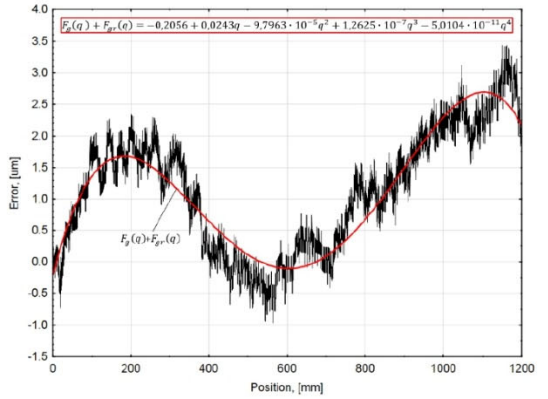

Figure 5. Average accuracy graph at 20 °C ambient temperature approximated by a parametric function. (Red line—approximating function and its equation).

The graph data are quite accurately approximated by a 4th order polynomial function that could be described by the following equation:

$$F_g(q) + F_{gr}(q) = F_G(q) = -0.2056 + 0.0243q - 9.7963 \times 10^{-5}q^2 + 1.2625 \times 10^{-7}q^3 - 5.0104 \times 10^{-11}q^4, \quad (7)$$

This determined function was used as a base for the further thermal and geometric error compensation value calculation. The approximating function was integrated into compensation electronics (FPGA), and the five measurements were repeated. The accuracy graph of an average position error of the compensated linear encoder is shown in Figure 6.

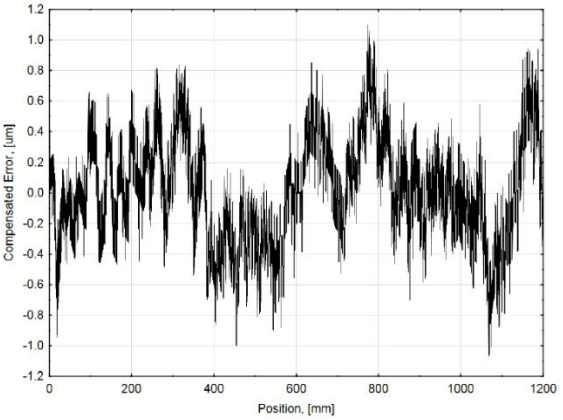

Figure 6. Average accuracy graph of compensated tested encoder at 20 °C ambient temperature.

In order to minimize encoder error at different ambient temperatures, the third component of the general error Equation (4) must be found. The mechanical construction and the thermal behavior of the linear encoder were investigated in a previous work [43] by using the finite element method (FEM). The computer simulation showed that the linear thermal expansion coefficient (CTE) of the measuring scale was greatly changed because of its fixing type, mass, and geometry differences between the scale and the extrusion, etc. Due to these reasons, the CTE of the scale was increased up to $\alpha_{corrected} = 22.9\ \mu m/(m\ ^\circ C)$. This value was used for the third member calculation, according the Equation (6). The ambient temperature difference from the nominal temperature was calculated according to the mean value of several external temperature sensor readings. The mathematical algorithm was supplemented and integrated into compensation electronics for other experiments at different ambient temperatures. The average uncompensated linear encoder accuracy graphs and the compensation functions, calculated according the mathematical algorithm, are combined in Figure 7.

How accurately the derived function describes the average uncompensated encoder error was evaluated by a standard deviation of error meanings with respect to the determined function.

$$\sigma_G = \sqrt{\frac{\sum_{i=0}^{N}(\overline{x_i} - F_G(q_i))^2}{N}}, \quad (8)$$

where σ_G—a standard deviation, $(\overline{x_1}, \overline{x_2}, \ldots, \overline{x_N})$—values of calibration process realizations, q_i—value of the argument q (linear position), which help to estimate the compensation function value F_G, and N—number of realizations. To evaluate ~96% of measurements, the standard deviation was multiplied by 2.1. Both values for each ambient temperature are listed in Table 3.

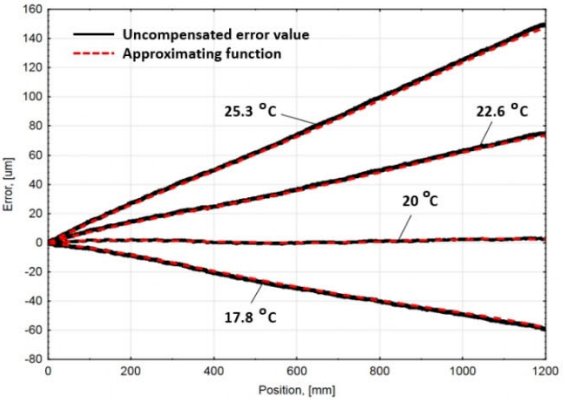

Figure 7. Combined average accuracy graph of uncompensated linear encoder average error at different ambient temperatures, and their compensation functions calculated according the presented mathematical algorithm.

Table 3. Parameters of approximating function and compensated tested encoder accuracy graphs.

Parameter	Ambient Temperature			
	17.8 °C	**20 °C**	**22.6 °C**	**25.3 °C**
Accuracy of approximating function (by mean of standard deviation)	±0.98 µm	±0.34 µm	±1.02 µm	±1.40 µm
Std. dev. of ~96% measurements (Std. dev. multiplied by 2.1)	±2.06 µm	±0.72 µm	±2.14 µm	±2.94 µm
Maximal error value (Non-compensated encoder)	0.07 µm	3.43 µm	75.47 µm	150.03 µm
Minimal error value (Non-compensated encoder)	−60.09 µm	−0.96 µm	0.01 µm	0.15 µm
Average accuracy of non-compensated encoder	±30.08 µm	±2.20 µm	±37.74 µm	±75.09 µm
Maximal error value (Compensated encoder)	0.57 µm	1.10 µm	2.51 µm	3.26 µm
Minimal error value (Compensated encoder)	−2.48 µm	−1.07 µm	−0.73 µm	0.64 µm
Average accuracy of compensated encoder	±1.52 µm	±1.08 µm	±1.62 µm	±1.95 µm

After applying the specified functions, the compensation electronics gave corrected position values. The average compensated linear encoder accuracy graphs and corresponding average uncompensated error values are shown in Figure 8.

The main indicators, such as maximum and minimum values and unidirectional systematic encoder error (average encoder accuracy), etc., are listed in Table 3.

4.1. Estimation of the Real Thermal Coefficient

The accuracy of the compensating value calculation highly depends on how precisely the approximating function is fitted to measured data. Unfortunately, the higher order polynomials or even more complex interpolation functions could cause a practical problem with their integration and calculation time. More efficient and more expensive calculation platforms could be needed. Another way to improve the precision of the presented

approach is to estimate the real coefficient of the linear thermal expansion (CTE). Because the mounting of the tested encoder during the performed experiments allows the free axial movement (the encoder could freely expand and contract), the real CTE estimation could be done by analyzing the experimental data of average uncompensated encoder error values.

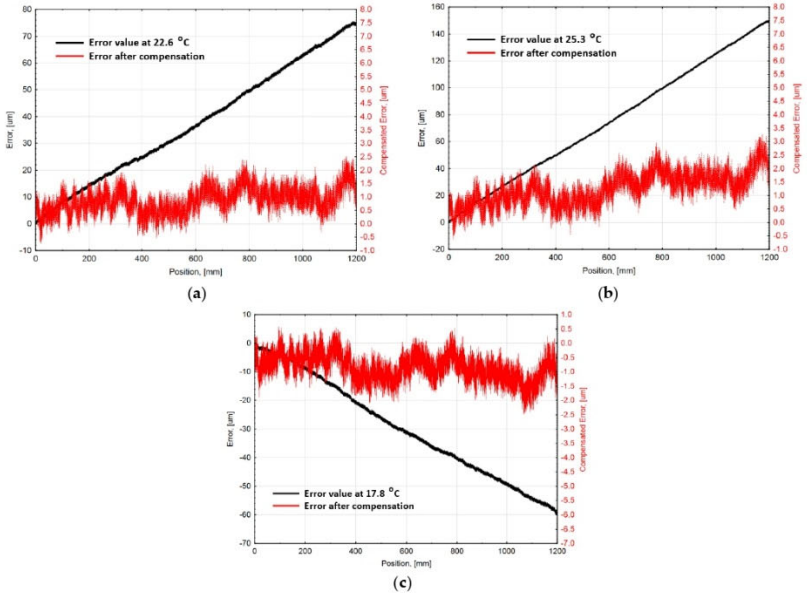

Figure 8. Compensated linear encoder average accuracy graphs (red line/right Y-axis units) with corresponding uncompensated error values (black line/left Y-axis units), at different ambient temperatures: (**a**) at 22.6 °C; (**b**) at 25.3 °C; and (**c**) at 17.8 °C.

The average accuracy graphs obtained at stable 17.8 °C and 22.6 °C ambient temperatures were taken. For a detailed interpretation, both graphs are represented in Figure 9a. The difference between the values of the graphs was calculated at every particular position and plotted in Figure 9b. The received meanings of the differences were approximated with the linear regression line, whose equation is:

$$y = 0.1111q + 1.011, \tag{9}$$

where y—approximated value of the differences, q—is the position value, number 0.1111 is a constant that represents the slope of the linear regression line, and constant 1.011 is the ordinate at the origin.

The real CTE α_{Real} is estimated as the ratio between the determined approximating line slope and the span of ambient temperatures [38]:

$$\alpha_{Real} = \frac{0.1111}{22.6 - 17.8} = 23.15 \left[\frac{\mu m}{m \cdot °C}\right], \tag{10}$$

The calculated value of the CTE is slightly different compared to the simulated $\alpha_{corrected}$. This determined value is greater than the theoretical thermal coefficient, which was used in FEM simulation as aluminum extrusion material property (23×10^{-6} m/(m°C). This suggests that the real CTE of aluminum extrusion is greater. In the literature, the CTE of the aluminum varies from 23×10^{-6}m/(m°C) to 24×10^{-6}m/(m°C). Such an experimental result allows to improve the computer model and the precision of the presented compensation algorithm.

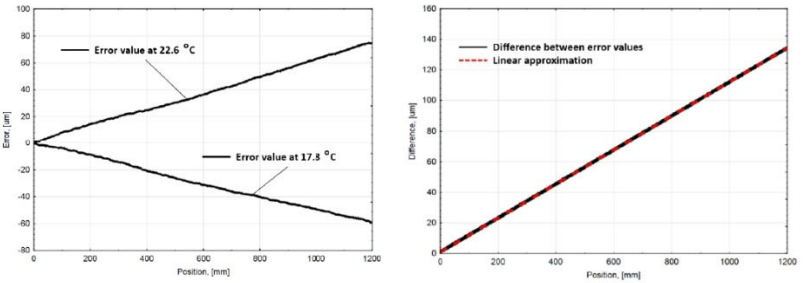

(**a**) (**b**)

Figure 9. (**a**) Accuracy graphs of uncompensated linear encoder at 17.8 °C and 22.6 °C; (**b**) Differences between accuracy graphs and linear fitting line to the difference.

4.2. Recalculation of the Compensated Results According to the Real CTE

The presented compensation algorithm was adjusted by including the estimated real thermal coefficient into the Equation (6). The compensated error values at different ambient temperatures were calculated and subtracted from the average uncompensated encoder values, recorded during the experiments. This allowed to determine the influence of the introduced changes and compare it to the performed test data. The recalculated compensated error graphs are shown in Figure 10.

The accuracy of approximating compensation functions based on a standard deviation and the parameters of compensated encoder errors are listed in Table 4.

Table 4. Parameters of approximating function and theoretically calculated encoder accuracy graphs (including experimentally estimated real thermal coefficient).

Parameter	Ambient Temperature		
	17.8 °C	**22.6 °C**	**25.3 °C**
Accuracy of approximating function (by mean of standard deviation)	±0.69 µm	±0.67 µm	±0.65 µm
Std. dev. of ~96% measurements (Std. dev. multiplied by 2.1)	±1.45 µm	±1.41 µm	±1.35 µm
Maximal error value (Compensated encoder)	0.95 µm	1.88 µm	1.92 µm
Minimal error value (Compensated encoder)	−1.89 µm	−1.04 µm	−1.04 µm
Compensated encoder accuracy	±1.42 µm	±1.46 µm	±1.48 µm

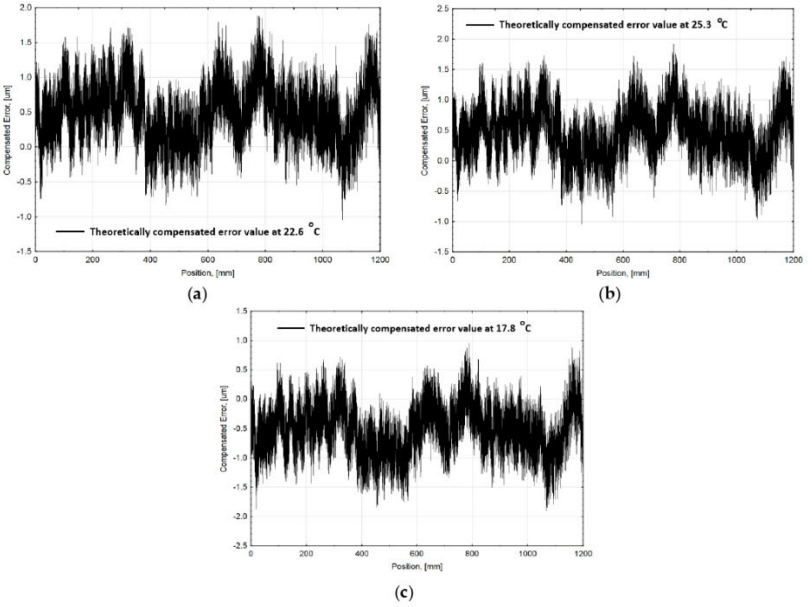

Figure 10. Theoretically recalculated compensated linear encoder accuracy graphs at different ambient temperatures: (**a**) at 22.6 °C; (**b**) at 25.3 °C; and (**c**) at 17.8 °C.

5. Discussion

The proposed mathematical algorithm is based on the approximation of geometric and thermoelastic linear encoder error by a simple parametric function and calculation of linear nature thermal error component in accordance to varying ambient temperature. Based on previous work's [46] accomplished computer modeling results and the practical tests, such a compensation technique was adapted to the selected linear optical encoder.

Performed experiments demonstrated that the designed subsequent electronics are suitable for the realization of the presented compensation approach. An FPGA-based calculation platform properly read tested linear optical encoder position value and compensated it according the installed mathematical function. All processes were performed in real-time; therefore, it could be applied into an industrial, scientific, or other technological application.

The experimental results demonstrate that geometric and introduced thermoelastic linear position measurement error could be drastically reduced:

- At nominal 20 °C ambient temperature, measured encoder average accuracy was ±2.20 µm. After the average position error graph approximation and position compensation, the recorded error was minimized to ±1.08 µm. The approximation accuracy evaluating ~96% measured positions reached ±0.72 µm.
- At different ambient temperatures (17.8 °C; 22.6 °C and 25.3 °C), encoder average accuracy respectively reached ±30.08 µm; ±37.74 µm, and ±75.09 µm without compensation. Applied mathematical algorithm at these temperatures could approximate encoder error correspondingly: ±2.06 µm; ±2.14 µm, and ±2.94 µm. Considering that

the maximal error value reaches up to ~150 µm, the average accuracy of approximation was accepted as reasonable.

- After the position compensation process, the average encoder accuracy at different temperatures was determined as the following: ±1.52 µm (at 17.8 °C); ±1.62 µm (at 22.6 °C), and ±1.95 µm (at 25.3 °C). Considering that the specified accuracy of a standard encoder is ±5 µm per meter, the compensated average encoder accuracy (including the uncertainty of the approximation at different temperatures) was within this range. It can be stated that the performance of the encoder remained under different thermal environmental conditions.
- The presented algorithm could be optimized according to experimentally estimated real CTE value. Embedding this value into the compensation allowed to improve the accuracy of the encoder error approximation which in turn decreased the total error. Theoretical calculations show that the encoder accuracy could reach: ±1.42 µm (at 17.8 °C); ±1.46 µm (at 22.6 °C); and ±1.48 µm (at 25.3 °C).

6. Conclusions

The approach of a thermal and geometric error compensation for a linear encoder is introduced in this article. Having designed the suitable technological equipment, performed experimental research, and analyzed the systematized results, the following conclusions are drawn:

1. The thermoelastic linear encoder deformation caused by external heat sources and changing ambient temperature is significant. Considering the linear thermal expansion coefficient, which greatly depends on an encoder design and used materials, and the working environment conditions, the linear position measurement uncertainty could have a big numerical value. This could lead to undesirable performance of the encoder or even a whole application.
2. The proposed error compensation model is suitable for thermoelastic and geometric error compensation. The performed experiments show that the introduced tested encoder error could be significantly reduced up to 98%. Usage of this kind's compensation might be cheaper and more appropriate solution compared to others, like encoder design including close to zero thermal expansion materials or control of working environment temperature.
3. The compensation algorithm implementation into FPGA-based calculation platform demonstrates the reliable performance. Such hardware selection can ensure an appropriate calculation speed for a real-time application. Due to its flexibility and low cost, it is possible to integrate this device into encoder design or use it like a subsequent electronics module.

However, certain details still exist that require in depth theoretical and experimental research, such as the dynamically changing temperature gradients, different encoder designs, and mounting methods, etc.

Author Contributions: D.G. designed and composed the experimental setup, contributed to the experiments, and wrote the paper; A.K. (Artūras Kilikevičius) performed the experiments and collected and processed the data; A.K. (Albinas Kasparaitis) supervised the research. All authors have read and agreed to the published version of the manuscript.

Funding: This research received no external funding.

Institutional Review Board Statement: Not applicable.

Informed Consent Statement: Not applicable.

Data Availability Statement: Not applicable.

Conflicts of Interest: The authors declare no conflict of interest.

Abbreviations

The following abbreviations are used in this manuscript:

CTE	Coefficient of Thermal Expansion
FPGA	Field-programmable Gate Array

References

1. Zhao, L.; Cheng, K.; Chen, S.; Ding, H.; Zhao, L. An approach to investigate moiré patterns of a reflective linear encoder with application to accuracy improvement of a machine tool. *Proc. Inst. Mech. Eng. Part B J. Eng. Manuf.* **2018**, *233*, 927–936. [CrossRef]
2. Bai, Q.; Liang, Y.; Cheng, K.; Long, F. Design and analysis of a novel large-aperture grating device and its experimental validation. *Proc. Inst. Mech. Eng. Part B J. Eng. Manuf.* **2013**, *227*, 1349–1359. [CrossRef]
3. Liu, C.; Jywe, W.; Hsu, T. The application of the double-redheads planar encoder system for error calibration of computer numerical control machine tools. *Proc. Inst. Mech. Eng. Part B J. Eng. Manuf.* **2004**, *218*, 1077–1089. [CrossRef]
4. Gao, W.; Kim, S.W.; Bosse, H.; Haitjema, H.; Chen, Y.; Lu, X.D.; Knapp, W.; Weckenmann, A.; Estler, T.; Kunzmann, H. Measurement technologies for precision positioning. *Cirp Ann. Manuf. Technol.* **2015**, *64*, 773–796. [CrossRef]
5. Ishii, N.; Taniguchi, K.; Yamazaki, K.; Aoyama, H. Performance improvement of machine tool by high accuracy calibration of built-in rotary encoders. In Proceedings of the 9th International Conference on Leading Edge Manufacturing in 21st Century, Hiroshima City, Japan, 13–17 November 2017.
6. Xie, L.-B.; Qiu, Z.-C.; Zhang, X.-M. Development of a 3-PRR precision tracking system with full closed-loop measurement and control. *Sensors* **2019**, *19*, 1756. [CrossRef]
7. Tang, T.; Chen, S.; Huang, X.; Yang, T.; Qi, B. Combining load and motor encoders to compensate nonlinear disturbances for high precision tracking control of gear-driven Gimbal. *Sensors* **2018**, *18*, 754. [CrossRef]
8. Chong, K.K.; Wong, C.W.; Siaw, F.; Yew, T.; Ng, S.; Liang, S.; Lim, Y.; Liong, L.S. Integration of an on-axis general sun-tracking formula in the algorithm of an open-loop sun-tracking system. *Sensors* **2009**, *9*, 7849–7865. [CrossRef]
9. Algburi, R.N.A.; Gao, H. Health assessment and fault detection system for an industrial robot using the rotary encoder signal. *Energies* **2019**, *12*, 2816. [CrossRef]
10. Han, Z.; Jianjun, Y.; Gao, L. External force estimation method for robotic manipulator based on double encoders of joints. *IEEE Int. Conf. Robot. Biomim.* **2018**. [CrossRef]
11. Peng, L.; Xiangpeng, L. Common sensors in industrial robots: A review. *J. Phys. Conf. Ser.* **2019**, *1267*, 012036.
12. Mikhel, S.; Popov, D.; Mamedov, S.; Klimchik, A. Advancement of robots with double encoders for industrial and collaborative applications. In Proceedings of the 23rd Conference of Open Innovations Association (FRUCT), Bologna, Italy, 13–16 November 2018; pp. 246–252.
13. Rodriguez-Donate, C.; Osornio-Rios, R.A.; Rivera-Guillen, J.R.; Romero-Troncoso, R.J. Fused smart sensor network for multi-axis forward kinematics estimation in industrial robots. *Sensors* **2011**, *11*, 4335–4357. [CrossRef] [PubMed]
14. Kimura, A.; Gao, W.; Hosono, K.; Shimizu, Y.; Shi, L.; Zeng, L. A sub-nanometric three-axis surface encoder with short-period planar gratings for stage motion measurement. *Precis. Eng.* **2012**, *36*, 576–585. [CrossRef]
15. Lee, C.B.; Kim, G.H.; Lee, S.K. Design and construction of a single unit multi-function optical encoder for a six-degree-of-freedom motion error measurement in an ultraprecision linear stage. *Meas. Sci. Technol.* **2011**, *22*, 105901. [CrossRef]
16. Li, Y.T.; Fan, K.C. A novel method of angular positioning error analysis of rotary stages based on the Abbe principle. *Proc. Inst. Mech. Eng. Part B J. Eng. Manuf.* **2018**, *232*, 1885–1892. [CrossRef]
17. Lou, Z.F.; Hao, X.P.; Cai, Y.D.; Lu, T.F.; Wang, X.D.; Fan, K.C. An embedded sensors system for real-time detecting 5-DOF error motions of rotary stages. *Sensors* **2019**, *19*, 2855. [CrossRef]
18. Ramesh, R.; Mannan, M.A.; Poo, A.N. Error compensation in machine tools—A review: Part I: Geometric, cutting-force induced and fixture-dependent errors. *Int. J. Mach. Tools Manuf.* **2000**, *40*, 1235–1256. [CrossRef]
19. Ramesh, R.; Mannan, M.A.; Poo, A.N. Error compensation in machine tools—A review: Part II: Thermal errors. *Int. J. Mach. Tools Manuf.* **2000**, *40*, 1257–1284. [CrossRef]
20. Mareš, M.; Horejš, O.; Havlik, L. Thermal error compensation of a 5-axis machine tool using indigenous temperature sensors and CNC integrated Python code validated with a machined test piece. *Precis. Eng.* **2020**, *66*, 21–30. [CrossRef]
21. Mareš, M.; Horejš, O. Modelling of cutting process impact on machine tool thermal behaviour based on experimental data. *Procedia Cirp* **2017**, *58*, 152–157. [CrossRef]
22. Zaplata, J.; Pajor, M. Piecewise compensation of thermal errors of a ball screw driven CNC axis. *Precis. Eng.* **2019**, *60*, 160–166. [CrossRef]
23. Li, Y.; Zhao, J.; Ji, S.; Liang, F. The selection of temperature-sensitivity points based on K-harmonic means clustering and thermal positioning error modeling of machine tools. *Int. J. Adv. Manuf. Technol.* **2019**, *100*, 2333–2348. [CrossRef]
24. Polyakov, A.N.; Parfenov, I.V. Thermal error compensation in CNC machine tools using measurement technologies. *J. Phys. Conf. Ser.* **2019**, *1333*, 062021. [CrossRef]
25. Yao, X.; Hu, T.; Yin, G.; Cheng, C. Thermal error modeling and prediction analysis based on OM algorithm for machine tools spindle. *Int. J. Adv. Manuf. Technol.* **2020**, *106*, 3345–3356. [CrossRef]

26. Tan, F.; Deng, C.; Xiao, H.; Luo, J.; Zhao, S. A wrapper approach-based key temperature point selection and thermal error modeling method. *Int. J. Adv. Manuf. Technol.* **2020**, *106*, 907–920. [CrossRef]
27. Lei, M.; Yang, J.; Wang, S.; Zhao, L.; Xia, P.; Jiang, G.; Mei, X. Semi-supervised modeling and compensation for the thermal error of precision feed axis. *Int. J. Adv. Manuf. Technol.* **2019**, *104*, 4629–4640. [CrossRef]
28. Shi, X.; Wang, W.; Mu, Y.; Yang, X. Thermal characteristics testing and thermal error modeling on a worm gear grinding machine considering cutting fluid thermal effect. *Int. J. Adv. Manuf. Technol.* **2019**, *103*, 4317–4329. [CrossRef]
29. Alejandre, I.; Artes, M. Machine tool errors caused by optical linear encoders. *Proc. Inst. Mech. Eng. Part B J. Eng. Manuf.* **2004**, *218*, 113–122. [CrossRef]
30. Lopez, J.; Artes, M.; Alejandre, I. Analysis of optical linear encoder's errors under vibration at different mounting conditions. *Measurement* **2011**, *44*, 1367–1380. [CrossRef]
31. Lopez, J.; Artes, M.; Alejandre, I. Analysis under vibrations of optical linear encoders based on different scanning methods using an improved experimental approach. *Exp. Tech.* **2012**, *36*, 35–47. [CrossRef]
32. Alejandre, I.; Artes, M. Method for the evaluation of optical encoders performance under vibration. *Precis. Eng.* **2007**, *31*, 114–121. [CrossRef]
33. Albrecht, C.; Klock, J.; Martens, O.; Schumacher, W. Online estimation and correction of systematic encoder line errors. *Machines* **2017**, *5*, 1. [CrossRef]
34. Mendenhall, M.H.; Windover, D.; Henins, A.; Cline, J.P. An algorithm for the compensation of short-period errors in optical encoders. *Metrologia* **2015**, *52*, 685. [CrossRef]
35. Ye, G.; Fan, S.; Liu, H.; Li, X.; Yu, X.; Yu, H.; Shi, Y.; Yin, L.; Lu, B. Design of a precise and robust linearized converter for optical encoders using a ratiometric technique. *Meas. Sci. Technol.* **2014**, *25*, 12. [CrossRef]
36. Yandayan, T.; Geckeler, R.D.; Just, A.; Krause, M.; Akgoz, S.A.; Aksulu, M.; Grubert, B.; Watanabe, T. Investigation of interpolation errors of angle encoders for high precision angle metrology. *Meas. Sci. Technol.* **2018**, *29*. [CrossRef]
37. Wang, Y.; Liu, Y.; Yan, X.; Chen, X.; Lv, H. Compensation of Moire fringe sinusoidal deviation in photoelectric encoder based on tunable filter. In Proceedings of the Engineering, Computer Science 2011 Symposium on Photonics and Optoelectronics (SOPO) NA, Wuhan, China, 16–18 May 2011. [CrossRef]
38. Alejandre, I.; Artes, M. Real thermal coefficient in optical linear encoders. *Exp. Tech.* **2004**, *28*, 18–22. [CrossRef]
39. Alejandre, I.; Artes, M. Thermal non-linear behaviour in optical linear encoders. *Int. J. Mach. Tools Manuf.* **2006**, *46*, 1319–1325. [CrossRef]
40. Yu, L.D.; Bao, W.H.; Zhao, H.N.; Jia, H.K.; Zhang, R. Application and novel angle measurement error compensation method of circular gratings. *Opt. Prec. Eng.* **2019**, *27*, 1719–1726.
41. Jia, H.K.; Yu, L.D.; Jiang, Y.Z.; Zhao, G.N.; Cao, J.M. Compensation of rotary encoders using Fourier expansion-back propagation neural network optimized by genetic algorithm. *Sensors* **2020**, *20*, 2603. [CrossRef]
42. Hu, F.; Chen, X.; Cai, N.; Lin, Y.J.; Zhang, F.; Wang, H. Error analysis and compensation of an optical linear encoder. *IET Sci. Meas. Technol.* **2018**, *12*, 561–566. [CrossRef]
43. Gurauskis, D.; Kilikevičius, A.; Borodinas, S.; Kasparaitis, A. Analysis of geometric and thermal errors of linear encoder for real-time compensation. *Sens. Actuators A Phys.* **2019**, *296*, 145–154. [CrossRef]
44. ISO 5725-1: 1994 (R2018). Accuracy (Trueness and Precision) of Measurement Methods and Results—Part 1: General Principles and Definitions. Available online: https://www.iso.org/standard/11833.html (accessed on 6 January 2021).
45. Fast and Simple Measurement of Position Changes. Available online: https://www.ichaus.de/upload/pdf/WP2en_EncoderInterface_14082012.pdf (accessed on 27 November 2020).
46. BiSS Interface. Available online: https://biss-interface.com/ (accessed on 27 November 2020).

Article 3. Gurauskis, D. et. al. (2020). Experimental Investigation of Linear Encoder`s Subdivisional Errors under different scanning speeds
(https://doi.org/10.3390/app10051766)

applied sciences

MDPI

Article

Experimental Investigation of Linear Encoder's Subdivisional Errors under Different Scanning Speeds

Donatas Gurauskis [1,*], Artūras Kilikevičius [2] and Sergejus Borodinas [3]

1 Department of Mechanical and Material Engineering, Vilnius Gediminas Technical University, LT-03224 Vilnius, Lithuania
2 Institute of Mechanical Science, Vilnius Gediminas Technical University, LT-03224 Vilnius, Lithuania; arturas.kilikevicius@vgtu.lt
3 Department of Applied Mechanics, Vilnius Gediminas Technical University, LT-10223 Vilnius, Lithuania; sergejus.borodinas@vgtu.lt
* Correspondence: donatas.gurauskis@vgtu.lt

Received: 27 January 2020; Accepted: 28 February 2020; Published: 4 March 2020

check for updates

Featured Application: The methodology described in the manuscript could be useful in a field of industrial automation for subdivisional linear-encoder error estimation and the improvement of final application performance in which the tested encoder is used.

Abstract: Optical encoders are widely used in applications requiring precise displacement measurement and fluent motion control. To reach high positioning accuracy and repeatability, and to create a more stable speed-control loop, essential attention must be directed to the subdivisional error (SDE) of the used encoder. This error influences the interpolation process and restricts the ability to achieve a high resolution. The SDE could be caused by various factors, such as the particular design of the reading head and the optical scanning principle, quality of the measuring scale, any kind of relative orientation changes between the optical components caused by mechanical vibrations or deformations, or scanning speed. If the distorted analog signals are not corrected before interpolation, it is very important to know the limitations of the used encoder. The methodology described in this paper could be used to determine the magnitude of an SDE and its trend. This method is based on a constant-speed test and does not require high-accuracy reference. The performed experimental investigation of the standard optical linear encoder SDE under different scanning speeds revealed the linear relationship between the tested encoder's traversing velocity and the error value. A more detailed investigation of the obtained results was done on the basis of fast Fourier transformation (FFT) to understand the physical nature of the SDE, and to consider how to improve the performance of the encoder.

Keywords: optical encoder; subdivisional error; resolution

1. Introduction

Optical encoders are usually the most reliable devices for precise displacement measurement and motion control. Due to their high accuracy, resolution, and repeatability, as well as their ability to work under different environmental conditions and their relatively low price, they are used in a variety of applications. Some examples are manually controlled machine tools and computer-numerical-control (CNC) machines [1–4], robotics [5–10], servosystems [11–14], monitoring and fault diagnosis systems [15–18], tracking systems [19,20], linear and rotary positioning stages [21–24], and other precision-positioning applications [25].

The overall accuracy and precision of the linear encoder mainly depend on the quality of the measuring scale graduation and nonlinear subdivisional error (SDE) in one signal period [26]. Standard photoelectric linear encoders typically have a measuring scale with a period of 20 or 40 µm [27,28]. In order to increase resolution, two analog electric signals generated by an encoder are converted to digital and interpolated [29,30]. The smallest increment that can be detected may then reach the nanometer level. High accuracy and resolution are very important for applications that require precise positioning and good repeatability. In some applications, a linear encoder is used not only for position estimation, but also to provide feedback for speed control. A higher resolution ensures more stable and accurate position and speed loop.

The SDE (also called the interpolation error) is a cyclic error that repeats with each period of encoder grating. It depends on the quality of a main measuring scale and of the generated electric signals. This error appears during the interpolation process because the encoder's distorted analog electric signals prevent the formation of a fine quadrature signal. In practice, the SDE does not cause any issues until its magnitude reaches the size of a measuring step. In other words, the magnitude of the SDE is a limit for the highest resolution. The minimal measurable incremental step has no point if the position error is greater. It is particularly important for applications requiring precise positioning and repeatability. In machines of which the feed axes or rotation tables are direct-driven, these nonlinear interpolation errors can cause not only positioning inaccuracies, but also result in loud noise, additional heat generation, and speed ripple [31].

The quality of the electrical signals highly depends on various aspects, like the optical-scanning principle, the design of a reading head and its ability to handle various deformations [32], mechanical vibrations [33–35], or temperature variations [36,37]. In order to improve signal quality and to make encoders more robust, manufacturers use advanced optical-scanning methods such as the single-field or interferential scanning principle [38,39], or they implement special-configuration multiple-track analyzer grating to eliminate higher-order harmonic signals [40]. Unfortunately, all such improvements require more complex encoder configurations and expensive optical parts. Another way to minimize SDE is electronic-signal correction. Nonideal signal parameters, such as relative amplitude, DC offset, phase shift, and nonsinusoidal shape, must be corrected before the interpolation process. Many studies dealt with this problem by using digital filtering and look-up tables, or by creating different algorithms for offline and dynamic compensation [41–45]. Because SDE is a short-range error that repeats each period, its compensation is a hard task.

It is very important to know the actual limits of the used displacement-measurement encoder so that the application can work smoothly and be properly tuned. SDE is one of the parameters that should be investigated first, especially if the electrical signals of the encoder are not corrected or compensated before an interpolation process. The methodology presented in this paper allows the estimation of interpolation-error magnitude and its trend across one period. The performed experimental investigation of the particular standard linear encoder interpolation error under different scanning speeds showed that the magnitude of this low-frequency error highly depends on the traversing speed of the encoder's reading head. Moreover, a detailed harmonic analysis of the SDE could help to understand the physical nature of the error, and improve the performance of the encoder and the whole application.

2. Metrological Process and Subdivisional Errors in Optical Encoders

Optical linear encoders use various types of optical-scanning principles (e.g., Talbot effect [46,47], Lau effect [48,49], Moiré effect [50–52], generalized grating imaging [53–56], interferometric [57–59]) to generate electric-output signals that are used to determine a precise position. Depending on subsequently used electronics, optical encoders can have different interfaces to ensure the reliable exchange of information [60]. One of the most widely used interfaces for incremental position measurement is two analog nearly sinusoidal voltage signals (Figure 1). Signals A and B are shifted by 90 electrical degrees and have an amplitude of typically 1 Vpp. One full period (360 electrical degrees)

of these signals corresponds to a period of grating on the measuring scale. Using the arctangent algorithm, it is easy to determine the relative position inside the period:

$$Xposition = \frac{p}{2\pi} arctan\left(\frac{S_A}{S_B}\right), \quad (1)$$

where *Xposition*, relative position between measuring scale and reading head; p, the period of the main scale; and S_A, S_B, values of output signals A and B in a certain position, respectively.

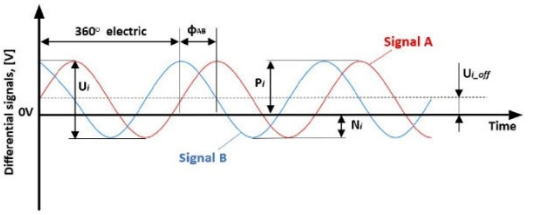

Figure 1. Definition of differential optical encoder signals. 1 Vpp interface.

Such a process is known as interpolation, and it is directly related to the quality of the signals. The 1 Vpp interface is mainly used in applications where such an interpolation and analog-signal digitalization processes are executed by the subsequent electronics of the end-user equipment.

Combining analog encoder signals into the *X* and *Y* axes of an oscilloscope, it is comfortable to observe and follow the quality and accuracy of the encoder. The ideal signals give a perfectly centered circular shape with a diameter corresponding to signal amplitude. Unfortunately, in real applications, encoder output signals are distorted due to imperfections in manufacturing, and assembly and optical-scanning operations, as well as negatively affected by variations of environmental conditions. Distortion of the signals causes SDE, which repeats in each period of the encoder grating. Variations of the signal background level (U_{A_off}, U_{B_off}) are usually caused by imperfections or contaminants of the encoder measuring scale. Different signal offsets could also be related to the improper adjustment of electronic parts. Such a distortion leads to a decentered Lissajous curve, as shown in Figure 2a. Different peak-to-peak amplitudes (U_A, U_B) of the A and B signals could appear due to uneven or inconsistent illumination of the photodetectors. This error leads to an elliptical Lissajous curve, as shown in Figure 2b. A phase shift from 90 electrical degrees made the curve oval, as shown in Figure 2c. The main reason for this type of error is the tilt between the gratings of the scanning reticle and the main measuring scale. All higher harmonics caused by optical effects and electronics make signals that are not perfectly sinusoidal. This type of error forms a noncircular Lissajous curve, as shown in Figure 2d.

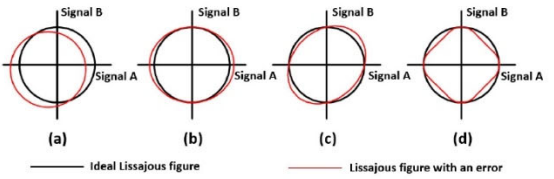

Figure 2. Lissajous curves of optical-encoder signals with relative subdivisional error (SDE): (**a**) offset error; (**b**) amplitude error; (**c**) phase-shift error; (**d**) signal-shape error.

3. Investigation Methodology and Experiment Setup

The magnitude of an SDE is usually determined by using a reference encoder or a laser interferometer. Independent position information from a reference device is compared with a tested linear encoder reading, and the difference between these measures is accepted as the error. In order to perform such a test, a high-accuracy reference is needed.

Another method that was realized in this paper is based on a constant-speed test. The tested encoder reading head was driven at constant speed, and its electric-output signals were recorded using a digital oscilloscope. Because of high sampling frequency, analog encoder signals were represented as a group of discrete points. The relative position values inside one grating period could be calculated by putting these discrete points of A and B signals into Equation (1). Claiming that scanning speed is constant, and knowing the used sampling rate that must be selected by taking into account the Nyquist–Shannon sampling theorem and the acceptable size of the sample, it is easy to compose the theoretically true position values at these points. For example, if the scanning speed is 100 mm/s, the grating period of the tested encoder is 20 µm, and the sampling frequency is 250 MHz, there are 50,000 sampling points per one period. The first point corresponds to a zero position value, and the last one (50,000) corresponds to 20 µm. All other points increase with a step of 0.0004 µm. Then, the calculated values according to the arctangent algorithm could be compared with theoretically determined "true" position values. The differences are accepted as metrological linear encoder errors inside one grating period. In order to obtain statistically reliable results, this procedure must be repeated for several periods or several separate measurements, and the average value must be used. The accuracy of this methodology highly depends on the instability of the scanning speed and the precision of the used equipment. However, this method is completely suitable to determine the magnitude level of the error and to notice its trend.

A standard optical (4-field scanning) linear encoder was selected for this experimental investigation. The special technological setup was designed to determine its metrological errors under different scanning speeds. A motorized translation stage based on direct-drive technology was used to drive-test the encoder's reading head at various constant speeds with high accuracy and low friction. The designed setup is shown in Figure 3.

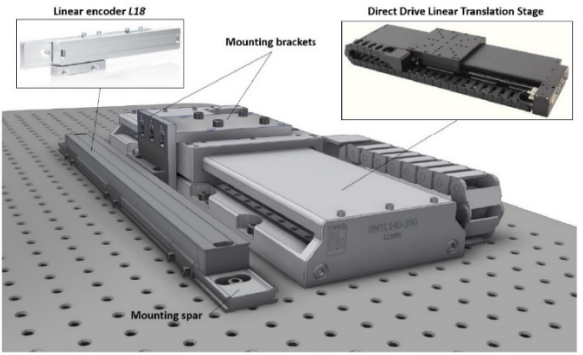

Figure 3. Designed experiment setup. Tested linear encoder was connected to direct-drive linear translation stage through mounting bracket.

The 3-phase ironless linear brushless servo motor of the translation stage was controlled by an ACS servo motion controller with a built-in driver. In the translation stage, an integrated noncontact

linear optical encoder was used as a feedback system for high-resolution positioning and fluent motion control. Electric signals were sampled and recorded by using a digital oscilloscope. Schematic representation of the experiment setup is shown in Figure 4.

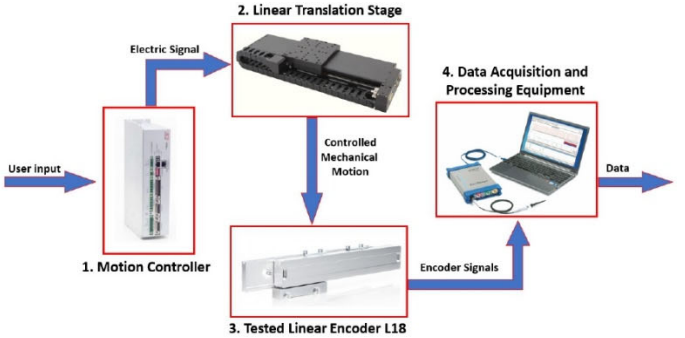

Figure 4. Schematic view of experiment setup.

Experiment setup consisted of:

1. Motion controller: servo motion controller with a built-in driver ACS Motion Control SPiiPlusCMnt.
2. Linear-translation stage: motorized direct drive linear translation stage "STANDA" 8MTL1401-300.
3. Tested linear encoder: optical (4-field scanning) linear encoder Precizika Metrology L18 (measuring length = 300 mm, grating period = 20 µm).
4. Data acquisition and processing equipment. digital oscilloscope PicoScope 3000 and notebook with appropriate software.

Collected data were processed with computer software MATLAB. Determined SDE dependency on different scanning speeds was statistically evaluated by using a linear-regression approach. In order to analyze the nature of these errors at each speed, a fast Fourier transformation (FFT) algorithm was used. Because these errors are cyclic, their harmonic analysis helps to define what kind of signal imperfections cause them. The first harmonic of the SDE is a result of a nonzero background level of the A and B signals. The second harmonic could be caused by unequal amplitudes or a phase shift. Third and higher harmonics are the result of high-order distortions of the electric signals. Usually, they are caused by diffractive effects in optical-light modulation processes. Thus, an error decomposed into harmonics can be mathematically expressed by the following formula:

$$\delta(x) = \sum_{i=1}^{n} (A_i cos(\frac{2\pi}{p} ix + \varphi_i)) + \varepsilon_n \; for \; 0 \le x \le p, \tag{2}$$

where $\delta(x)$ denotes the SDE inside one period of the encoder grating, A_i and φ_i indicate the amplitude and the phase of the harmonic, and x denotes the relative position inside a period p. The number of the harmonic is marked as n, and ε indicates the random error.

4. Results and Discussion

First, performance of the tested linear encoder was checked under different scanning speeds. The maximal traversing velocity specified by a vendor of the encoder was 1 m/s. The Lissajous curves of several signal periods at 100, 500, and 1000 mm/s are shown in Figure 5.

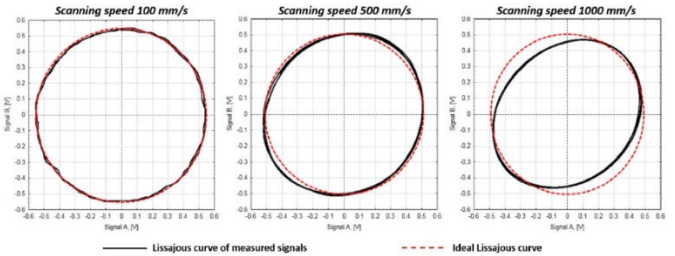

Figure 5. Lissajous curves of several signal periods at different scanning speeds: 100, 500, and 1000 mm/s.

From these graphs, it is clear that encoder performance started to differ when scanning speed was increased. The Lissajous curve changed its size and shape. Higher SDE was introduced. Moreover, several tested signal periods slightly varied from one another. This added additional uncertainty that had to be evaluated. For a more detailed investigation, the reading head of the tested encoder was driven at traversing velocities from 100 to 1100 mm/s with a step of 100 mm/s. The output electric signals were recorded by using a sampling frequency of 250 MHz, and the SDE was determined according to the methodology described in a previous section. Six different signal periods were randomly chosen to calculate the average value of the SDE at each speed level. As an example, the graphical representation of the electric signals and their combination in the X–Y plot when the reading head was driven at 300 mm/s is shown in Figure 6.

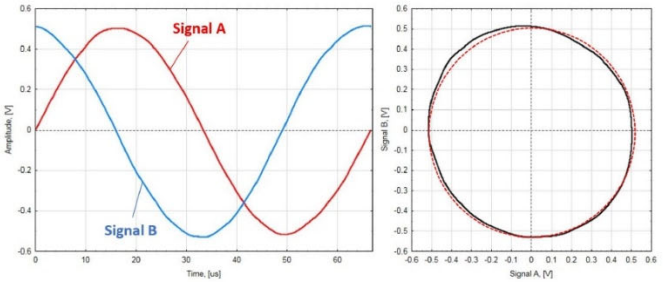

Figure 6. Electric signals A and B and their representation in the X–Y plot. Encoder was working at 300 mm/s traversing velocity.

Calculated average SDE at this speed is shown in Figure 7. FFT analysis showed that the first, second, and third harmonics had the greatest influence on the error amplitude. Therefore, all three first harmonics are shown in the same graph to present the impact of each. The total magnitude of the error was ±0.185 µm. The second harmonic, which was repeated twice per period, created the biggest error value.

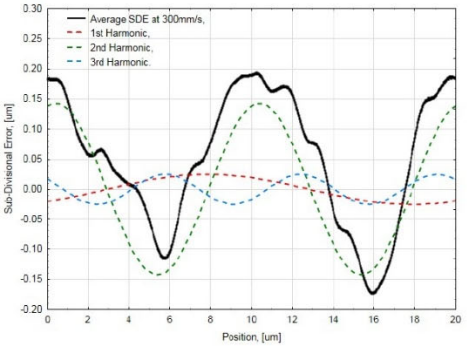

Figure 7. Average SDE and its decomposition into three first harmonics when scanning speed is 300 mm/s.

Similar data processing was made for all tested speeds. Calculated total error values were plotted into one graph, as shown in Figure 8. Results showed a strong linear relationship between scanning speed and total SDE. More than 85% of the experimentally determined error values could be mathematically associated with the increasing traversing speed of the encoder (R-squared = 0.8581). The low *p*-value confirmed that the applied linear-regression model was statistically significant (*p*-value = 0.00004 < 0.05). The biggest error was ±0.52 µm at 1100 mm/s. Two magnitudes at 900 and 1000 mm/s were quite distinct and distinguished from the linear relation.

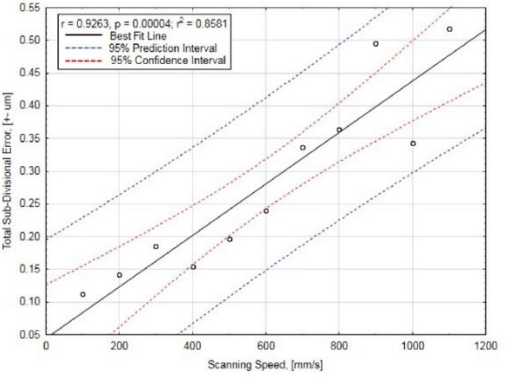

Figure 8. Total SDE dependency on scanning speed. Data points and their statistical parameters.

To understand the physical meaning of the error that occurs during the scanning process, the magnitude and behavior of the first three error harmonics were analyzed. Their dependency on the tested encoder's scanning speed is shown in Figure 9.

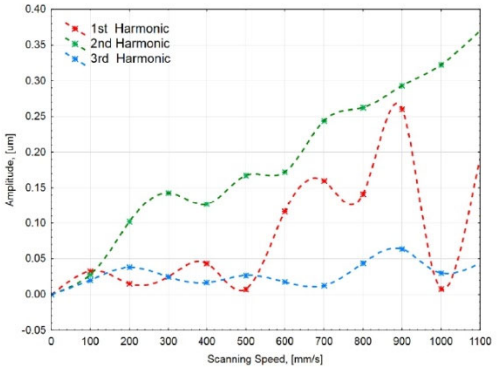

Figure 9. Three first harmonics of determined SDEs at different scanning speeds.

The biggest part of the SDE at each speed was caused by the second harmonic. This harmonic demonstrates a strong linear relationship (R-square = 0.96) to traversing velocity. Its size proportionally increased with increasing speed. This kind of error behavior is a result of signal-amplitude variation, phase shift, or their combination.

The first harmonic of the error demonstrates a nonlinear relationship. Amplitude values started to increase when the encoder reached a speed above 500 mm/s. An extreme jump of values was noticed in the range of 900–1000 mm/s. In this region, magnitude relatively dropped from 0.26 to 0.01 µm. This harmonic is a result of the emerged electric signals offset from a zero level.

The variation of the third harmonic meaning was not large in comparison with others. Its amplitude reached the highest value of 0.06 µm. This magnitude was noticed at a scanning speed of 900 mm/s, as with the first harmonic. Usually, this third harmonic is a result of variation in the optical-scanning process.

The following conclusions could be drawn from the obtained results:

- The initial overview of the Lissajous curves showed that the SDE of the tested encoder depended on the scanning speed. More detailed analysis at different velocities is necessary to figure out the dependency.
- Statistical investigation showed a strong linear relationship between SDE and scanning speed. In this case, it is important to know the maximal traversing velocity at which the encoder runs in a specific application. Different maximal speed gives a different maximal SDE value and sets a distinct limitation for the highest resolution. In another case, when the SDE retains the same meaning in the whole speed range, or its relationship is nonlinear, the maximal SDE value should be determined.
- The maximal recommended traversing velocity of the encoder was 1 m/s. Working in this range, maximal SDE was ±0.49 µm, reached at 900 mm/s. After interpolation of these encoder signals, the resolution should be more than 0.5 µm. Otherwise, the interpolation error is bigger than the measuring step.
- At each speed, the biggest part of the SDE budget formed the second harmonic. This directly correlates to increasing velocity. This means that the difference of the signal amplitudes or the phase shift increased with speed. Amplitude, offset, or phase errors could be caused by the physics of the optical-scanning principle, and the dynamical behavior and improper adjustment of the electric components (like photodiodes, used processing chips, or analog amplifiers), or the

quality of the used cable and other effects. It is necessary to pay attention to these aspects not only during the design process, but also while choosing a suitable encoder for a specific application. For example, the tested encoder's working principle was based on the four-field scanning method. If the application requires more stability to scanning speed, or if there is an increased possibility of measuring scale contamination, the optical encoder based on the single-field scanning principle must be selected.

- The calculated total SDE values at 900 and 1000 mm/s velocities were distinct from the determined linear relationship. The magnitudes of the first and third harmonics reached their maximum values at 900 mm/s. When analyzing the first harmonic graph, in speeds above 500 mm/s the offset error of the encoder signals started to greatly vary. It is very likely that the dynamic behavior of the encoder was affected in this range of speed. The reading head is a complex mechanical part containing optical and electronic components, and flexible spring-based suspension, so even the smallest translation, distance variation, tilt, or other change in a relative position between scanning reticle and measuring scale could be generated by resonant frequency, friction, or other forces. For more detailed analysis, the generated frequencies at these speeds should be determined and compared with the natural frequencies of the encoder.
- FFT analysis showed that the major part of the SDE was made up of only a few first harmonics. That means that the trend of the SDE could be quite accurately approximated by using a simple equation that contains information of only the three first harmonics ($n = 3$).

$$\delta(x) = \sum_{i=1}^{n=3} (A_i cos(\frac{2\pi}{p} ix + \varphi_i)) \; for \; 0 \le x \le p \tag{3}$$

After some extra processing of the experimental-investigation data, the multivariable function of the SDE value could be derived. This function could tell the approximated SDE value at a relative position inside the period at any scanning speed.

$$\delta(x,v) = f(x,v) + \varepsilon, \; for \begin{cases} 0 \le x \le p \\ 0 < v \le v_{Max} \end{cases} ; \; x, v \in Z, \tag{4}$$

where $f(x)$ is a multivariable approximation function of the SDE value, of which the arguments are relative position x and scanning speed v. ε indicates the random error, and v_{Max} denotes the maximal traversing velocity of the encoder. This kind of equation could be used for real-time SDE compensation.

5. Conclusions

Linear encoders are often used in applications for the precise displacement measurement of a moving unit to control positioning and speed. In order to properly accomplish these tasks, encoder parameters such as accuracy and resolution are critical. In practice, a SDE in an optical encoder is unavoidable. The magnitude of this error is a major factor that limits maximal resolution and causes a speed ripple. When analog encoder signals are interpolated without any error correction or compensation approach, it is very important to know the limitations of the used encoder. The method described in this paper presents a way to determine the magnitude and trend of the linear encoder SDE.

Experimental investigation of the standard optical linear encoder SDE under different scanning speeds was accomplished according to the presented methodology. Deeper analysis of the determined errors helped to reveal their physical nature and the limits of the encoder. On the basis of the obtained results, it is possible to specify the weak points of the tested device to help to improve its performance. Mapped and approximated SDE at different speeds could be used as a multivariable function for positioning-error compensation. This is our future research direction.

Author Contributions: D.G. introduced and composed the presented methodology, designed and completed the experiment setup, contributed to the experiments, and wrote the paper; A.K. performed the experiments, and

collected and processed the data; S.B. supervised the research. All authors have read and agreed to the published version of the manuscript.

Funding: This research received no external funding.

Conflicts of Interest: The authors declare no conflict of interest.

Abbreviations

The following abbreviations are used in this manuscript:

SDE Subdivisional error
FFT Fast Fourier transformation

References

1. Zhao, L.; Cheng, K.; Chen, S.; Ding, H.; Zhao, L. An approach to investigate moiré patterns of a reflective linear encoder with application to accuracy improvement of a machine tool. *Proc. Inst. Mech. Eng. Part B J. Eng. Manuf.* **2018**, *233*, 927–936. [CrossRef]
2. Bai, Q.; Liang, Y.; Cheng, K.; Long, F. Design and analysis of a novel large-aperture grating device and its experimental validation. *Proc. Inst. Mech. Eng. Part B J. Eng. Manuf.* **2013**, *227*, 1349–1359. [CrossRef]
3. Liu, C.; Jywe, W.; Hsu, T. The application of the double-readheads planar encoder system for error calibration of computer numerical control machine tools. *Proc. Inst. Mech. Eng. Part B J. Eng. Manuf.* **2004**, *218*, 1077–1089. [CrossRef]
4. Du, Z.; Zhang, S.; Hong, M. Development of a multi-step measuring method for motion accuracy of NC machine tools based on cross grid encoder. *Int. J. Mach. Tools Manuf.* **2010**, *50*, 270–280. [CrossRef]
5. Ishii, N.; Taniguchi, K.; Yamazaki, K.; Aoyama, H. Performance improvement of machine tool by high accuracy calibration of built-in rotary encoders. In Proceedings of the 9th International Conference on Leading Edge Manufacturing in 21st Century, Japan Society of Mechanical Engineers, Hiroshima, Japan, 13–17 November 2017.
6. Algburi, R.N.A.; Gao, H. Health assessment and fault detection system for an industrial robot using the rotary encoder signal. *Energies* **2019**, *12*, 2816. [CrossRef]
7. Han, Z.; Jianjun, Y.; Gao, L. External force estimation method for robotic manipulator based on double encoders of joints. In Proceedings of the IEEE International Conference on Robotics and Biomimetics (ROBIO), Kuala Lumpur, Malaysia, 12–15 December 2018.
8. Peng, L.; Xiangpeng, L. Common sensors in industrial robots: A review. *J. Phys. Conf. Ser.* **2019**, *1267*, 012036.
9. Mikhel, S.; Popov, D.; Mamedov, S.; Klimchik, A. Advancement of robots with double encoders for industrial and collaborative applications. In Proceedings of the 23th Conference of Open Innovations Association (FRUCT), Bologna, Italy, 13–16 November 2018.
10. Rodriguez-Donate, C.; Osornio-Rios, R.A.; Rivera-Guillen, J.R.; Romero-Troncoso, R.J. Fused smart sensor network for multi-axis forward kinematics estimation in industrial robots. *Sensors* **2011**, *11*, 4335–4357. [CrossRef]
11. Vazquez-Gutierrez, Y.; O'Sullivan, L.; Kavanagh, R.C. Study of the impact of the incremental optical encoder sensor on the dynamic performance of velocity servosystems. *J. Eng.* **2019**, *2019*, 3807–3811. [CrossRef]
12. Vazquez-Gutierrez, Y.; O'Sullivan, L.; Kavanagh, R.C. Small-signal modeling of the incremental optical encoder for motor control. *IEEE Trans. Ind. Electron.* **2019**. [CrossRef]
13. Vazquez-Gutierrez, Y.; O'Sullivan, L.; Kavanagh, R.C. Evaluation of three optical-encoder-based speed estimation methods for motion control. *J. Eng.* **2019**, *2019*, 4069–4073. [CrossRef]
14. Zhang, Z.; Olgac, N. Zero magnitude tracking control for servo system with extremely low-resolution digital encoder. *Int. J. Mechatron. Manuf. Syst.* **2018**, *10*. [CrossRef]
15. Zhao, M.; Jia, X.; Lin, J.; Lei, Y.; Lee, J. Instantaneous speed jitter detection via encoder signal and its application for the of planetary gearbox. *Mech. Syst. Signal Process.* **2018**, *98*, 16–31. [CrossRef]
16. Li, B.; Zhang, X.; Wu, J. New procedure for gear fault detection and diagnosis instantaneous angular speed. *Mech. Syst. Signal Process.* **2017**, *85*, 415–428. [CrossRef]

17. Ariznavarreta-Fernandez, F.; Gonzalez-Palacio, C.; Menendez-Diaz, A.; Ordonez, C. Measurement system with angular encoders for continuous monitoring of tunnel convergence. *Tunn. Undergr. Space Technol.* **2016**, *56*, 176–185. [CrossRef]
18. Zhao, M.; Lin, J. Health assessment of rotating machinery using a rotary encoder. *IEEE Trans. Ind. Electron.* **2018**, *65*, 2548–2556. [CrossRef]
19. Tang, T.; Chen, S.; Huang, X.; Yang, T.; Qi, B. Combining load and motor encoders to compensate nonlinear disturbances for high precision tracking control of gear-driven Gimbal. *Sensors* **2018**, *18*, 754. [CrossRef] [PubMed]
20. Chong, K.K.; Wong, C.-W.; Siaw, F.-L.; Yew, T.-K.; Ng, S.-S.; Liang, M.-S.; Lim, Y.-S.; Lau, S.-L. Integration of an on-axis general sun-tracking formula in the algorithm of an open-loop sun-tracking system. *Sensors* **2009**, *9*, 7849–7865. [CrossRef] [PubMed]
21. Kimura, A.; Gao, W.; Kim, W.; Hosono, K.; Shimizu, Y.; Shi, L.; Zeng, L. A sub-nanometric three-axis surface encoder with short-period planar gratings for stage motion measurement. *Precis. Eng.* **2012**, *36*, 576–585. [CrossRef]
22. Lee, C.B.; Kim, G.H.; Lee, S.K. Design and construction of a single unit multi-function optical encoder for a six-degree-of-freedom motion error measurement in an ultraprecision linear stage. *Meas. Sci. Technol.* **2011**, *22*. [CrossRef]
23. Li, Y.T.; Fan, K.C. A novel method of angular positioning error analysis of rotary stages based on the Abbe principle. *Proc. Inst. Mech. Eng. Part B J. Eng. Manuf.* **2018**, *232*, 1885–1892. [CrossRef]
24. Lou, Z.F.; Hao, X.P.; Cai, Y.D.; Lu, T.F.; Wang, X.D.; Fan, K.C. An embedded sensors system for real-time detecting 5-DOF error motions of rotary stages. *Sensors* **2019**, *19*, 2855. [CrossRef] [PubMed]
25. Gao, W.; Kim, S.W.; Bosse, H.; Haitjema, H.; Chen, Y.L.; Lu, X.D.; Knapp, W.; Weckenmann, A.; Estler, W.T.; Kunzmann, H. Measurement technologies for precision positioning. *CIRP Ann. Manuf. Technol.* **2015**, *64*, 773–796. [CrossRef]
26. Smith, G.T. *Machine Tool Metrology. An Industrial Handbook*; Springer: Berlin, Germany, 2016; pp. 159–177.
27. Heidenhain. Linear Encoders for Numerically Controlled Machine Tools. Available online: https://www.heidenhain.com/fileadmin/pdb/media/img/571470-2C_Linear_Encoders_For_Numerically_Controlled_Machine_Tools.pdf (accessed on 22 January 2020).
28. Fagor Automation. Feedback Systems. Available online: https://www.fagorautomation.com/en/p/feedback-systems/ (accessed on 22 January 2020).
29. Ye, G.; Wu, Z.; Xu, Z.; Wang, Y.; Shi, Y.; Liu, H. Development of a digital interpolation module for high-resolution sinusoidal encoders. *Sens. Actuators A Phys.* **2019**, *285*, 501–510. [CrossRef]
30. Ye, G.; Liu, H.; Wang, Y.; Lei, B.; Shi, Y.; Yin, L.; Lu, B. Ratiometric-linearization -based high-precision electronic interpolator for sinusoidal optical encoders. *IEEE Trans. Ind. Electron.* **2018**, *65*, 8224–8231. [CrossRef]
31. Ye, G.; Xing, H.; Liu, H.; Li, Y.; Lei, B.; Niu, D.; Li, X.; Lu, B.; Liu, H. Total error compensation of non-ideal signal parameters for Moire encoders. *Sens. Actuators* **2019**, *298*. [CrossRef]
32. Alejandre, I.; Artes, M. Machine tool errors caused by optical linear encoders. *J. Eng. Manuf.* **2004**, *218*, 113–122. [CrossRef]
33. Lopez, J.; Artes, M.; Alejandre, I. Analysis of optical linear encoders errors under vibration at different mounting conditions. *Measurement* **2011**, *44*, 1367–1380. [CrossRef]
34. Lopez, J.; Artes, M.; Alejandre, I. Analysis under vibrations of optical linear encoders based on different scanning methods using an improved experimental approach. *Exp. Tech.* **2012**, *36*, 35–47. [CrossRef]
35. Lopez, J.; Artes, M. A new methodology for vibration error compensation of optical encoders. *Sensors* **2012**, *12*, 4918–4933. [CrossRef]
36. Alejandre, I.; Artes, M. Real thermal coefficient in optical linear encoders. *Exp. Tech.* **2004**, *28*, 18–22. [CrossRef]
37. Alejandre, I.; Artes, M. Thermal non-linear behaviour in optical linear encoders. *Int. J. Mach. Tools Manuf.* **2005**, *46*, 1319–1325. [CrossRef]
38. Rozman, J.; Pletersek, A. Linear optical encoder system with sinusoidal signal distortion below −60 dB. *IEEE Trans. Instrum. Meas.* **2010**, *59*, 1544–1549. [CrossRef]
39. Li, M.; Liang, Z.; Zhang, R.; Wu, Q.; Xin, C.; Jin, L.; Xie, K.; Zhao, H. Large-scale range diffraction grating displacement sensor based on polarization phase-shifting. *Appl. Opt.* **2020**, *59*, 469–473. [CrossRef]

40. Ye, G.; Liu, H.; Jiang, W.; Li, X.; Jiang, W.; Yu, H.; Shi, Y.; Yin, L.; Lu, B. Design and development of an optical encoder with sub-micron accuracy using a multiple-tracks analyser grating. *Rev. Sci. Instrum.* **2017**, *88*. [CrossRef]
41. Albrecht, C.; Klock, J.; Martens, O.; Schumacher, W. Online estimation and correction of systematic encoder line errors. *Machines* **2017**, *5*, 1. [CrossRef]
42. Mendenhall, M.H.; Windover, D.; Henins, A.; Cline, J.P. An algorithm for the compensation of short-period errors in optical encoders. *Metrologia* **2015**, *52*, 685. [CrossRef]
43. Ye, G.; Fan, S.; Liu, H.; Li, X.; Yu, H.; Shi, Y.; Yin, L.; Lu, B. Design of a precise and robust linearized converter for optical encoders using a ratiometric technique. *Meas. Sci. Technol.* **2014**, *25*. [CrossRef]
44. Yandayan, T.; Geckeler, R.D.; Just, A.; Krause, M.; Akgoz, S.A.; Aksulu, M.; Grubert, B.; Watanabe, T. Investigation of interpolation errors of angle encoders for high precision angle metrology. *Meas. Sci. Technol.* **2018**, *29*. [CrossRef]
45. Wang, Y.; Liu, Y.; Yan, X.; Chen, X.; Lv, H. Compensation of Moire fringe sinusoidal deviation in photoelectric encoder based on tunable filter. In Proceedings of the 2011 Symposium on Photonics and Optoelectronics (SOPO), Wuhan, China, 16–18 May 2011. [CrossRef]
46. Kao, C.F.; Huang, H.L.; Lu, H. Optical encoder based on Fractional-Talbot effect using two-dimensional phase grating. *Opt. Commun.* **2010**, *283*, 1950–1955. [CrossRef]
47. Kao, C.F.; Lu, H. Optical encoder based on the fractional Talbot effect. *Opt. Commun.* **2005**, *250*, 16–23. [CrossRef]
48. Crespo, D.; Alonso, J.; Tomas, M.; Eusebio, B. Optical encoder based on the Lau effect. *Opt. Eng.* **2000**, *39*, 817–822. [CrossRef]
49. Sudol, R.; Thompson, B.J. Lau effect: Theory and experiment. *Appl. Opt.* **1981**, *20*, 1107–1116. [CrossRef] [PubMed]
50. Li, X. Displacement measurement based on the Moire fringes. *Int. Soc. Opt. Eng.* **2011**. [CrossRef]
51. Wu, J.; Zhou, T.T.; Yuan, B.; Wang, L.-Q. A digital Moire fringe method for displacement sensors. *Front. Inform. Technol. Electron. Eng.* **2016**, *17*, 946–953. [CrossRef]
52. Zhao, B.; Miao, J.; Xie, H.; Asundi, A. Modeling of grating/Moire based micro sensor. *Microsyst. Technol.* **2001**, *7*, 107–116. [CrossRef]
53. Ye, G.; Liu, H.; Xie, H.; Asundi, A. Optimizing design of an optical encoder based on generalized grating imaging. *Meas. Sci. Technol.* **2016**, *27*. [CrossRef]
54. Ye, G.; Liu, H.; Fan, S.; Li, X.; Yu, H.; Lei, B.; Shi, Y.; Yin, L.; Lu, B. A theoretical investigation of generalized grating imaging and its application to optical encoders. *Opt. Commun.* **2015**, *354*, 21–27. [CrossRef]
55. Liu, H.; Ye, G.; Shi, Y.; Yin, L.; Chen, B.; Lu, B. Multiple harmonics suppression for optical encoders based on generalized grating imaging. *J. Mod. Opt.* **2016**, *63*, 1564–1572. [CrossRef]
56. Iwata, K. Interpretation of generalized grating imaging. *J. Opt. Soc. Am.* **2008**, *25*, 2244–2250. [CrossRef]
57. Lee, C.-K.; Wu, C.-C.; Chen, S.-J.; Yu, L.-B.; Chang, Y.-C.; Wang, Y.-F.; Chen, J.-Y.; Wu, J.W.-J. Design and construction of linear laser encoders that possess high tolerance of mechanical run out. *Appl. Opt.* **2004**, *43*, 5754–5762. [CrossRef]
58. Liu, C.-H.; Jywe, W.-Y.; Wang, M.-S.; Huang, H.-L. Development of a three-degrees-of-freedom laser linear encoder for error measurement of a high precision range. *Rev. Sci. Instrum.* **2007**, *78*. [CrossRef]
59. Liu, C.H.; Cheng, C.H. Development of a multi-degree-of-freedom laser encoder using +- 1 order and +- 2 order diffraction rays. In Proceedings of the 10th International Symposium of Measurement Technology and Intelligent Instruments, Daejeon, Korea, 29 June–2 July 2011.
60. Heidenhain. Interfaces. Available online: https://www.heidenhain.com/en_US/documentation/fundamentals/interfaces/ (accessed on 22 February 2020).

Article 4. Gurauskis, D. and Kilikevičius, A. (2020). Dynamic Behaviour Analysis of Optical Linear Encoder under Mechanical Vibrations

(https://doi.org/10.5755/j01.mech.26.1.23070)

ISSN 1392–1207. MECHANIKA. 2020 Volume 26(1): 35–41

Dynamic Behaviour Analysis of Optical Linear Encoder under Mechanical Vibrations

Donatas GURAUSKIS*, Artūras KILIKEVIČIUS**
**Department of Mechanical Engineering, Vilnius Gediminas Technical University, J. Basanavičiaus 28, 03224 Vilnius, Lithuania, E-mail: donatas.gurauskis@vgtu.lt*
***Institute of Mechanical Science, Vilnius Gediminas Technical University, J. Basanavičiaus 28, 03224 Vilnius, Lithuania, E-mail: arturas.kilikevicius@vgtu.lt*

crossref http://dx.doi.org/10.5755/j01.mech.26.1.23070

1. Introduction

Optical linear encoders play noticeable role in performance of computer numerical controlled machines (CNC) [1], coordinate measuring machines (CMM), robotics [2], positioning stages [3], tracking systems [4] and other precision positioning applications [5]. Usually, the accuracy of technological process, performed by the equipment, depends on the used encoder`s accuracy. It is obvious that the good performance of the encoder is very important.

In practice, mechanical vibrations are one of the factors which cause errors in linear displacement measurement encoders. Resonance in measuring device parts like aluminium extrusion or reading head, either in supporting elements of the application could cause additional undesirable motion of a scanning carriage (cursor) along a measuring scale. Such motion inevitably affects accuracy. Essentially, dynamic behaviour of the encoder depends on its construction. J. López et al. investigates the behaviour of the linear encoder under vibrations based on different optical scanning methods [6,7], and encoder`s errors under vibration at different mounting conditions [8]. Although, there are developed methodologies to evaluate optical encoders performance under vibration [9] or compensate vibration caused errors [10], but in order to have a good understanding of ongoing processes in mechanical construction of each encoder, more detailed investigation such as modal analysis is required.

In this paper, the dynamic behaviour of enclosed type optical encoder based on reflective light modulation is investigated. Its dynamic response to external mechanical excitation, generated by the electrodynamic shaker, is recorded by accelerometers and the most precarious resonant frequencies are determined. In order to establish how the encoder elements, behave at these resonances, the modal analysis is done.

2. Experimental details

The optical linear encoder analysed in this work is incremental. It is reflective type and its measuring scale is fabricated on the stainless-steel tape surface by a laser. This provides the opportunity to reach measuring length up to 30 meters. Meanwhile, encoders with a glass scale reach approximately about 3 meters. In cases when encoder`s length must be more than 2 meters, several of modular aluminium extrusions are added together. Stainless-steel tape with an engraved measuring scale is fitted into encoder`s aluminium extrusion, respectively stretched by using a special spring-based mechanism and tightened at both ends. Another stainless-steel tape is used as a guideway for the precise scanning carriage positioning and motion during the displacement measurement process. Main parts of the tested linear encoder are shown in Fig. 1.

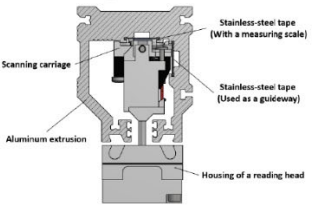

Fig. 1 Construction of tested linear encoder

The main idea of this experimental research is to analyse dynamic behaviour and determine resonant frequencies which could cause errors of the encoder. Theoretically, errors appear due to additional undesirable motion between the measuring scale and the reticle, mounted onto the scanning carriage. Even a small motion or oscillation generates electrical signals, which incorrectly represent the real displacement value.

Because the most important motion is along the measuring scale, the dynamic responses of the encoder`s aluminium extrusion and reading head are investigated only in this direction (meet the y axis in Fig. 2). Linear encoder is tightly mounted onto the laboratory table in such way, that its reading head has no ability to move with regard to aluminium extrusion. Two piezoelectric accelerometers are respectively mounted on top of the extrusion and housing of the reading head. Massive electrodynamic shaker is positioned close to the encoder to generate external mechanical excitation with the amplitude of about 100 mm/s^2 at each frequency. It imitates vibrations that occur in real applications. Excited encoder`s parts start to oscillate. When shaker generated excitation frequency is getting closer to the resonant frequencies of the encoder`s elements, the oscillation amplitudes increase. These resonant frequencies are the most dangerous, because the encoder starts to generate some kind of electric signals, even though there is no wanted displacement to measure. Despite the fact that the accuracy is directly affected, high frequency oscillations, caused by vibrations, remains during the displacement measurement

process. This generates higher harmonics and the analogue encoder signals become distorted. Interpolation process of such encoder signals is disturbed, and higher resolution becomes hardly reachable. The composition of the experimental setup is shown in Fig. 2.

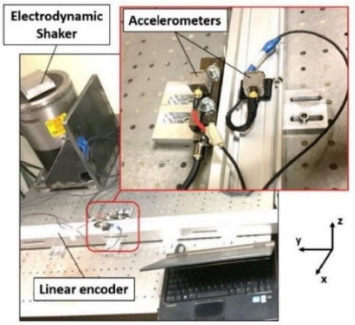

Fig. 2 Experimental setup used for encoder investigation

In order to reveal encoder`s behaviour and determine resonant frequencies, the device is tested under the sweep of sine wave form vibrations. Later, the amplitudes of aluminium extrusion and reading head responses under various resonant and other frequencies are measured. The biggest differences between the recorded amplitude values of oscillating elements distinguish excitations, which potentially generate the biggest errors. To check it, electrical 1 V peak-to-peak encoder`s output signals are recorded by a digital oscilloscope during the all experiment.

Used experimental equipment consists of:

1. Processing equipment. Data acquisition hardware "B&K" 3660-163D.

2. Electrodynamic shaker. Head "B&K" 4812, permanent magnet body "B&K" 4805, and amplifier "B&K" 2707.

3. Accelerometers. 3-axis piezoelectric accelerometer "B&K" 4506.

4. Data acquisition and processing equipment. Digital oscilloscope "PicoScope" 3000 and notebook.

The schematic representation of the experimental setup is shown in Fig. 3.

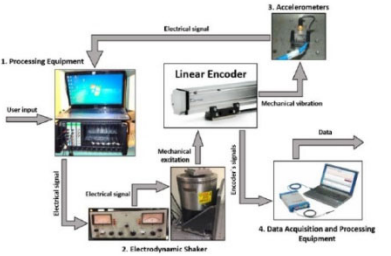

Fig. 3 Schematic representation of experimental setup

At each resonance mechanical elements oscillate in different manner. Modal analysis shows the oscillation shape of the elements. This simulation is performed by using the finite element method (FEM) in a computer software "COMSOL". A simplified 3D model of the encoder is created and divided into finite number of free tetrahedral (tets) elements with a predefined extra fine size. Boundary conditions such as fixing points of extrusion and reading head imitates encoder`s mounting in real application.

A simplified 3D model is shown in Fig. 4. Materials and their mechanical properties for each one of simulated device elements are listed in Table 1.

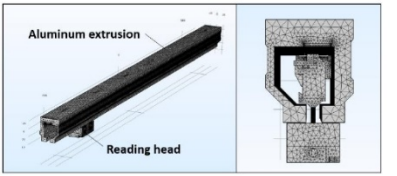

Fig. 4 Simplified 3D encoder model for FEM simulation

Table 1

Materials and mechanical properties of encoder elements

Element	Material	Mechanical properties		
		Density ρ, kg/m^3	Young's modulus E, GPa	Poisson's ratio ν
Extrusion	Aluminum 6060	2700	70	0,33
Reading head	Aluminum 6082T6	2700	69	0,33
Measuring scale	Stainless-steel AISI 420	7700	190	0,28
Springs (reading head suspension)	Stainless-steel AISI 302	7800	200	0,28

Optical encoder generates two sinusoidal output signals S_A and S_B. They should have same size amplitudes A_A and A_B, zero offset from background level ($B_A = B_B = 0$) and must be shifted by 90 electrical degrees ($\varphi_B - \varphi_A = \pi/2$). These signals could be mathematically expressed as:

$$S_A = A_A F_A\left(2\pi\frac{x}{p} + \varphi_A\right) + B_A, \quad (1)$$

$$S_B = A_B F_B\left(2\pi\frac{x}{p} + \varphi_B\right) + B_B, \quad (2)$$

where: F_A, F_B is the shape (sinusoidal) of the signals; x is the position and p is the period.

The linear displacement could be easily determined according these signals by using arctangent algorithm:

$$x_{arctan} = \frac{p}{2\pi} arctan\left(\frac{S_A}{S_B}\right). \quad (3)$$

Output signals could be visually represented by the Lissajous curve. The curve appears in an oscilloscope screen, when one signal is plotted against another in x and y axis. Full circular shape corresponds to a relative motion between the reticle and the measuring scale, which is equal to a period of raster elements on them. The period of the tested encoder`s scale is 40 μm. Typically, external mechanical vibration initiates smaller motion between the optical components than one period. In case, when the reading head is mounted in fixed position as well as the aluminum extrusion, generated output signals are presented as a circumference arc of the Lissajous curve. From the size of arc, it is possible to determine and the size of error, generated by an external mechanical vibration.

During the displacement measurement process, encoder`s generated signals have multiple periods, so it is hard to exactly determined the amount of dynamic error. However, a specific mode shapes of the encoder mechanical components lead to a gap or tilt variation between the reticle and the glass scale. Disturbed optical interaction could present a loss of contrast and uneven light distribution on surfaces of used photodiodes. These variations make changes in signals` amplitudes, phase, offsets and even the shape. Metrological errors presented in optical linear encoder could be determined by analysing the Lissajous curve and its distortion from an ideal shape [11]. The following equations are derived to evaluate these errors.

$$U_{off}(x) = \frac{p}{2\pi} cos\left(\frac{2\pi}{p}x\right)\frac{\Delta B}{A}, \quad (4)$$

$$U_{amp}(x) = \frac{p}{4\pi} sin\left(4\pi\frac{x}{p}\right)\frac{\Delta A}{A}, \quad (5)$$

$$U_{phase}(x) = \frac{p}{2\pi} cos^2\left(\frac{2\pi}{p}x\right)\Delta\varphi, \quad (6)$$

$$U_{shape}(x) = \frac{p}{2\pi} sin\left(8\pi\frac{x}{p}\right)\Delta T, \quad (7)$$

where: U_{off}, U_{amp}, U_{phase} and U_{shape} stand for metrological errors respectively caused by signal offset, variation of amplitudes, phase shift and not sinusoidal shape of the signals.

Other conditions for these formulas: $A_B = A$; $A_A = A + \Delta A$; $B_A = \Delta B$; $\varphi_A = \Delta\varphi$; $\varphi_B = \pi / 2$.

3. Results and discussion

Firstly, encoder's response to sine sweep vibration test is done. The shaker is set to generate sinusoidal excitation from 0 to 3200 Hz. Collected data from the accelero-

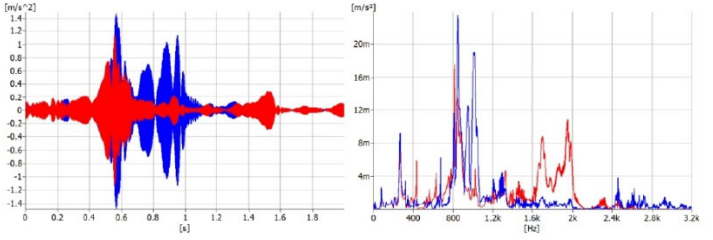

a b

Fig. 5 Response graphs: a) acceleration amplitude versus time, b) auto-spectrum. (Aluminium extrusion response – blue line; reading head response – red line)

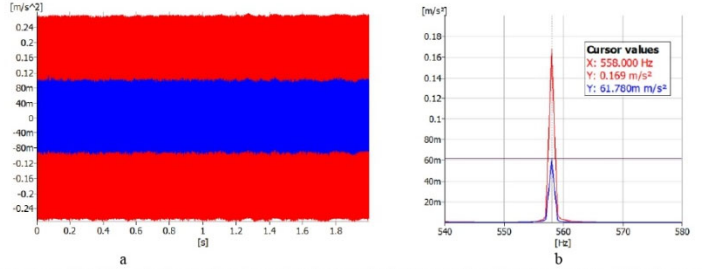

a b

Fig. 6 Response to 558 Hz excitation graphs: a) acceleration amplitudes versus time, b) auto-spectrum. (Aluminium extrusion response – blue line; reading head response – red line)

meters presents the frequency response of the aluminium extrusion and the reading head. Acceleration amplitude versus time and auto-spectrum graphs are plotted in Fig. 5. Resonant frequencies 382, 433, 534, 558, 629,5, 753 and 815,5 Hz are selected for more detailed investigation.

Secondly, linear encoder is excited with a discrete sine vibration up to 2000 Hz with a step of 100 Hz, including selected resonant frequencies. The values of frequency response amplitudes are recorded by the accelerometers. For example, aluminium extrusion and reading head responses to 558 Hz selected resonant frequency are shown in Fig. 6.

In this case the acceleration amplitude of the reading head oscillations reaches 169 mm/s^2 and the extrusion oscillates at 61,78 mm/s^2. The difference between amplitudes is almost three times.

According measured amplitude values the revised graphs of frequency responses to sine wave form mechanical vibration are plotted. The graph composed for the reading head is shown in Fig. 7.

Several sharp peaks could be clearly seen in this graph. According the accomplished modal analysis, some of these peaks quite accurately correspond to the determined modes. They are marked on the graph. Other modes may not have such clearly visible effect at investigated direction y. Oscillation modes: 1, 2, 3 and 6 are depicted in Fig. 8. Only the reading head and its mode shapes are shown in these images for a better visualization. It is obvious, that all excludedmodes are related to the motion of the scanning carriage and occur at tested frequencies of 433, 558, 815,5 and about 2000 Hz. Mechanical assembly and encoder`s mounting type could also change and the dynamic behaviour, so resonant frequencies of simulated modes and modes of the real encoder may slightly differ. Another graph composed of the aluminum extrusion response data is shown in Fig. 9.

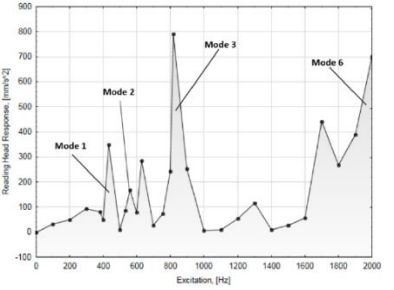

Fig. 7 Reading head frequency response graph with marked modes

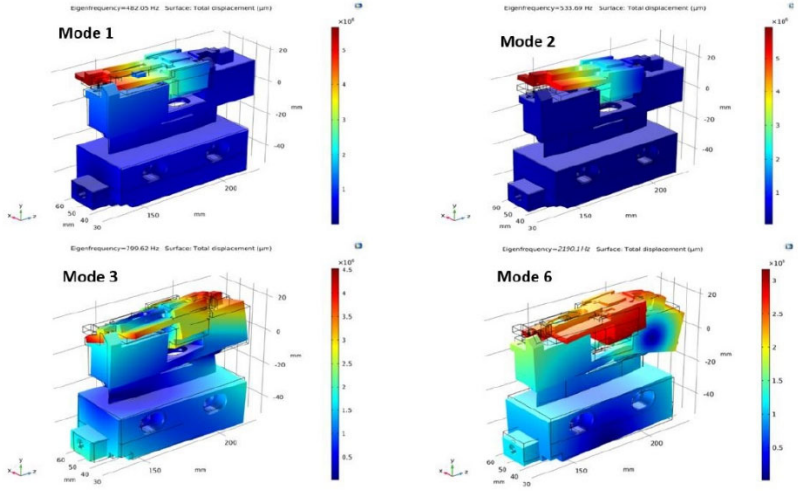

Fig. 8 Mode shapes of encoder`s reading head

Noticeable peaks correspond to the simulated modes: 7, 12, 13, 15 and 19. The shapes of these modes could be seen in Fig. 11. The swell type motion of the aluminum extrusion (mode 7 and mode 13) and the stainless-steel tape with a measuring scale (mode 12, mode 15 and mode 19) is generated at frequencies of 300, 800, 900, 1200 and 1700 Hz respectively. Other peaks seen in both discussed graphs could appear due to resonances of the experimental setup or the synergetic effect of the other factors.

When the oscillation amplitude values of the aluminum extrusion and the reading head are similar at the same frequency, the motion between the main optical com-

39

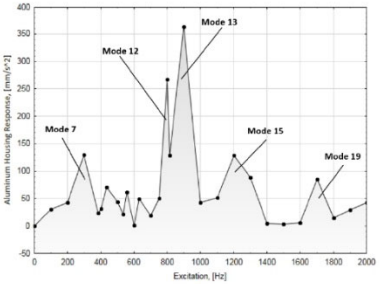

Fig. 9 Aluminum extrusion frequency response graph with marked modes

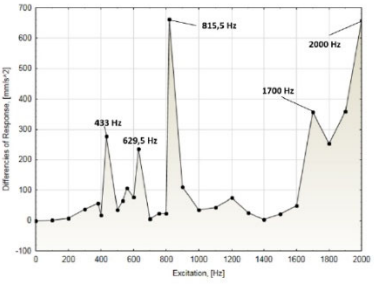

Fig. 10 Differences between response amplitude values of reading head and aluminum extrusion

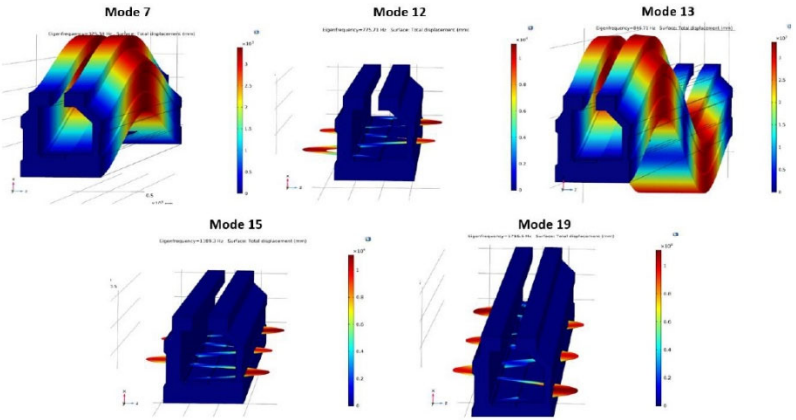

Fig. 11 Mode shapes of encoder`s aluminum extrusion

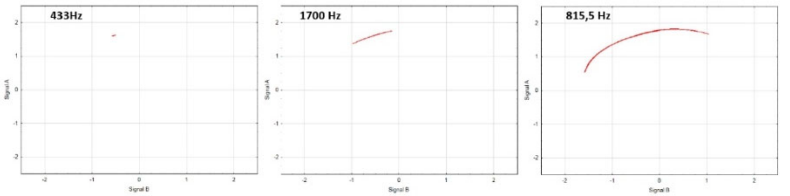

Fig. 12 Circumference arcs of Lissajous curves at 433, 1700 and 815,5 Hz

ponents is relatively small, even then the amplitude values are big. Much bigger relative motion appears in cases, when one of the elements oscillates with appreciably bigger amplitude. The differences between the response amplitudes are plotted in Fig. 10.

This graph shows potentially the most dangerous frequencies which could generate displacement measurement errors. The peaks appear at 433; 629,5; 815,5; 1700 and 2000 Hz.

In order to check the influence of these resonant frequencies the electric output signals generated by the encoder are analyzed. Three examples of Lissajous curves of

electrical signals recorded at 433; 815,5 and 1700 Hz are shown in Fig. 12. The corresponding arcs show that encoder`s performance under vibration is affected. The generated error reaches <1 μm at 433 Hz; ~4 μm at 1700 Hz and ~11 μm at 815,5 Hz.

Electrical signals are recorded and during the displacement measurement process, to see how external mechanical excitation affects its performance. The Lissajous curve of working encoder under 815,5 Hz excitation is shown in Fig. 13.

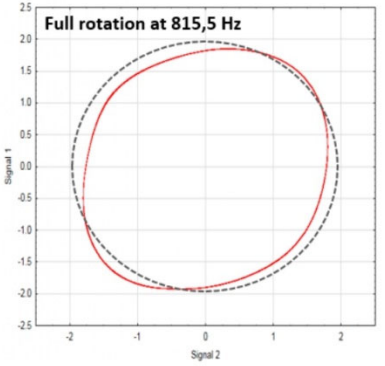

Fig. 13 Lissajous curve of working encoder under 815,5 Hz mechanical excitation (Lissajous curve of the tested encoder - solid red line; ideal circular curve – dashed black line)

Properly working linear encoder generates good quality sin and cos signals. The Lissajous curve of such signals looks like almost perfect circle. The graph above shows that the electrical signals are distorted. Shape of the curve are not circular and represents uneven amplitudes of electric signals. Slightly non-centered elliptical shape configuration tells about the phase distortion and different offsets of the output signals.

4. Conclusions

In this study, the dynamic behaviour of the linear optical encoder under mechanical vibrations is analysed. The main resonant frequencies and corresponding mode shapes of the encoder`s elements are determined. Potentially the most dangerous frequencies, which could cause the biggest displacement measurement errors are distinguished.

The results could be summarized as follow:

1) Accomplished sine sweep vibration test shows that there are resonant frequencies in the studied frequency range. Motion of the reading head along the encoder`s measuring scale is considered as the most dangerous and is selected like a point of interest in this work.

2) Determined resonances generate errors up to ~11 μm. Accuracy of the encoder is ±10 μm/m by itself. This means that mechanical vibrations can significantly worsen the performance of the tested device.

3) The Lissajous curve of working encoder under vibrations shows that analogue electrical signals are distorted. Amplitudes, offsets and phase of the signals vary during the displacement measurement process. This is usually related to a tilt or air gap variations between the reticle and the measuring scale. It means, that not only the forward and backward oscillations are generated.

4) Determined mode shapes expose that the biggest errors are generated due to the swell type motion of the aluminum extrusion and the stainless-steel tape. They are also directly related to a various motion of the scanning carriage.

5) In order to improve encoder performance under mechanical vibrations, changes in mechanical design of the reading head may help to reduce resonant frequencies. Especially it is important to do in a range from 50 to 2000 Hz, which is mentioned in standard EN 60068-2-6 (sinusoidal vibrations). Most linear encoders must support conditions according this standard.

Due to various mounting types and different length of aluminum extrusion, it is hard to describe its exact dynamic behaviour. However, the stainless-steel tape in all cases are relatively stretched and fixed on both ends. Considering such encoder`s construction, the following steps could be discussed to improve its dynamic behaviour under vibrations:

1) The harder stretch of the stainless-steel tape may increase the stiffness of the assembly and as a consequence, the resonant frequencies should become higher. To achieve this, raster elements of the incremental track should be made with a correspondingly corrected period.

2) Depending on the length of the aluminum extrusion assembly, several additional fixing pins could be integrated into design. These pins could be respectively placed to press a tape at points, where its modal shape reaches maximal peaks.

Unfortunately, these cases require changes in encoder`s mechanical design or the technological process of scale engraving. Either way, more detailed experimental investigation is required.

References

1. **Alejandre I.; Artés M.** 2004. Machine tool errors caused by optical linear encoders, Journal of Engineering Manufacture 218(1): 113-122. https://doi.org/10.1243/095440504772830255.
2. **Rodriguez-Donate, C.; Osornio-Rios, R. A.; Rivera-Guillen, J. R.; Romero-Troncoso, J.** 2011. Fused smart sensor network for multi-axis forward kinematics estimation in industrial robots, Sensors 11(4): 4335-4357. https://doi.org/10.3390/s110404335.
3. **ChaBum, L.; Gyu, H. K.; Sun-Kyu, L.** 2011. Design and construction of a single unit multi-function optical encoder for a six-degree-of-freedom motion error measurement in an ultraprecision linear stage, Meas. Sci. Technol. 22(105901): 8. https://doi.org/10.1088/0957-0233/22/10/105901.
4. **Chong, K.; Wong, C.; Siaw, F.; Yew, T.; Ng, S.; Liang, M.; Lim, Y.; Lau, S.** 2009. Integration of an on-axis general sun-tracking formula in the algorithm of an open -loop sun-tracking system, Sensors 9: 7849-7865. https://doi.org/10.10.3390/s91007849.
5. **Gao, W.; Kim, S. W.; Bosse, H.; Haitjema, H.; Chen,**

Y. L.; Lu, X. D.; Knapp, W.; Weckenmann, A.; Estler, W.T.; Kunzmann, H. 2015. Measurement technologies for precision positioning, Manufacturing technologies 64(2): 773-796. https://doi.org/10.1016/j.cirp.2015.05.009.

6. **López, J.; Artés, M.; Alejandre, I.** 2012. Analysis under vibrations of optical linear encoders based on different scanning methods using an improved experimental approach, Experimental techniques 36(6): 35-47. https://doi.org/10.1111/j.1747-1567.2011.00749.x.
7. **López, J.; Artés, M.; Alejandre, I.** 2009. Vibration behaviour analysis of optical linear encoders based on different scanning methods. Proceeding of the SEM Annual Conference. Society for Experimental Mechanics Inc.
8. **López, J.; Artés, M.; Alejandre, I.** 2011. Analysis of optical linear encoders` errors under vibration at different mounting conditions, Measurement 44(8): 1367-1380. https://doi.org/10.1016/j.measurement.2011.05.004.
9. **Alejandre, I.; Artés, M.** 2007. Method for the evaluation of optical encoders performance under vibration, Precision Engineering 31(2): 114-121. https://doi.org/10.1016/j.precisioneng.2006.03.004.
10. **López, J.; Artés, M.** 2012. A new methodology for vibration error compensation of optical encoders, Sensors 12(4): 4918-4933. https://doi.org/10.3390/s12040491.
11. **Sanchez-Brea, L. M.; Morlanes, T.** 2008. Metrological errors in optical encoders, Measurement Science and Technology 19(115104): 8. https://doi.org/10.1088/0957-0233/19/11/115104.

D. Gurauskis, A. Kilikevičius

DYNAMIC BEHAVIOUR ANALYSIS OF OPTICAL LINEAR ENCODER UNDER MECHANICAL VIBRATIONS

S u m m a r y

Mechanical vibrations are probably inevitable and occur in more or less all machine tools and other technological equipment. In case the linear encoder is used for moveable parts positioning in such machines, vibrations could cause additional errors. This paper investigates the dynamic behaviour of the optical linear encoder under mechanical vibrations. Potentially the most harmful frequencies are determined experimentally, and the corresponding mode shapes are simulated by using the finite element method (FEM). Obtained results describe tested encoder`s construction dynamic response to external excitation and could be used to improve its design.

Keywords: Linear encoder, mechanical vibrations, reading head.

Received April 01, 2019
Accepted February 03, 2020

Summary in Lithuanian

Įvadas

Problemos formulavimas

Optiniai linijiniai keitikliai yra vieni patikimiausių prietaisų, skirtų tiksliam linijiniam poslinkiui matuoti ir automatizuotų mechanizmų judančių mazgų judesiui valdyti. Dėl didelio matavimo tikslumo, itin didelės skiriamosios gebos, gero pakartojamumo ir sąlyginai mažos kainos jie yra naudojami įvairiausiose pramonės, mokslo ir inžinerijos srityse, tokiose kaip: rankinio ar kompiuterinio valdymo metalo apdirbimo staklėse (Zhao *et al.* 2018*)*; automatizuotose gamybos linijose; medicinoje; karinėje pramonėje; stebėjimo ir gedimų diagnostikos įrenginiuose; tiksliose linijinio pozicionavimo sistemose (Lee *et al.* 2011) ir kituose preciziniuose įrenginiuose (Gao *et al.* 2015). Nenuostabu, jog esant tokiam plačiam pritaikomumui, keitikliams tenka dirbti pačiomis įvairiausiomis darbinėmis sąlygomis, kurios turi didesnę ar mažesnę įtaką šių matavimo prietaisų veikimui. Negana to, tikslumo reikalavimai aukščiau paminėtiems technologiniams įrenginiams ir juose integruotoms matavimo sistemoms vis griežtėja.

Mechanizmų atliekamo technologinio proceso tikslumas ir kokybė didele dalimi priklauso nuo naudojamos matavimo sistemos patikimumo. Akivaizdu, jog tinkamas linijinių keitiklių veikimas yra itin svarbus. Deja, dažnu atveju, su pozicionavimo tikslumu susijusios technologinio proceso paklaidos yra siejamos su tiesioginėmis įrenginio deformacijomis, konstrukcijoje vyraujančiomis mechaninėmis vibracijomis ar temperatūriniais efektais, priimant, jog matavimo sistemos paklaidos sandas sudaro tik mažą dalį visos paklaidos (Alejandre and Artes 2004).

Linijiniuose keitikliuose vyraujančios paklaidos sukeltos mechaninių deformacijų montavimo metu, precizinių skalių gamybos ar prietaiso surinkimo netikslumai, termoelastinės paklaidos atsirandančios dėl temperatūrinių efektų ar keitiklio elementų virpesiai sukelti išorinių mechaninių vibracijų gali sutrikdyti matavimo sistemos veikimą ir pakenkti matavimo tikslumui bei pakartojamumui. Didelės dominuojančios aukšto dažnio interpoliacijos paklaidos vertės gali riboti galimą maksimalią rezoliuciją. Sistemose, kuriose judančių elementų judesiai yra valdomi tiesioginės pavaros (angl. direct-drive) sistema, šios keitiklio paklaidos gali sukelti triukšmingą pavaros veikimą, greičio svyravimus ir papildomą šilumos kiekio susidarymą (Ye *et al.* 2019).

Sumažinti matavimo sistemos paklaidas ir pasiekti aukštus kokybės reikalavimus galima tik kuriant naujas sistemas, kuriose būtų integruoti naujausi mokslo ir technikos pasiekimai, o taip pat ir tobulinant esamus matavimo prietaisus pagal šiuolaikinius precizinės inžinerijos principus. Daugelio pasaulio šalių mokslininkai nuolat analizuoja optinius keitiklius, kuria naujus jų veikimo principus, bei tobulina gamybos technologijas. Nemažą indėlį kuriant precizines matavimo sistemas ir jų kalibravimo įrenginius, bei stiklinių ir plieninių matavimo skalių gamybos technologijas įneša ir Lietuvos universitetai bei mokslininkai.

Šiame darbe pagrindinis dėmesys skiriamas teoriniam ir eksperimentiniam optinių linijinių poslinkių matavimo keitiklių paklaidų ir jas sukeliančių veiksnių tyrimui. Siekiant nustatyti vyraujančių matavimo paklaidų pobūdį ir išsiaiškinti jų prigimtį atliktas nuoseklus linijinių keitiklių tyrimas esant skirtingoms darbo sąlygoms, įskaitant aplinkos šiluminius efektus, mechanines vibracijas bei skirtingą nuskaitymo greitį. Išanalizuoti ir susisteminti duomenys panaudoti kuriant terminių ir geometrinių paklaidų kompensavimo modelį ir pasiūlant techninius paklaidų nustatymo, tyrimo ir minimizavimo metodologijų realizavimo sprendimus.

Darbo aktualumas

Poslinkio matavimo paklaidos vyraujančios optiniuose linijiniuose keitikliuose gali sutrikdyti tikslios įrenginio pozicijos nustatymą ar sukelti judesio nesklandumus. Tai daro įtaką įrenginio atliekamo technologinio proceso kokybei, o kartais netgi gali sugadinti patį mechanizmą. Siekiant išvengti šių pasekmių, reikalinga atkreipti dėmesį į tokių matavimo sistemų elgseną įvairiomis eksploatavimo sąlygomis.

Pažangūs foto litografinės gamybos, sistemos mazgų surinkimo ir optinių linijinių keitiklių kalibravimo procesai yra atliekami laikantis griežtų standartų ir reikalavimų. Visi minėti procesai atliekami specialiose švariose ir termostabiliose laboratorijose, naudojant preciziškai sukalibruotą įrangą. Tokiomis idealiomis sąlygomis sukalibruoto prietaiso parametrai, kaip tikslumas, yra nurodomi vartotojo specifikacijose. Tačiau termoelastinių deformacijų ar mechaninių vibracijų poveikis dažnai taip ir išlieka diskusijų objektu. Bet koks naudotojo bandymas išnagrinėti ar pagerinti linijinio keitiklio tikslumą reikalauja detalių žinių apie prietaiso konstrukciją ir veikimo principus, kurios dažniausia išlieka gamybine paslaptimi. Todėl yra reikalingos universalios matavimo paklaidų vertinimo ir analizės metodikos.

Į šią problemą žvelgiant iš gamintojo pusės, matavimo paklaidų mažinimas įrenginių gamybos tikslumo didinimo sąskaita ne visada yra įmanomas. Negana to, dažniausia tai

yra technologiškai ir ekonomiškai neefektyvi išeitis. Norint sukurti aplinkos sąlygoms minimaliai jautrų matavimo prietaisą reikia panaudoti pažangiausių mokslo ir technikos pasiekimų optikos, elektronikos, tiksliosios mechanikos, medžiagų inžinerijos ir kitose srityse. Šiuo atveju kitokios paklaidų mažinimo priemonės, tokios kaip realaus laiko kompensacija, gali atverti plačias galimybes, kai vyraujančios matavimo paklaidos yra kalibruojamos, įsimenamos ir eliminuojamos technologinio proceso metu.

Bet kokiu atveju, pats tinkamiausias sprendimas yra galimas tik atlikus kompleksinį matavimo sistemos tyrimą. Identifikuotas sistemingasis paklaidų susidarymo pobūdis gali būti eliminuojamas naudojant paklaidų kompensavimo metodus, o atsitiktinė paklaidos dedamoji gali būti mažinama įvairiais techniniais sprendimais.

Tyrimo objektas

Darbo tyrimų objektas yra optinis linijinių poslinkių matavimo keitiklis, bei jo matavimo paklaidos, kurios susidaro prietaisui veikiant realiomis darbinėmis sąlygomis. Kad būtų tinkamai ištirtos keitiklyje vyraujančios matavimo paklaidos reikia išnagrinėti:

- termoelastinių deformacijų susidarymą veikiant skirtingoms temperatūrinėms sąlygoms ir jų poveikį matavimo tikslumui;
- dalijamosios vidaus žingsnio paklaidos priklausomybę nuo skirtingų poslinkio matavimo greičių;
- išorinių mechaninių vibracijų įtaką matavimo paklaidos susidarymui, bei galimus šios įtakos mažinimo sprendimus.

Darbo tikslas

Šio darbo tikslas yra teoriškai ir eksperimentiškai ištirti susidarančias optinio linijinių poslinkių matavimo keitiklio paklaidas veikiant įvairioms darbinės aplinkos sąlygoms, siekiant sukurti metodus ir pasiūlyti techninius sprendimus tokių optinių matavimo sistemų kokybei gerinti.

Darbo uždaviniai

Darbo tikslui pasiekti reikalinga spręsti sekančius uždavinius:

1. Susisteminti moksline bei technine literatūra paremtas žinias apie optinius linijinius keitiklius: išanalizuoti egzistuojančias tokio tipo sistemas, jų veikimo principus ir konstrukcijas; išskirti didžiausią įtaką matavimo procesui darančius veiksnius; sudaryti matavimo paklaidų biudžetą ir išskirti pagrindinius paklaidų šaltinius; išanalizuoti naudojamus teorinius matavimo paklaidų skaičiavimo ir eksperimentinius paklaidų įvertinimo metodus; išanalizuoti matavimo paklaidų mažinimo metodikas ir naudojamus techninius sprendimus.
2. Analitinių ir skaitinių metodų pagalba teoriškai ištirti pasirinkto linijinio keitiklio veikimą esant skirtingoms aplinkos sąlygoms: veikiant išoriniasm šilumos šaltiniams ir kintančiai aplinkos temperatūrai; vyraujant skirtingam poslinkio matavimo greičiui; bei veikiant išorinėms mechaninėms vibracijoms.

2.1. Sudaryti skaitinį tiriamojo optinio linijinio keitiklio modelį ir atlikti kompiuterinį modeliavimą siekiant ištirti termoelastinių deformacijų sukeliamas matavimo paklaidas, bei sukurti sisteminės šios paklaidos dedamosios matematinį skaičiuojamosios kompensacijos algoritmą.

2.2. Sukurti dalijamosios vidaus žingsnio paklaidos įvertinimo ir analizės metodiką, esant skirtingiems poslinkio matavimo greičiamas.

2.3. Skaitinių metodų pagalba nustatyti rezonansinius dažnius, bei atitinkamas deformacijos formas.

3. Atliki sekančius eksperimentinius tyrimus:

3.1. Taikant sudarytą geometrinių ir termoelastinių deformacijų sukeltų matavimo paklaidų kompensavimo metodiką, atlikti tyrimus ir įvertinti sukurto algoritmo tinkamumą ir patikimumą.

3.2. Pritaikyti sukurtą metodiką ir eksperimentiškai nustatyti interpoliacijos paklaidų susidarymo priklausomybę nuo skirtingų poslinkio matavimo greičių.

3.3. Atlikti eksperimentinį dinaminio poveikio tyrimą. Susieti išmatuotus linijinio keitiklio elementų virpesius su atliktos kompiuterinės modalinės analizės rezultatais ir nustatyti kokios modos (keitiklio deformacijos) sukelia didžiausią atsako amplitudę. Įvertinti išorinių mechaninių virpesių poveikį matavimo paklaidos susidarymui.

Tyrimų metodika

Darbe atliktų tyrimų metodikos yra paremtos atitinkamų mokslo sričių žiniomis, kurios yra susistemintos atlikus analitinę mokslinės bei techninės literatūros apžvalgą.

Teoriniai tyrimai yra atlikti remiantis medžiagų mokslo bei kieto kūno kontinuumo mechanikos principais. Tiriamajame linijiniame keitiklyje vykstantys temperatūriniai procesai nagrinėjami pasitelkiant termodinamikos dėsnius. Energijos tvermės ir virsmo dėsnis leidžia spręsti šilumos perdavimo problemą ir įvertinti nusistovėjusį temperatūrinį gradientą. Atsiradusių temperatūrinių įtempių bei terminio plėtimosi skaičiavimas padeda nustatyti termoelastines deformacijas, kurios yra tiesiogiai susijusios su tiriamąja linijinio poslinkio matavimo paklaida.

Dinaminiai linijinio keitiklio tyrimai remiasi savitųjų sistemos rezonansinių dažnių nustatymu bei modaline virpesių analize. Baigtinių elementų metodas (BEM) yra naudojamas kaip labiausia tinkamas būdas tokio pobūdžio trimačių uždavinių, aprašomų diferencialinėmis lygtimis su dalinėmis išvestinėmis, skaitiniam sprendimui. Kompiuteriniam modeliavimui pasitelktas programinės įrangos paketas *„COMSOL“*.

Empiriniai duomenys surinkti eksperimentinių tyrimų metu, kurie yra atlikti mechanikos mokslo instituto (VGTU) bei UAB „Precizika Metrology“ laboratorijose. Lazerinė kalibravimo sistema *„Keysight 5530“* yra panaudota kaip etaloninė matavimo sistema tiriamojo keitiklio paklaidų nustatymui. Precizinė įmonių *“Brüel & Kjær”* ir *“Hottiger”* virpesių žadinimo bei matavimo įranga panaudota dinaminių tiriamojo objekto parametrų analizei. Suprojektuotas ir sukomplektuotas eksperimentinis stendas, kurio pagrindą sudaro įmonės *„STANDA“* motorizuotas tiesioginės pavaros linijinio pozicionavimo staliukas, panaudotas linijinio keitiklio interpoliacijos paklaidų priklausomybės nuo skirtingo poslinkio matavimo greičio nustatymui. Diferencialinių inkrementinio keitiklio išėjimo

signalų įrašymui panaudota duomenų rinkimo ir apdorojimo sistema paremta skaitmeniniu osciloskopu *„PicoScope 3000“*. Visi eksperimentiniai matavimai atlikti remiantis matavimų teorijos pagrindais siekiant sumažinti galimą neapibrėžtumą.

Surinktų duomenų patikimumas įvertintas pasitelkiant matematinės statistikos skaičiavimus. Detalesnis linijinio keitiklio interpoliacijos paklaidų tyrimas atliktas remiantis harmonine paklaidos analize. Duomenų apdorojimui ir grafiniam rezultatų reprezentavimui panaudoti kompiuterinės programinės įrangos paketai: *“Matlab”*; *“Statistica”*; *“Origin”* ir *“Microsoft Excel”*.

Darbo mokslinis naujumas

Rengiant disertaciją buvo pasiekti šie inžinerijos mokslo naujumai:

1. Atskleisti uždaro tipo linijinių keitiklių poslinkio matavimo paklaidų sistemingieji dėsningumai veikiant išoriniams aplinkos poveikiams, kuriems gali būti taikoma skaičiuojamoji paklaidų kompensacija.
2. Sudarytas, išanalizuotas ir techninėmis priemonėmis realizuotas matematinis temperatūrinių bei geometrinių tiriamojo linijinio keitiklio paklaidų kompensavimo modelis.
3. Pristatyta linijinių keitiklių metrologinių paklaidų nustatymo, bei šių paklaidų tyrimo metodologija.
4. Ištirtos dinaminės tiriamojo linijinio keitiklio savybės veikiant išorinėms mechaninėms vibracijoms, bei nustatytas jų poveikis poslinkio matavo paklaidų susidarymui.

Darbo rezultatų praktinė reikšmė

Disertacijoje yra sprendžiamas kompleksinis uždavinys apimantis būtinus teorinius ir eksperimentinius tyrimus, siekiant išanalizuoti ir suprasti linijiniuose keitikliuose vyraujančius procesus, kurie pasireiškia matavimo sistemai dirbant įvairiomis aplinkos sąlygomis. Tam įgyvendinti buvo sukurti metodologiniai bei praktinio pritaikymo sprendimai, kurių dėka sprendžiamos analitinės, empirinės bei skaitinės užduotys. Gauti rezultatai panaudoti matavimo sistemos elgsenos įvertinimui ir realaus laiko paklaidų kompensavimo modelio sudarymui. Pasiūlytas metodas yra patogus ir lengvai realizuojamas pasitelkiant standartines skaitmeninio valdymo priemones, kurios gali būti integruotos į linijinių keitiklių matavimo sistemas.

Darbe pateikti metodai ir techniniai sprendimai gali būti naudingi inžinieriams ir mokslininkams dirbantiems su precizinėmis matavimo sistemomis, jų kūrimu ir tobulinimu.

Ginamieji teiginiai

1. Uždaro tipo linijinių keitiklių termoelastiniai, bei dinaminiai procesai ir jų dėsningumai gali būti tiriami ir įvertinami naudojant kompleksinę metodiką.
2. Linijinių keitiklių geometrinės ir temperatūros paklaidos užrašomos ir realiu laiku kompensuojamos naudojant supaprastintas parametrines funkcijas.
3. Pasiūlytas praktinis realaus laiko paklaidų kompensavimo sprendimas yra efektyvus ir tinkamas termoelastinių ir geometrinių linijinio keitiklio paklaidų

kompensavimui, priimant, jog keitiklio tikslumas išlieka gamintojo deklaruoto dydžio ribose.

Darbo rezultatų aprobavimas

Disertacijos tema atspausdinti 8 moksliniai straipsniai:

- keturi, disertacijoje pateikti, straipsniai atspausdinti recenzuojamuose Clarivate Analytics Web of Science duomenų bazės moksliniuose leidiniuose, turinčiuose citavimo rodiklį;
- vienas straipsnis atspausdintas Clarivate Analytics Web of Science duomenų bazės Conference Proceedings moksliniame žurnale, be citavimo rodiklio;
- trys straipsniai atspausdinti kitų tarptautinių duomenų bazių moksliniuose žurnaluose.

Disertacijoje atliktų tyrimų rezultatai paskelbti trijose mokslinėse konferencijose:

- kasmetinėje jaunųjų mokslininkų konferencijoje " Science – Future of Lithuania", 2017, Vilniuje;
- 15th tarptautinėje konferencijoje "Piezoelectric Materials and Applications in Actuators (IWPMA)", 2018, Kobe, Japonijoje;
- 16th tarptautinėje konferencijoje "Piezoelectric Materials and Applications in Actuators (IWPMA)", 2019, Lyon, Prancūzijoje.

Disertacijos struktūra

Disertaciją sudaro: įvadas, analitinės literatūros apžvalga, tyrimo metodologijos aptarimas, apibendrinti tyrimo rezultatai ir išvados, literatūros sąrašas, keturi pridedami moksliniai straipsniai ir santrauka Lietuvoje.

Darbo apimtis 145 puslapiai, kuriuose: 50 pateiktų lygčių, 28 paveikslai, 2 lentelės ir 36 darbe cituojamos literatūros šaltiniai ir 4 pridedamai moksliniai straipsniai.

Tyrimų rezultatai ir išvados

Šioje dalyje bendrame kontekste pateikiama pridedamuose 1–4 straipsniuose pateiktų išvadų santrauka. Siekiama susieti darbų rezultatus su bendrais darbo tikslais. Kiekvieno iš skirtingų aplinkos veiksnių, lemiančių linijinio keitiklio matavimo paklaidas, tyrimai pateikiami atskiruose moksliniuose straipsniuose. Geometrinių ir temperatūrinių paklaidų teorinis tyrimas ir jų kompensavimo algoritmo sukūrimas pateiktas pridedamame 1 straipsnyje. Praktinis sukurtos realaus laiko kompensavimo realizavimas ir atlikti eksperimentiniai tyrimai pateikiami 2 straipsnyje. 3 straipsnyje pateikiamas eksperimentinis vidaus žingsnio (kitaip vadinamos interpoliacijos paklaida) paklaidos tyrimas esant skirtingiems poslinkių nuskaitymo greičiams. Mechaninių virpesių įtaka kodavimo įrenginio matavimo paklaidoms ištirta ir pateikta pridedamame 4 straipsnyje. Taip pat pateikiamos bendrosios baigiamojo darbo išvados.

Straipsnio 1 tyrimų rezultatai

Straipsnyje 1 pateikiama geometrinių bei temperatūrinių linijinių poslinkių matavimo keitiklio paklaidų analizė bei sudaromas skaičiuojamosios kompensacijos matematnis modelis. Siekiant išsamiau atskleisti problemą, įvadinėje straipsnio dalyje pristatomi matavimo sistemose vyraujantys temperatūriniai procesai ir aptariami temperatūrinių matavimo paklaidų mažinimo metodai. Straipsnyje atliktų tyrimų objektu pasirinktas uždaro tipo optinis linijinis keitikis. Atliktas tiriamąjame objekte nusistovinčių temperatūrinių laukų ir termoelastinių deformacijų sukeltų matavimo paklaidų kompiuterinis modeliavimas, paremtas baigtinių elementų metodu (BEM). Gauti rezultatai atskleidžia sistemingą temperatūrinės paklaidos elgseną, kai keitiklį veikia pastovaus galingumo išoriniai šilumos šaltiniai, bei kintanti aplinkos temperatūra. Tai sudaro prielaidą matematinio temperatūrinių paklaidų modelio sudarymui. Pasiūlytas skaičiuojamosios kompensacijos modelis pagrįstas geometrinių ir termoelastinių linijinio ketiklio paklaidų aproksimavimu paprastomis parametrinėmis funkcijomis ir sisteminių, tiesinės prigimties, temperatūrinių paklaidų skaičiavimu pagal aplinkos temperatūros svyravimus. Išvesta dvimatė funkcija sudaro pagrindą kompensacinės vertės Δ apskaičiavimui.

$$\Delta(q,T) = F_g(q) + F_{gr}(q) + F_a(\Delta T, q). \tag{3.1}$$

Jos argumentai yra poslinkis q ir temperatūros reikšmė T, išmatuota viename specialiai pasirinktame keitiklio profilio taške, kuris geriausiai apibūdina vidutinį temperatūros pokytį. $F_g\ (q)$ – nustatytos geometrinės klaidos aproksimacinė funkcija; $F_{gr}\ (q)$ – termoelastinės paklaidos aproksimacinė funkcija, kai šiluminis gradientas išilgai tiesinės kodavimo skalės yra pastovus, o aplinkos temperatūra stabili; $F_a\ (\Delta T,\ q)$ – šiluminės paklaidos sudedamoji dalis, išreiškianti matavimo skalės tiesinę deformaciją kintant aplinkos temperatūrai.

$$F_a(\Delta T, q) = \alpha_{corrected} \cdot \Delta T \cdot q. \tag{3.2}$$

Čia: $\alpha_{corrected}$ – tai pataisytas matavimo skalės linijinio šiluminio plėtimosi koeficientas (nustatomas analizuojant aliuminio korpuso ir nerūdijančio plieno matavimo skalės sąveiką); ΔT – aplinkos temperatūros T skirtumas nuo vardinės Tn ($\Delta T = Tn - T$), o q – išmatuotas poslinkis (matuojamoji padėtis).

Straipsnyje 1 analizuojamo linijinio keitiklio matavimo paklaidos kompensavimo dydžio grafinis vaizdas gali būti pateiktas kaip 3D diagrama, kaip parodyta Pav.1.

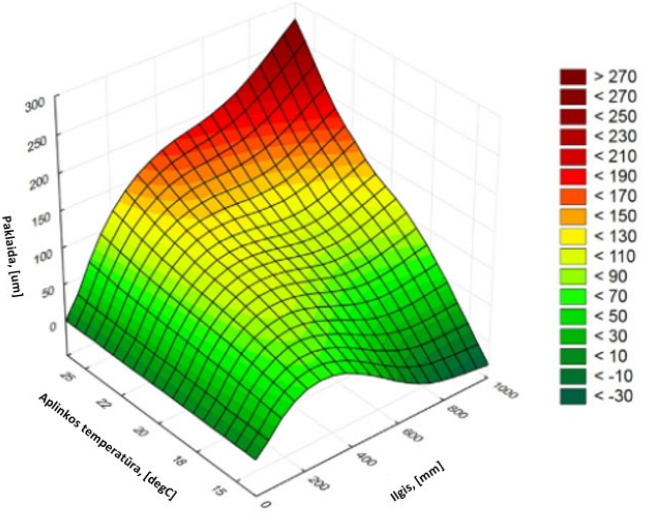

1 pav. Kompensuojamos paklaidos priklausomybė nuo išmatuoto poslinkio dydžio ir aplinkos temperatūros

Tokį skaičiuojamąjį matavimo paklaidų mažinimo metodą galima realizuoti naudojant standartinę skaičiavimo įrangą, kuri būtų naudojama kaip išorinis elektronikos modulis jungiamas prie įrenginio arba integruota į pačio keitiklio konstrukciją.

Straipsnio 2 tyrimų rezultatai

Straipsnyje 2 pateiktas optinio linijinio keitiklio temperatūrinių ir geometrinių paklaidų realaus laiko kompensacijos metodas. Ankstesniame moksliniame straipsnyje 1 sudarytas matematinis skaičiuojamosios kompensacijos modelis yra realizuotas panaudojant lauku programuojamo loginio masyvo (angl. FPGA) platformą. Principinė sukomplektuotos technologinės keitiklio pozicijos kompenavimo įrangos blokinė schema parodyta Pav.2.

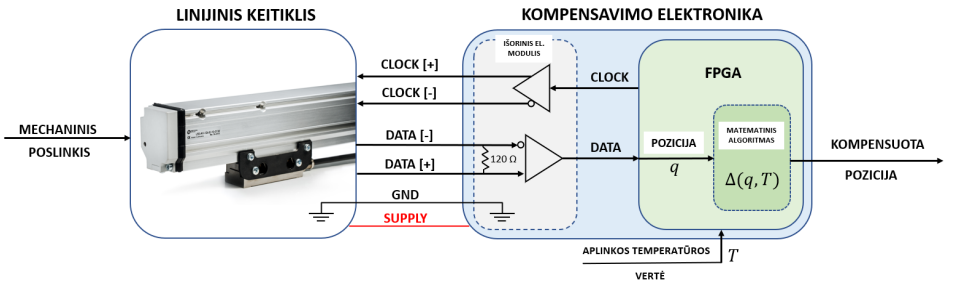

2 pav. Principinė blokinė keitiklio pozicijos kompensavimo įrangos schema

Eksperimentinio tyrimo metu, sukomplektuotos technologinės įrangos pagalba, buvo atliekamas išvestos dvimatės kompensacinės funkcijos skaičiavimas ir linijinio keitiklio padėties rodmenų koregavimas realiuoju laiku. Uždaro tipo linijinio optinio keitiklio elgsena ištirta esant keturioms skirtingoms aplinkos temperatūroms. Termo stabilioje laboratorijoje išmatuotas keitiklio tikslumas esant 20 ± 0,2 ºC temperatūrai priimamas kaip nominalus. Šios nustatytos paklaidos vidurkių grafiką aproksimuojanti parametrinė funkcija toliau yra naudojama geometrinių ir temperatūrinių paklaidų kompensavimo vertėms apskaičiuoti. Palyginamieji kompensuotos ir nekompensuotos keitiklio matuojamosios pozicijos paklaidos grafikai pateikti Pav.3.

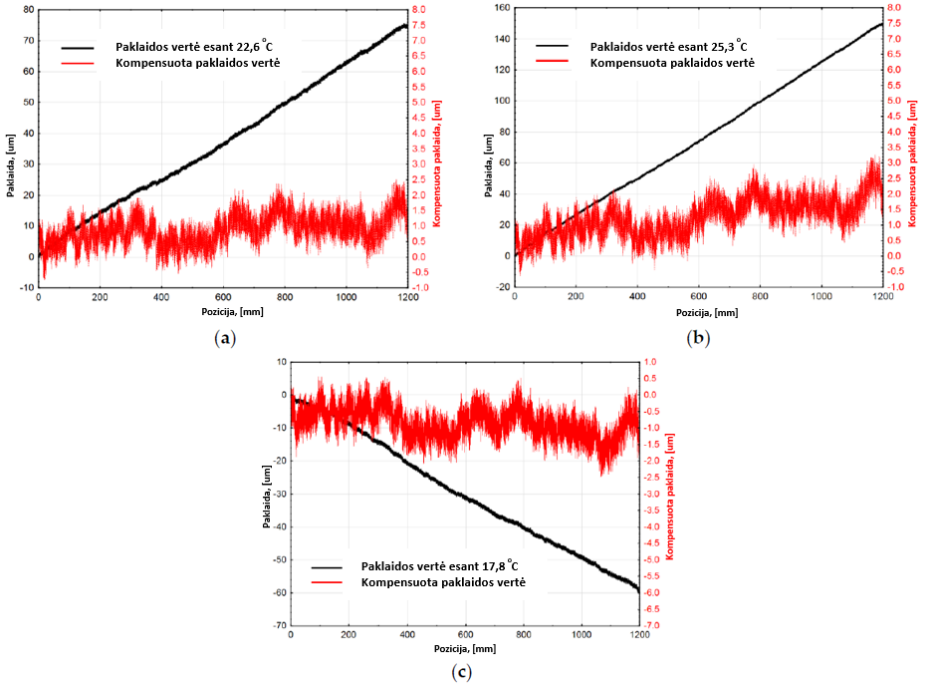

3 pav. Kompensuotos keitiklio paklaidos grafikai (raudona linija / dešinės Y ašies vienetai) ir atitinkami nekompensuotos keitiklio paklaidos grafikai (juoda linija / kairės Y ašies vienetai) prie skirtingų aplinkos temperatūrų: **(a)** 22,6 ºC; **(b)** 25,3 ºC; **(c)** 17,8 ºC

Gauti rezultatai rodo, jog termoelastinių deformacijų sukelta matavimo paklaida gali būti sėkmingai sumažinta iki 98 procentų. Pasiūlytas paprastų paklaidas aproksimuojančių funkcijų ir elektroninės įrangos pasirinkimas užtikrina skaičivimo spartą, kuri yra tinkama realaus laiko sistemoms. Straipsnyje taip pat pristatomas temperatūrinių paklaidų kompensavimo algoritmo patikslinimo metodas. Jis pagrįstas optinio keitiklio matuojamosios skalės realaus linijinio temperatūrinio plėtimosi koeficiento (angl. CTE) vertės apskaičiavimu iš eksperimentiškai surinktų duomenų. Glaustas rezultatų palyginimas pateiktas lentelėje 1.

Lentelė 1. Temperatūrinių paklaidų kompensavimo tyrimo rezultatai

Parametras	Aplinkos temperatūra			
	17,8 °C	**20 °C**	**22,6 °C**	**25,3 °C**
Nekompensuota vidutinė keitiklio paklaida, [µm]	± 30,08	± 2,20	± 37,74	± 75,09
Kompensuota vidutinė keitiklio paklaida, [µm]	± 1,52	± 1,08	± 1,62	± 1,95
Apskaičiuota keitiklio paklaida naudojant eksperimentiškai nustatytą temperatūrinio plėtimosi koeficientą, [µm]	± 1,42	-	± 1,46	± 1,48

Pasiūlytas paprastų parametrinių aporksimuojančių funkcijų ir standartinių elektroninių skaičiavimo priemonių pasirinkimas leidžia užtikrinti pakankamą skaičiavimo spartą, tinkančią realaus laiko kompensacijos realizavimui.

Straipsnio 3 tyrimo rezultatai

Straipsnis 3 pateikia eksperimentinį linijinio keitiklio dalijamosios vidinio žingsnio paklaidos (angl. Sub-divisional error, SDE) tyrimą esant skirtingiems poslinkio nuskaitymo greičiams. Įvadinėje mokslinio straipsnio dalyje aptariami metrologiniai procesai vykstantys optiniuose keitikliuose ir dalijamosios paklaidos svarba bei jos daroma įtaka matavimo sistemos veikimui. Siekiant nustatyti skirtingų nuskaitymo greičių įtaką dalijamosios paklaidos formavimuisi, sukurta metodika, pagrįsta eksperimentiniu pastovaus greičio bandymu. Tyrimų metu linijinio keitiklio poslinkio matavimo procesas buvo realizuotas esant skirtingiems nuskaitymo greičiams nuo 100 mm/s iki 1100 mm/s. Analoginiai keitiklio išėjimo signalai buvo įrašomi, o dalijamosios aukšto dažnio matavimo paklaidos reikšmės ir jos kitimo tendencija įvertinama pritaikant skaičiuojamąjį arktangento algoritmą (atan2). Statistinės tiesinės regresijos analizė, atlikta apskaičiuotiems duomenims, parodo tiesioginį ryšį tarp nustatytos paklaidos absoliutaus dydžio ir keitiklio nuskaitymo galvutės linijino judėjimo greičio (R=0,8581). Nustatytos absoliučiosios SDE paklaidos pavaizduotos grafike pateiktame Pav.4.

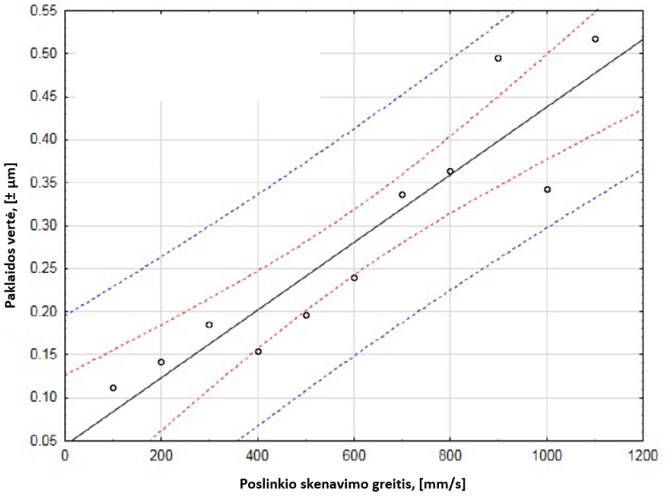

4 pav. Absoliučių SDE paklaidos verčių priklausomybės nuo poslinkio skenavimo greičio grafikas

Išsamesniam tyrimui atlikta harmoninė nustatytų dalijamųjų paklaidų analizė pagrįsta greitąja Furje transformacija (angl. FFT). Dalijamosios paklaidos išskaidomos į atskirus harmoninius komponentus. Pastebėta, jog pirmosios trys harmonikos sudaro didžiąją dalį paklaidos vertės. Didžiausią dalį iš jų sudaro antroji harmonika. Nustatyta, jog pastaroji tiesiogiai koreliuoja su poslinkio nuskaitymo greičiu ir atsiranda dėl didėjančio keitiklio išėjimo signalų amplitudžių ar fazių skirtumo. Trijų pirmųjų harmonikų ir poslinkio skenavimo greičio priklausomybės grafikas pateiktas Pav.5.

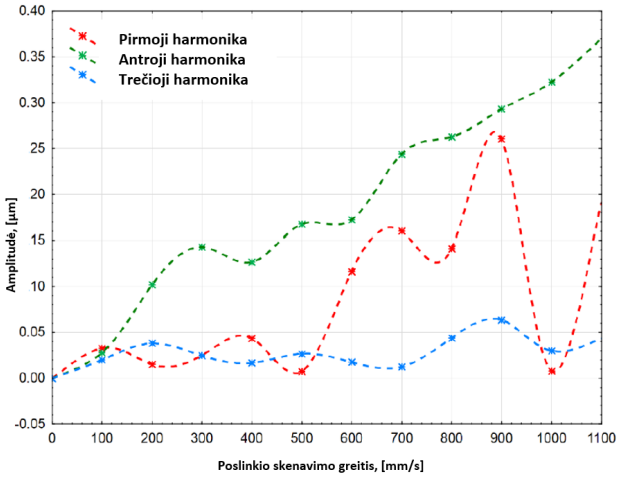

5 pav. Nustatytų SDE paklaidų grafikų pirmųjų trijų harmonikų priklausomybės nuo poslinkio skenavimo greičio grafikas

Siekiant sumažinti tokio tipo paklaidas pasiūlytas techninis sprendimas integruoti mažiau skenavimo dažniui jautrų „vieno skenavimo laukelio“ (angl. single-field) optinį signalų formavimo metodą arba išorinę išėjimo signalų monitoringo ir koregavimo elektroninę įrangą. Kitas siūlomas metodas yra skaičiuojamoji keitiklio padėties rodmenų kompensacija. Atlikus papildomą surinktų eksperimentinių duomenų apdorojimą galima išvesti dvimatę funkciją, kurios argumentai yra atitinkama interpoliuota keitiklio pozicija vidiniame matuojamosios skalės žingsnyje, bei pagal poslinkio skenavimo dažnį nustatytas matavimo greitis. Apskaičiuota tokios funkcijos reikšmė galėtų nusakyti apytikslę aproksimuotos dalijamosios paklaidos vertę esant tam tikram skenavimo greičiui ir gali būti naudojama kaip kompensuojamasis dydis matavimo sistemose.

Straipsnio 4 tyrimo rezultatai

Straipsnyje 4 pateikta optinio linijinio keitiklio dinaminės elgsenos analizė veikiant išorinėms mechaninėms vibracijoms. Eksperimentinių tyrimų metu uždaro tipo keitiklio korpusas bei nuskaitymo galvutė įtvirtinami fiksuotoje padėtyje ant elektrodinaminio vibro stendo. Nepageidaujamas nuskaitymo karietėlės judesys išilgai matuojamosios skalės, atsirandantis keitiklio konstrukciją veikiant vibracijai, yra esminis šio tyrimo aspektas. Naudojamas vibro stendas generuoja žinomo dydžio mechaninį periodinį judesį, o pjezoelektrinių akselerometrų pagalba matuojami nuskaitymo galvutės ir keitiklio aliuminio korpuso atsakai. Eksperimentų metu įrašomi analoginiai inkrementiniai keitiklio išėjimo signalai padeda nustatyti sugeneruotos dinaminės paklaidos vertę naudojant skaičiuojamąjį arktangento algoritmą (atan2), bei vizualiai analizuoti atitinkamas Lissajous kreives. Pirmiausia buvo ištirtas linijinio keitiklio atsakas į kintančio dažnio sinusines vibracijas ir nustatyti testo metu išryškėję savitieji konstrukcijos dažniai. Sekančiame etape vibro stendas žadino linijinį keitiklį periodinėmis vibracijomis nuo 100 Hz iki 2000 Hz, kas 100 Hz žingsniu įtraukiant ir prieš tai nustatytus rezonansinius dažnius. Tokiu būdu nustatomos keitiklio nuskaitymo galvutės ir korpuso atsako amplitudžių vertės. Atlikta kompiuterinė modalinė tiriamojo keitiklio analizė pagrįsta baigtinių elementų metodu. Remiantis šios analizės ir eksperimentų metu surinktais duomenimis, didžiausios keitiklio elementų atsako vertės susietos su atitinkamomis modalinėmis vibracijos formomis. Teoriškai, didžiausia keitiklio paklaida turėtų būti sugeneruojama kai vieno iš keitiklio elementų: nuskaitymo galvutės arba korpuso virpesių išilgine skalės kryptimi amplitudė yra gerokai didesnė už kito elemento. Įvertinant šią prielaidą sudarytas šių elementų atsako skirtumų grafikas prie skirtingų žadinimo dažnių. Jis pateikiamas Pav.6.

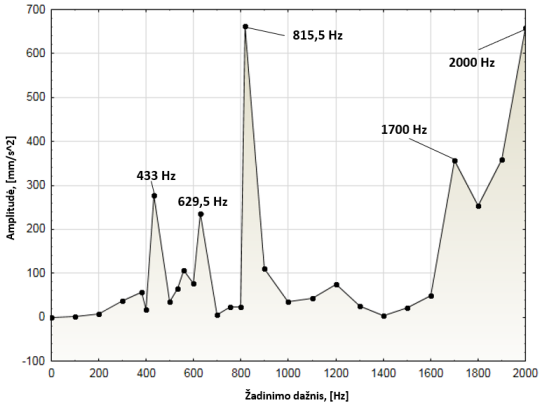

6 pav. Keitiklio nuskaitymo galvutės ir aliuminio korpuso atsako amplitudžių skirtumo grafikas

Gauti rezultatai išryškina potencialiai pavojingiausius dažnius, kuriais žadinama keitiklio konstrukcija ima rezonuoti ir gali sugeneruoti didžiausias matavimo paklaidas. Eksperimentiškai nustatytos paklaidos vertės šiuose dažniuose siekia iki ~11 μm. Tai yra reikšmingas dydis, kadangi matavimo skalės periodas siekia 40 μm. Siekiant pamatyti, kokią įtaką šios išorinės mechaninės vibracijos turi elektriniams keitiklio išėjimo signalams, pastarieji yra įrašyti ir poslinkio matavimo metu. Kaip pavyzdys, Pav.7 pateikiama Lissajous kreivė veikiant 85,5 Hz išoriniam žadinimui

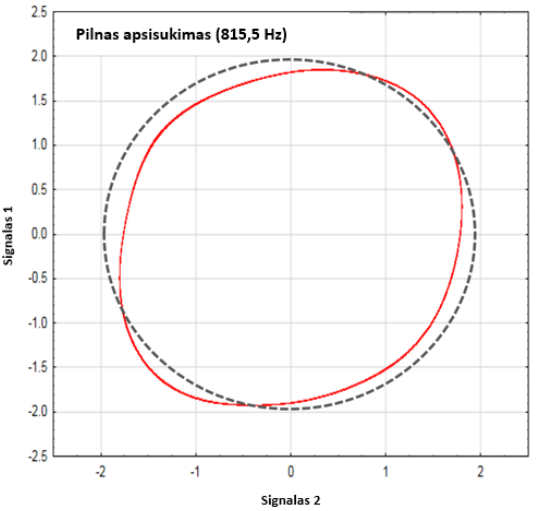

7 pav. Lissajous kreivė keitiklio veikiamo 815,5 Hz išorinėmis mechaninėmis vibracijomis: raudona linija – testuojamo keitiklio Lissajous kreivė; brūkšninė juoda linija – idealaus apskritimo kreivė

Pateikti technologiniai mechaninių vibracijų sukeltų paklaidų mažinimo metodai siūlo didesnio dydžio plieninės skalės įtempimą, tokiu būdu padidinant sistemos standumą, arba papildomų mechaninių elementų integravimą juostos fiksacijai keliuose taškuose. Aptartas dinaminio poveikio tyrimas gali būti pritaikomas kaip matavimo sistemų analizės metodas.

Bendrosios išvados

Teoriškai ir eksperimentiškai ištyrus optinio linijinio keitiklio veikimą skirtingomis darbinės aplinkos sąlygomis gauti šie rezultatai:

1. Atlikta mokslinės ir techninės literatūros apžvalga rodo, jog realių aplinkos sąlygų, tokių kaip: šiluminis poveikis, mechaninės vibracijos, įvairios deformacijos ir poslinkiai gamybos ir montavimo metu daro reikšmingą įtaką matavimo paklaidos susidarymui. Pastebimas naujų patikimų šios problemos sprendimo metodų poreikis. Trūksta išsamesnio tyrimo apie linijinio keitiklio dalijamųjų matavimo paklaidų susidarymą esant skirtingiems poslinkio nuskaitymo greičiams.

2. Atlikus analitinius ir skaitinius linijinio keitiklio veikimo skirtingomis darbinėmis sąlygomis tyrimus, suformuluojamos šios mokslinės išvados:

2.1. Pastebėtas sistemingas termoelastinių deformacijų pobūdis, kuris sukuria prielaidą pristatytos skaičiuojamosios temperatūros paklaidų kompensacijos sudarymui ir jos realizavimui standartinėmis techninėmis priemonėmis. Sukurtas matematinis skaičiuojamosios kompensacijos modelis.

2.2. Sukurta dalijamosios vidaus žingsnio paklaidos įvertinimo ir analizės metodologija. Šis metodas leidžia nustatyti vyraujančią interpoliacijos paklaidos tendenciją ir ją išanalizuoti nenaudojant didelio tikslumo etaloninio keitiklio ar kitos precizinės metrologinės įrangos.

2.3. Atlikta skaitinė linijinio keitiklio modalinė analizė. Nustatyti savitieji sistemos dažniai bei virpėjimo formos leidžia perprasti komponentų virpėjimo prigimtį.

3. Atlikti eksperimentiniai tyrimai leidžia suformuoti šias mokslines išvadas:

3.1. Atlikti bandymai rodo, jog sudarytas matematinis kompensacijos modelis yra tinkamas linijinių keitiklių geometrinės ir termoelastinės paklaidos nustatymui ir kompensavimui. Matavimo paklaida gali būti sumažinta iki 98%. Pristatytas skaičiuojamosios kompensacijos metodas, realizuotas lauko programuojamų vartų masyvo (angl. FPGA) skaičiavimo platforma, pademonstravo pakankamą skaičiavimo našumą ir yra tinkamas naudoti realaus laiko sistemose.

3.2. Atliktas dalijamosios linijinio keitiklio paklaidos tyrimas atskleidžia tiesinę šios paklaidos priklausomybę nuo poslinkio nuskaitymo greičio. Didėjant keitiklio nuskaitymo galvutės perslinkimo greičiui - dalijamosios paklaidos absoliutusis dydis didėja. Antroji harmonika sudaro didžiąją nustatytos paklaidos dalį ir gali būti interpretuojama kaip atsirandantis kintantis skirtumas tarp analoginių keitiklio išėjimo signalų amplitudžių arba jų tarpusavio fazės.

3.3. Atlikti eksperimentiniai dinaminiai linijinio keitiklio tyrimai (pagal IEC/EN 60068-2 standartą) rodo matavimo paklaidos susidarymą, kuris siekia iki ~11 μm. Toks paklaidos susidarymas siejamas su atitinkamais plieninės matavimo skalė, korpuso ar nuskaitymo galvutės judesiais nustatytais modalinės analizės metu.

Darbe pristatyta kompleksinė metodologija, kuri gali būti pritaikyta uždaro tipo linijinių keitiklių temperatūros ir dinaminėms paklaidoms tirti. Aptarti nustatytų paklaidų matematinio aprašymo ir praktinio paklaidų kompensavimo realizavimo pavyzdžiai gali būti integruoti į naujos kartos matavimo sistemas arba padėti jau esamų sistemų tyrimams, bei jų tobulinimui.

Ateityje, šioje disertacijoje pristatytus darbus galima būtų tęsti taikant konkrečius techninius bei eksperimentinius sprendimus:

1. Temperatūrinių paklaidų skaičiuojamosios kompensacijos modelį būtų galima patobulinti pritaikant pažangesnius matematinius aproksimavimo metodus. Dinamiškai laike kintantis išorinių šilumos šaltinių ir aplinkos temperatūros poveikis gali būti įvertinti ir pridėti kaip korekcinė vertė pristatytame kompensavimo algoritme.
2. Atliktų tyrimų metu nustatytas dalijamosios matavimo paklaidos vertes esant skirtingiems greičiams galima papildomai apdoroti ir išvesti dvimatę funkciją paklaidų kompensavimui. Tokia funkcija galėtų būti integruota į jau pristatytą temperatūrinių paklaidų kompensavimo algoritmą. Tokiu būdu linijinis keitiklis taptų atsparus ne tik šiluminiams poveikiams, bet ir mažiau jautrus nuskaitymo greičiui.
3. Siekiant sumažinti mechaninių vibracijų poveikį, patartina pritaikyti techninius sprendimus, tokius kaip: naudoti didesnį plieninės matavimo skalės įtempimą, ar į aliuminio korpusą integruoti juostos prispaudimo elementus. Tokiu būdu būtų padidintas sistemos standumas ir rezonansiniai keitiklio elementų dažniai. Vieno laukelio (angl. „single-field“) elektrinių signalų formavimo sistemos integravimas sumažintų sistemos jautrumą išoriniam mechaniniam žadinimui, o tuo pačiu ir nuskaitymo greičio įtakai.

Daugumos iš šių pasiūlymų įgyvendinimui reikalinga pakeisti keitiklio konstrukciją ar gamybos technologinius aspektus. Bet kuriuo atveju yra reikalingi išsamesni teoriniai ir eksperimentiniai tyrimai

Donatas GURAUSKIS

INVESTIGATION OF THE MEASUREMENT ERRORS FORMATION IN OPTICAL LINEAR ENCODERS

Doctoral Dissertation

Technological Sciences,
Mechanical Engineering (T 009)

MATAVIMO PAKLAIDŲ FORMAVIMOSI OPTINIUOSE LINIJINIUOSE KEITIKLIUOSE TYRIMAS

Daktaro disertacija

Technologijos mokslai,
Mechanikos inžinerija (T 009)

2022 05 13. 12 sp. l. Tiražas 20 egz.
Leidinio el. versija *https://doi.org/10.20334/2022-024-M*
Vilniaus Gedimino technikos universitetas
Saulėtekio al. 11, 10223 Vilnius
Spausdino UAB „Ciklonas“,
Žirmūnų g. 68, 09124 Vilnius